Insights into Directional Motor-Driven RNA Localization from the *Xenopus* Oocyte

James A. Gagnon

B.S. Worcester Polytechnic Institute, 2003

Submitted in partial fulfillment of the requirements for the degree of Doctor of Philosophy in the Division of Biology and Medicine at Brown University

Providence, Rhode Island

May 2011

This dissertation by James A. Gagnon is accepted in its present form by the Division of Biology and Medicine as satisfying the dissertation requirement for the degree of Doctor of Philosophy

Date _____ _____
Director, Dr. Kimberly Mowry

Recommended to the Graduate Council

Date _____ _____
Reader, Dr. Mark Johnson

Date _____ _____
Reader, Dr. Richard Freiman

Date _____ _____
Reader, Dr. Albert Dahlberg

Date _____ _____
Reader, Dr. Robert Singer

Approved by the Graduate Council

Date _____ _____
Dr. Peter Weber
Dean of the Graduate School

James A. Gagnon
Brown University
185 Meeting Street
Sidney Frank Hall Box GL-269, Providence, RI 02912
(Cell) 508.736.9587, (Lab) 401.863.2439, (Fax) 401.863.1201
James_Gagnon@brown.edu

EDUCATION & RESEARCH

Brown University
Providence, Rhode Island
Molecular Biology, Cell Biology and Biochemistry Department - Ph.D. Candidate
Fall 2003 - Present
P.I.: Dr. Kimberly Mowry
"Insights into Directional Motor-Driven RNA Localization from the Xenopus Oocyte"

iGEM (International Genetically Engineered Machines Competition)
2006-2009 Teams – Co-Founder of Brown University Team, Graduate Student Mentor

Projects
- Construction of a heavy metal detector (winner of Best Environmental Project 2008)
- Modeling and partial construction of a gene expression limiter
- Construction of a tri-stable genetic toggle switch

Additional Activities

- Key fundraiser, obtained laboratory space and solicited donated equipment
- Developed and implemented introductory molecular biology lab technique seminars
- Developed standardized molecular cloning protocols
- Video Work:
  Nanodrop promotional video, resulted in two free spectrophotometers
  A series of interviews with synthetic biology researchers for IET.TV

University of Massachusetts Medical School
Research Assistant / Senior Undergraduate Thesis
Summer 2002 – Summer 2003

P.I.: Dr. Jane Lian / Dr. Steve Jones (joint project)

Worcester Polytechnic Institute
B.S. Biology, Molecular Genetics Concentration
Minor - Computer Science
May 2003

PUBLICATIONS

Gagnon JA, Kreiling JA, Mowry KL. *In vivo analysis of RNA localization reveals a new role for dynein and the basis for directional transport in Xenopus oocytes.* (Manuscript in preparation)

Gagnon JA, Mowry KL. *Visualization of mRNA localization in Xenopus oocytes.* Methods Mol Biol. 2010 (In Press)

Gagnon JA, Mowry KL. *Visualizing RNA localization in Xenopus oocytes.* J Vis Exp. 2010 Jan 14;(35).

Gagnon JA, Mowry KL. *RNA Transport In Ovo: Simultaneous Visualization of Two RNAs.* Mol Reprod Dev. 2009 76:1115.

Messitt TJ, **Gagnon JA**, Kreiling JA, Pratt CA, Yoon YJ, Mowry KL. *Multiple kinesin motors coordinate cytoplasmic RNA transport on a subpopulation of microtubules in Xenopus oocytes.* Dev Cell. 2008 15:426-36.

Lewis RA, **Gagnon JA**, Mowry KL. *PTB/hnRNP I is required for RNP remodeling during RNA localization in Xenopus oocytes.* Mol Cell Biol. 2008 28:678-86.

Lohmueller J, Neretti N, Hickey B, Kaka A, Gao A, Lemon J, Lattanzi V, Goldstein P, Tam LK, Schmidt M, Brodsky AS, Haberstroh K, Morgan J, Palmore T, Wessel G, Jaklenec A, Urabe H, **Gagnon JA**, and Cumbers J. *Progress toward construction and modeling of a tri-stable toggle switch in E. coli.* IET Synthetic Biology. 2007 1:1-2:25-28

Lengner CJ, Steinman HA, **Gagnon J**, Smith TW, Henderson JE, Kream BE, Stein GS, Lian JB, Jones SN. *Osteoblast differentiation and skeletal development are regulated by Mdm2-p53 signaling.* J Cell Biol. 2006 172:909-21.

AWARDS & ACTIVITIES

NIH Training Grant Fellow, Brown University	2006-2007
John G. Peterson Fellowship, Brown University	2008-2009
Associate Member, Faculty of 1000	2009
Member of RNA Society	2006-2009
Graduate Admissions Committee: Graduate Student Representative	2006
Graduate Student Council Representative, Brown University	2005-2007
Brown University Community Council Representative	2006
Sheridan Teaching Certification for Secondary Education	2006-2008

PRESENTATIONS

Society of Developmental Biology Regional Meeting selected speaker, April 2009
"Mechanisms directing localization of maternal determinants revealed by in vivo imaging in Xenopus oocytes."

RNA Society Meeting poster, Madison WI, May 2007
"PTB/hnRNP I is Required for RNP Remodeling during RNA Localization in Xenopus Oocytes."

Synthetic Biology 3.0 Conference poster, Zurich Switzerland, June 2007
"Progress Towards Construction of a Tri-Stable Toggle Switch."

FASEB Summer Research Conference poster, Tuscon AZ, June 2005
"Mechanisms Directing Vegetal RNA Localization in the Xenopus oocyte."
Honorable Mention – Best Poster

WPI Senior Thesis Conference poster, Worcester MA, May 2003
"The Role of Mdm2/p53 in Osteogenesis and Skeletal Development."
2nd Runner Up – Best Poster

Table of Contents

Chapter 1: Introduction

The central dogma of molecular biology, oversimplified and drilled into high school students every year for decades, focuses on the unidirectional flow of biological information from DNA through RNA to proteins (Crick, 1970). While this may generally suffice for prokaryotic gene expression, where transcription and translation are coupled, this flowchart underemphasizes the crucial regulatory mechanisms that underlie eukaryotic gene expression. As our tools and theoretical understanding have grown, RNA has emerged as a major point for regulation of gene expression. As a single messenger RNA (mRNA) molecule has the ability to generate hundreds or even thousands of proteins, mRNAs are generally kept at low abundance in the cell, and mis-expression of some mRNAs could jeopardize the survival of the cell or even the organism. To avoid these consequences, cells must carefully regulate the production, distribution, and degradation of mRNA. Gene expression after transcription can be modulated in a startling number of ways; we are just beginning to understand the implications and complexity of mechanisms such as RNA splicing, small RNA mediated gene silencing, and subcellular localization of mRNAs (reviewed in Moore, 2005; Sharp, 2009). Moreover, regulation of RNA plays a crucial role during early development. In the oocyte and embryo, maternally loaded mRNAs and proteins initiate and control many aspects of development. Perhaps most well studied is the role of mRNAs in the establishment of cell polarity.

Cell Polarity

Cell polarity must be established at many points during the development of multicellular organisms to initiate embryonic patterning and differentiation, and in somatic cells to determine cell identity and regulate cell motility (reviewed in St Johnston and Ahringer, 2010). During metazoan oogenesis and embryogenesis, symmetry must be broken to define the animal–vegetal and dorsal–ventral axes that inform the asymmetric body plan. One crucial method for initiating asymmetry is RNA localization, the enrichment of RNA in a subcellular region to spatially control protein expression. This mechanism has been repeatedly employed across many eukaryotic species to spatially and temporally control the expression of important patterning factors. A high-throughput in situ hybridization screen in *Drosophila* embryos revealed that up to 70% of endogenous transcripts exhibit subcellular localization (Lecuyer et al., 2007), suggesting that RNA localization may play a broad role in controlling gene expression during early development.

Detailed characterization of localized transcripts within a multitude of invertebrate and vertebrate organisms has revealed conserved mechanisms of RNA localization (reviewed in Holt and Bullock, 2009; Martin and Ephrussi, 2009; Singer, 2008). A theme has emerged in which RNA binding proteins initially recognize cis-acting motifs, usually in the 3' UTR of localized transcripts, to form a core mRNP in the nucleus. After nuclear export, additional factors are recruited to direct cytoplasmic fate, including translational repressors and often

molecular motors, which actively transport translationally silenced mRNPs to a subcellular compartment using the cytoskeletal network. Finally, RNPs are released from their translationally silent state, and localized translation initiates to generate polarized gene expression.

Mechanisms of RNA Localization

Several mechanisms for generating localized RNA in the cell have been defined (reviewed in Bashirullah et al., 1998; Lipshitz and Smibert, 2000; Martin and Ephrussi, 2009; St Johnston, 2005). I will discuss the three main mechanisms of RNA localization below.

Local Protection from Degradation

In this mechanism, RNA is degraded or translationally repressed everywhere except the correct region of localization (Figure 1A). One example is *nanos* mRNA, which is required for posterior embryonic patterning of the *Drosophila* embryo (Lehmann and Nusslein-Volhard, 1991). While it was initially thought that expression of Nanos at the posterior pole was due to prior localization of the mRNA (Gavis and Lehmann, 1994), it was later shown that only 4% of *nanos* mRNA is localized in the egg (Bergsten and Gavis, 1999). Later during embryogenesis, this pool of *nanos* mRNA at the posterior pole is stabilized, while transcripts in the bulk cytoplasm are actively removed by Smaug- mediated deadenylation and degradation (Bashirullah et al., 1999; Zaessinger et al., 2006).

Restriction of *nanos* mRNA to the posterior pole is controlled by selective protection of the transcript from degradation in this region.

Diffusion and Entrapment

A second mechanism involves random diffusion of RNA thoughout the cytoplasm while anchoring machinery traps transcripts selectively at the destination (Figure 1B). One example is the *Xcat2* mRNA, which functions in germ plasm specification (MacArthur et al., 1999). *Xcat2* mRNA localizes during early *Xenopus* oogenesis to a structure termed the mitochondrial cloud (Zhou and King, 1996a). *Xcat2* mRNA localizes even in the presence of drugs that disrupt microtubules (Zhou and King, 1996a). This suggests that it localizes independently of molecular motors, which track on the cytoskeleton. Further analysis of *Xcat2* mRNA localization using live imaging approaches demonstrated that *Xcat2* mRNA in the cytoplasm moves at rates consistent with diffusion, until being immobilized upon reaching the mitochondrial cloud (Chang et al., 2004). *Xcat2* mRNA localizes by diffusing through the cytoplasm until capture and enrichment at the mitochondrial cloud.

Active Transport

While these examples support mechanisms of RNA localization without active transport, the most well studied mechanism for localizing RNA is through motor-driven RNA transport (Figure 1C) (reviewed in St Johnston, 2005; Tekotte and Davis, 2002).

Molecular Motors

Members of all three families of molecular motors have been shown to transport RNA in systems as diverse as yeast, flies and mammals. In most cases, molecular motors are thought to join the RNA complex via adapter proteins, and carry out transport along the cytoskeleton in a directed manner, delivering RNA to a specific destination. I will focus on previously defined roles for the ATP-dependent molecular motors myosin, kinesin, and dynein in transport of mRNA in both invertebrate and vertebrate organisms.

Myosin

The myosin molecular motor superfamily represents a diverse set of genes containing 20 structurally and functionally distinct classes (reviewed in Krendel and Mooseker, 2005). Myosin motors operate on the actin microfilament cytoskeleton. Myosin motors are best known to control muscle contraction (reviewed in Adelstein and Eisenberg, 1980). More recently, essential non-muscle functions for myosin have been described in cell adhesion, cell motility, signal transduction and cargo transport (reviewed in Bridgman, 2009; Vicente-Manzanares et al., 2009). Most myosin motors contain an N-terminal motor domain used for actin binding and ATP hydrolysis, a neck domain required for light chain attachment, and a C-terminal tail domain for cargo binding (Figure 2A) (reviewed in Rayment and Holden, 1994).

Myosin is required for transport of mRNAs in the budding yeast *Saccharomyces cerevisiae*. One such mRNA, *ASH1* mRNA, has arguably the best-understood mechanism of mRNA localization. Ash1p is a transcription factor that represses mating type switching in the daughter cell (but not the mother) by blocking expression of HO endonuclease (reviewed in Gonsalvez et al., 2005). Polarized expression of Ash1p is restricted to the daughter cell of the budding yeast by active localization of *ASH1* mRNA (Long et al., 1997). An RNA-binding protein, She2p, recognizes *ASH1* mRNA from the milieu of other RNAs through elements in the *ASH1* 3' UTR, and recruits Myo4p, a class V myosin motor, via the adapter protein She3p (Bohl et al., 2000; Jansen et al., 1996; Long et al., 2000; Long et al., 1997). This complex of *ASH1* mRNA/She2p/She3p/Myo4p transports on the actin cytoskeletal network to the daughter cell (reviewed in Gonsalvez et al., 2005).

Myosin is also involved in transport of mRNAs in vertebrate cells. Motile fibroblasts must constantly polymerize new actin filaments at the leading edge of the cell for movement, and localization of β-actin RNA is required for this process (Condeelis and Singer, 2005; Kislauskis et al., 1997; Lawrence and Singer, 1986). β-actin RNA transport is dependent on the actin cytoskeleton and myosin motors (Latham et al., 2001; Sundell and Singer, 1991). It is interesting to note that not only β-actin RNA is localized to the leading edge, but also RNAs that encode a complex involved in actin polymerization and branching (Mingle et al., 2005). These data support a model in which local translation of actin and growth

of new cytoskeleton at the leading edge is regulated by localization of RNA by myosin motors.

Kinesin

The kinesin superfamily spans diverse classes of molecular motors, which transport cargo such as organelles, proteins and mRNAs on the intracellular microtubule network of many eukaryotic cells (reviewed in Hirokawa et al., 2009; Vale, 2003). Most well studied are the N-kinesins, which are plus end directed motors. Much variation can be seen in component organization within the N-kinesin family, but they all contain a kinesin motor domain and a structurally important coiled coil domain (reviewed in Hirokawa et al., 2009). This family is most clearly exemplified by kinesin-1 (Vale et al., 1985). Kinesin-1 (Figure 2B) is a heterotetrameric protein complex consisting of two identical kinesin heavy chains (KHC) and two kinesin light chains (KLC). The KHC homodimer is responsible for binding microtubules and hydrolyzing ATP, while the KLC homodimer appears to work with KHC to bind cargo (Hirokawa et al., 1989). A second N-kinesin relevant to this thesis, Kinesin-2, also transports cargo to the plus ends of microtubules, but has a quite distinct structure. Kinesin-2 (Figure 2C) is a heterotrimeric protein complex: two motor subunits, termed Klp3a and Klp3b, and a cargo adapting protein, the kinesin adapting protein (KAP) (De Marco et al., 2001).

Kinesin molecular motors are involved in RNA localization in several systems. Localization of *oskar* mRNA in the *Drosophila* oocyte defines the posterior pole and segregates germ plasm for future generation of germ cells (Cha et al., 2002). Knocking out kinesin-1 specifically interfered with the accumulation of *oskar* mRNA at the posterior pole, suggesting that localization of *oskar* RNA requires kinesin-1 (Brendza et al., 2000). However, it has been shown that kinesin light chain is dispensible for kinesin-1 dependent transport of *oskar* mRNA (Palacios and St Johnston, 2002), suggesting that a non-canonical kinesin- based transport mechanism may localize *oskar* mRNA. Kinesin could also localize *oskar* RNA indirectly; kinesin-1 is required for cytoplasmic flows which could mediate the accumulation of *oskar* mRNA at the posterior pole (Palacios and St Johnston, 2002), or *oskar* mRNA could be linked to an organelle localized by kinesin-1. The molecular mechanism by which kinesin-1 is recruited to target mRNAs for transport remains unknown (reviewed in St Johnston, 2005).

Kinesin-1 also appears to have a role in transport of RNAs in neurons. RNAs are transported to distant processes in neurons, both to the synapses of dendrites and down the axon (reviewed in Kiebler and Bassell, 2006; Sossin and DesGroseillers, 2006). System-wide approaches have characterized hundreds of transcripts that are localized in mammalian neurons (Eberwine et al., 2002; Poon et al., 2006; Suzuki et al., 2007). Local translation of RNA oculd allow neurons to quickly respond to chemical signals at the synapse, and may mediate synaptic plasticity (reviewed in Holt and Bullock, 2009; Wang et al., 2010).

Because these cytoplasmic extensions contain highly polarized microtubule networks, with the minus ends of microtubules at the cell body and plus ends at the cell periphery, Kinesin-1 is a clear candidate for transport of mRNAs and other cargos in an anteriograde fashion to the synapse. Evidence supporting a role for kinesin-1 in transport of RNAs came from biochemical purification and mass spectrometric analyses of kinesin complexes from mouse brain tissue, which revealed many RNA binding proteins and at least two RNAs (Kanai et al., 2004). Transport of these large RNA granules *in vivo* was perturbed by kinesin-1 gain-of-function and loss-of-function experiments, clearly demonstrating a role for kinesin in transport of RNA in neurons (Kanai et al., 2004). Similar dominant negative experiments show a role for kinesin-1 in *shank1* mRNA transport in rat neurons (Falley et al., 2009). Although abundant evidence suggests a link between RNA localization, spatially restricted translation and synaptic plasticity, the underlying molecular mechanisms are only beginning to be elucidated (Wang et al., 2009; Wang et al., 2010).

Studies in the *Xenopus* oocyte have revealed a direct role for kinesin molecular motors in RNA localization. Kinesin-1 and kinesin-2 are members of the Vg1 mRNP and are required for vegetal RNA localization (Betley et al., 2004; Messitt et al., 2008; Yoon and Mowry, 2004; Chapter 2). Interestingly, disruption of either kinesin-1 or kinesin-2 interferes with Vg1 localization, indicating that both motors are involved in transport of Vg1 (Messitt et al., 2008; Chapter 2). Co-immunoprecipitation experiments demonstrated that kinesin-1 and kinesin-2

interact *in vivo* in an RNA-dependent fashion, suggesting that both motors are simultaneously bound to the Vg1 RNP. Why both kinesin motors are involved remains unclear. Cross-rescue experiments in which kinesin-1 overexpression can rescue a kinesin-2 dominant negative phenotype (and vice versa) suggest that kinesin motors are limiting for Vg1 localization (Messitt et al., 2008; Chapter 2). It has been hypothesized that the *Xenopus* homolog of Staufen (XStau) recruits kinesin-1 to the Vg1 mRNP in the cytoplasm, where it associates with microtubules to direct transport to the vegetal pole (Messitt et al., 2008; Yoon and Mowry, 2004; Chapter 2).

Dynein

In contrast to the diverse myosin and kinesin gene families, the dynein family of molecular motors contains only two classes, the axonemal dyneins and cytoplasmic dynein. Axonemal dyneins are solely involved in coordinating the beating of flagella and cilia, leaving the cytoplasmic dynein motor responsible for all transport of cargos to the minus end of microtubules and several mitotic functions (reviewed in Karki and Holzbaur, 1999). Cytoplasmic dynein (Figure 2D) is a multi-protein complex that consists of a catalytic homodimeric heavy chain and many non-catalytic subunits, which appear to be dispensible for dynein mobility but may function to adapt different cargos and regulate dynein function (reviewed in Kardon and Vale, 2009). Distinct from the dynein complex is the cargo adapter complex dynactin (Figure 2E). Dynactin was first identified as an activator of dynein dependent transport of cargos (Gill et al., 1991), and is now

known to be required for almost all cellular functions of dynein (reviewed in Schroer, 2004). Dynactin is a protein complex of at least eleven subunits, and targets dynein to subcellular locations, affects dynein processivity and adapts dynein to cargo (reviewed in Schroer, 2004). It may also be involved in coordinating transport of cargos bound by both kinesin and dynein molecular motors (see below). Several additional co-factor complexes are required for dynein function during cytokinesis and organelle transport (reviewed in Kardon and Vale, 2009).

Dynein transports localized mRNAs in *Drosophila* oocytes and embryos. Localization of the *bicoid* mRNA during oogenesis produces a morphogen gradient of Bicoid protein that patterns the anterior-posterior axis of the developing *Drosophila* embryo (Berleth et al., 1988; Driever and Nusslein-Volhard, 1988). Disruption of dynein-cargo interactions interferes with *bicoid* mRNA localization to the dorsoanterior pole of the oocyte, suggesting a role for dynein in transport (Duncan and Warrior, 2002; Januschke et al., 2002). Tracking *bicoid* RNA transport in live oocytes further defined a role for dynein in continually transporting *bicoid* mRNA. Disruption of dynein function results in the delocalization of *bicoid* mRNA, suggesting that dynein continuously maintains localization to the anterior pole (Weil et al., 2006). Recent high resolution electron microscopy studies confirmed an association between dynein and *bicoid* RNA (Weil et al., 2010). Taken together, these data strongly support a role for

dynein in transporting *bicoid* mRNA to the minus ends of microtubules in the *Drosophila* oocyte.

Dynein is also responsible for transport of the pair-rule and *wingless* mRNAs to the apical cytoplasm of *Drosophila* embryos, and localized expression of these factors is responsible for coordinating segmentation (Bullock and Ish-Horowicz, 2001; Bullock et al., 2004; Wilkie and Davis, 2001). Dynein associates with these transcripts via the adapter proteins BicaudalD (BicD) and Egalitarian (Egl) (Bullock and Ish-Horowicz, 2001). Recent elegant work has clarified the molecular mechanism, demonstrating that Egl directly binds localized mRNAs, and recruits the dynein transport complex via a direct interaction with BicD (Dienstbier et al., 2009). This represents one of the few molecular mechanisms in which factors have been identified that specifically recognize a localized mRNA and attach it to a molecular motor for transport.

Motor Coordination

The majority of cargos are transported bidirectionally in cells. In fact, even some localized RNAs appear to exhibit only a slight bias in directionality during transport (Zimyanin et al., 2008). How bidirectional transport, presumably controlled by differential motor activity, is coordinated during transport of cargos remains poorly understood. Some evidence hints that dynactin may be able to bridge interactions between dynein and kinesin motors. Dynactin can interact with kinesin-2 and appears to increase processivity of kinesin-2 through

microtubule binding (Berezuk and Schroer, 2007; Deacon et al., 2003). An interaction between dynactin and kinesin-5 has also been reported, though it is unclear whether this represents motor coordination or merely transport of kinesin-5 by dynein (Blangy et al., 1997; Uteng et al., 2008). Dynein and kinesin activities appear to be tightly coupled, as disruption of either motor tends to decrease transport in both directions (Ally et al., 2009; Deacon et al., 2003; Ling et al., 2004; Martin et al., 1999; Uchida et al., 2009; Waterman-Storer et al., 1997). One model of vesicular trafficking proposes that a dual-motor complex is formed, and both motors must be present for the transport complex to function, and the motors alternate in activity (Gross et al., 2007; Welte, 2004). An alternate hypothesis argues that a stoichiometric ratio of bound motors dictates directionality in a "tug of war" mechanism (Hendricks et al., 2010; Holzbaur and Goldman, 2010).

RNA Anchoring

After transport, localized RNAs must be maintained at their final destination to ensure polarized expression. One mechanism for maintenance is anchoring, whereby RNAs transition from active transport to static particles bound at the destination. RNA anchoring has been observed in many systems, but remains poorly understood.

Anchoring of *ASH1* mRNA appears to involve multiple factors in the bud tip. The C terminal peptide of Ash1p is required for anchoring *ASH1* mRNA, suggesting

that translation of Ash1p produces an anchor for future transcripts (Gonzalez et al., 1999). Also, knocking out several genes causes defects ascribed to loss of *ASH1* mRNA anchoring (Beach et al., 1999; Frey et al., 2001; Gonsalvez et al., 2005; Irie et al., 2002; Tadauchi et al., 2001), though it remains unclear whether these factors play a direct role in anchoring or have an indirect effect due to roles in translational control or maintainance of the actin cytoskeletal network. There appears to be a strong mechanistic link between translational repression and anchoring of *ASH1* mRNA (reviewed in Gonsalvez et al., 2005).

Anchoring of pair-rule transcripts in the *Drosophila* embryo requires microtubules but not actin, and involves a novel transition in dynein activity from RNA transport to static anchor (Delanoue and Davis, 2005). In this situation, dynein mediates transport of *ftz* mRNA, and then transitions to a very different role as a static anchor, in which ATPase activity and the co-factors BicD and Egl, all required for mRNA transport, are now dispensible for its function as an anchor (Delanoue and Davis, 2005). An analogous situation has been observed for *gurken* localization in *Drosophila* oocytes (Delanoue et al., 2007). Interestingly, the myosin motor plays a role in anchoring *oskar* mRNA at the posterior pole. Oocytes with null mutations in the myosin-V motor fail to accumulate *oskar* mRNA in a tight cresent; instead, *oskar* mRNA often remains near but not tightly associated with the posterior cortex (Krauss et al., 2009), suggesting a role for myosin-V in mediating anchoring *oskar* mRNA at the cortex. These data together support novel functions for molecular motors in RNA anchoring.

Vg1 mRNA is anchored at the vegetal cortex of the *Xenopus* oocyte through a mechanism that requires actin, cytokeratin, and microtubule networks (Alarcon and Elinson, 2001; Yisraeli et al., 1990). A family of non-coding RNAs is localized to the vegetal cortex before Vg1 (Zearfoss et al., 2003); antisense oligo-mediated interference with one of these, *Xlsirt*, releases previously localized Vg1 mRNA from the cortex, suggesting a role in anchoring (Kloc and Etkin, 1994). One model proposes that *Xlsirt* mediates interactions between Vg1 mRNA and the cytoskeleton (Kloc and Etkin, 1994; Kloc et al., 2005). Prrp, an RNA binding protein that binds to Vg1 RNA, has been proposed to be involved in anchoring as it can interact with actin binding proteins (Zhao et al., 2001), though its role in the mechanism of RNA anchoring is unproven. Although several factors have been implicated in anchoring of Vg1 mRNA, the underlying mechanisms remain entirely unknown.

Cytoskeletal Polarity

The cytoplasm of most eukaryotic cells contains a complex network of actin filaments, microtubules and intermediate filaments known collectively as the cytoskeleton. Beyond simply functioning as the structural component of the cell, the cytoskeleton is responsible for spatial organization of the nucleus, organelles, vesicles and various proteins and RNAs. Substantial evidence shows that the cytoskeleton also plays an active role in mediating intracellular signaling and translation (reviewed in Kim and Coulombe, 2010).

Polarity of the cytoskeleton can be crucial for RNA localization. Polarity of active RNA transport can be achieved if molecular motors are able to navigate a complex cytoskeletal network towards a destination. The organization of actin polymers and microtubules has proven critical to this process. For example, transport of *ASH1* mRNA by myosin motors is dependent on actin (Long et al., 1997), and mutants that interfere actin organization affect *ASH1* mRNA localization (Aronov and Gerst, 2004; Takizawa et al., 1997).

The reorganization of the microtubule network can have an obvious impact on RNA localization. For example, during stages 7-10 of *Drosophila* oogenesis, microtubules are polarized with minus ends at the anterior and plus ends at the posterior (Clark et al., 1994). This results in dynein-dependent transport of *gurken* RNA to the anterior pole (MacDougall et al., 2003). A distinct network of microtubules associated with the oocyte nucleus then mediates the second step of *gurken* mRNA localization, during which dynein directs *gurken* mRNA to the dorso-anterior pole of the oocyte (MacDougall et al., 2003). Thus, the *gurken* RNA localization complex localizes in a multi-step process dependent on discrete and polarized microtubule arrays that emerge during development.

Vg1 RNA also localizes in a transport pathway dependent on oocyte microtubule polarity. Initial reports implicating plus-end directed kinesin motors as responsible for transport of Vg1 mRNA (Betley et al., 2004; Yoon and Mowry,

2004) were met with some skepticism because of the previously published orientation of microtubules with minus ends at the vegetal cortex of oocytes (Pfeiffer and Gard, 1999). It was unclear how Vg1 mRNA would be transported to the cortex by kinesin motors. Closer examination of microtubule polarity using a marker for plus ends confirmed this orientation in early stage oocytes, when endogenous Vg1 mRNA is unlocalized, but defined a subpopulation of microtubule plus ends that emerged at the vegetal cortex coincident with Vg1 mRNA localization (Messitt et al., 2008; Chapter 2). The establishment of this subpopulation of microtubules could trigger the localization of Vg1 mRNA by kinesin-1 and/or kinesin-2. Developmentally timed reorganization of the cytoskeleton can play an active role in spatial and temporal control of RNA transport.

RNA Localization in *Xenopus* Oocytes

Studies of the frog *Xenopus laevis* have begun to elucidate some of the mechanisms that govern RNA localization. The large size and easy availability of oocytes has uniquely enabled biochemical approaches that have defined many of the cis-elements and trans-factors that mediate mRNA transport in a physiologically relevant context. The development of numerous *in vivo* imaging approaches has supplemented this work by adding spatial and temporal dimensions to our understanding (Chang et al., 2004; Cote et al., 1999; Deshler et al., 1997; Gagnon and Mowry, 2009, 2010; Havin et al., 1998; Kress et al.,

2004; Lewis et al., 2008; Mowry and Melton, 1992; Yisraeli and Melton, 1988; Yoon and Mowry, 2004).

A number of mRNAs are localized during oogenesis through several distinct mechanisms. The so-called "early" pathway localizes RNAs to the mitochondrial cloud in stage I oocytes by a diffusion and entrapment mechanism (Chang et al., 2004). After mitochondrial cloud breakdown, these RNAs remain associated with the vegetal cortex and play essential roles in germ cell development (reviewed in King et al., 2005). The "late" pathway of vegetal RNA localization operates during stages III and IV of oogenesis, when mRNAs involved in germ layer specification are localized to the vegetal pole using an active transport mechanism that requires microtubules, actin and kinesin molecular motors (Birsoy et al., 2006; Messitt et al., 2008; Yisraeli et al., 1990; Zhang et al., 1998). Several RNAs are also localized to the animal pole of the oocyte; however, their localization is poorly understood and may not be required for appropriate development (reviewed in King et al., 2005).

Vg1 mRNA Localization

Vg1 mRNA encodes a member of the TGF-β superfamily of secreted growth factors, and plays an essential role in mesoderm and endodermal patterning in the *Xenopus* embryo (Birsoy et al., 2006; Weeks and Melton, 1987). Vg1 mRNA utilizes the late pathway to localize to the vegetal pole of *Xenopus* oocytes during oogenesis (Figure 3), resulting in expression of Vg1 protein in vegetal

blastomeres (reviewed in King et al., 2005). Mis-expression of Vg1 in the animal hemisphere induces ectopic mesoderm and a second organizing center, abrogating further development and highlighting the importance of spatially controlled Vg1 expression (Birsoy et al., 2006; Dale et al., 1993; Thomsen and Melton, 1993).

Vg1 mRNA is recognized in the nucleus by at least two RNA binding proteins, hnRNP I/PTB and Vg1RBP/Vera (Cote et al., 1999; Czaplinski et al., 2005; Deshler et al., 1997; Kress et al., 2004; Mowry, 1996). After nuclear export, the complex is remodeled to promote its fate in the cytoplasm (Lewis et al., 2008). Staufen, another RNA binding protein, joins the complex and may mediate interactions with molecular motors and other cytoplasmic factors (Yoon and Mowry, 2004). Additional factors have been hypothesized to join the complex to mediate translational repression during transport and anchoring at the vegetal cortex (Colegrove-Otero et al., 2005; Zhao et al., 2001). Distinct cis- elements that mediate both localization and translational repression of Vg1 RNA have been identified and dissected, including a 340 nucleotide sequence in the 3' UTR sufficient for vegetal localization (VLE, Vegetal Localization Element, Figure 3) (Gautreau et al., 1997; Lewis et al., 2004; Mowry and Melton, 1992; Otero et al., 2001). Vg1 mRNA localization requires the microtubule cytoskeleton for transport (Yisraeli et al., 1990), suggesting involvement of molecular motors. Recently, we and others have demonstrated roles for kinesin-1 and kinesin-2 in transport of Vg1 (Betley et al., 2004; Messitt et al., 2008; Chapter 2). Kinesin-1

and kinesin-2 appear to operate cooperatively to transport Vg1 mRNA and a subpopulation of microtubule plus ends emerges at the vegetal pole during early oogenesis that may promote kinesin- dependent transport of Vg1 mRNA to the vegetal cortex (Messitt et al., 2008; Chapter 2). After transport, Vg1 mRNA is anchored at the vegetal cortex after transport, dependent on a non-coding RNA and the actin cytoskeleton (Kloc and Etkin, 1994; Yisraeli et al., 1990).

Open Questions About Vg1 RNA Localization

Although much is known about Vg1 mRNA localization, significant gaps remain in our mechanistic understanding. Disruption of kinesin function using a mutant that locks kinesin at the region of cargo binding has defined a region of the lower vegetal cytoplasm in which Vg1 mRNA transport is kinesin dependent (Messitt et al., 2008; Chapter 2). How Vg1 reaches this region is unclear. Perhaps it requires the function of another molecular motor, or other undefined machinery for accumulation at the midpoint of the vegetal cytoplasm. Additionally, no information on rates of RNA transport or directionality can be determined for localized or unlocalized RNAs from static imaging approaches. The absence of a live cell imaging system has hindered our understanding of these critical issues. The development of such a system is necessary to address important questions about the mechanisms of Vg1 mRNA transport in different regions of the oocyte. We recently uncovered a subpopulation of microtubules in the lower vegetal cytoplasm with opposite orientation to the bulk cytoplasm microtubules (Messitt et al., 2008; Chapter 2). The orientation of microtubules in the vegetal cytoplasm

allows us to make predictions about the directionality of motor driven RNA transport in distinct regions of the vegetal cytoplasm. Specifically, we predict unidirectional transport in the upper vegetal cytoplasm, and bidirectional transport in the lower vegetal cytoplasm in the presence of mixed polarity microtubules. It is these issues that I will address in this thesis. The research herein substantially adds to our understanding of the mechanisms of motor-driven directional RNA transport in the *Xenopus* oocyte.

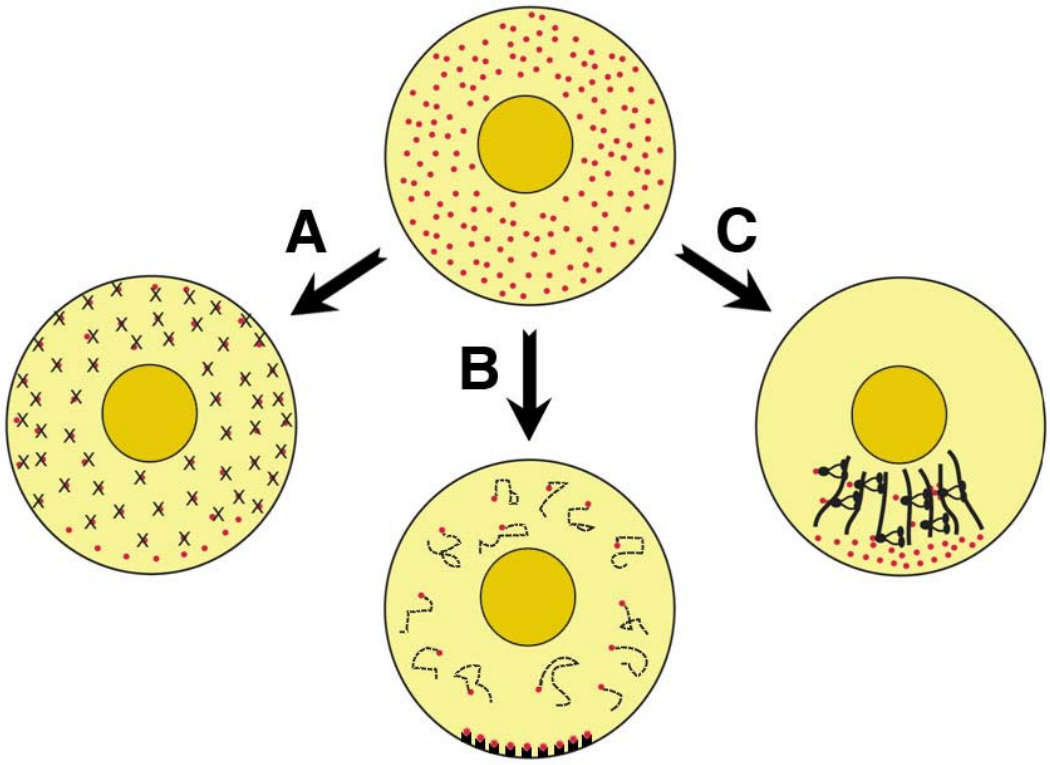

Figure 1. *Mechanisms of RNA Localization.* (A) Local protection from degradation. RNAs distributed uniformly achieve localization through protection from degradation at a subcellular localization. (B) Diffusion and entrapment. RNAs diffuse throughout the cytoplasm, and accumulate through capture at the destination. (C) Active transport. RNAs are moved on the cytoskeleton by molecular motors to their final destination.

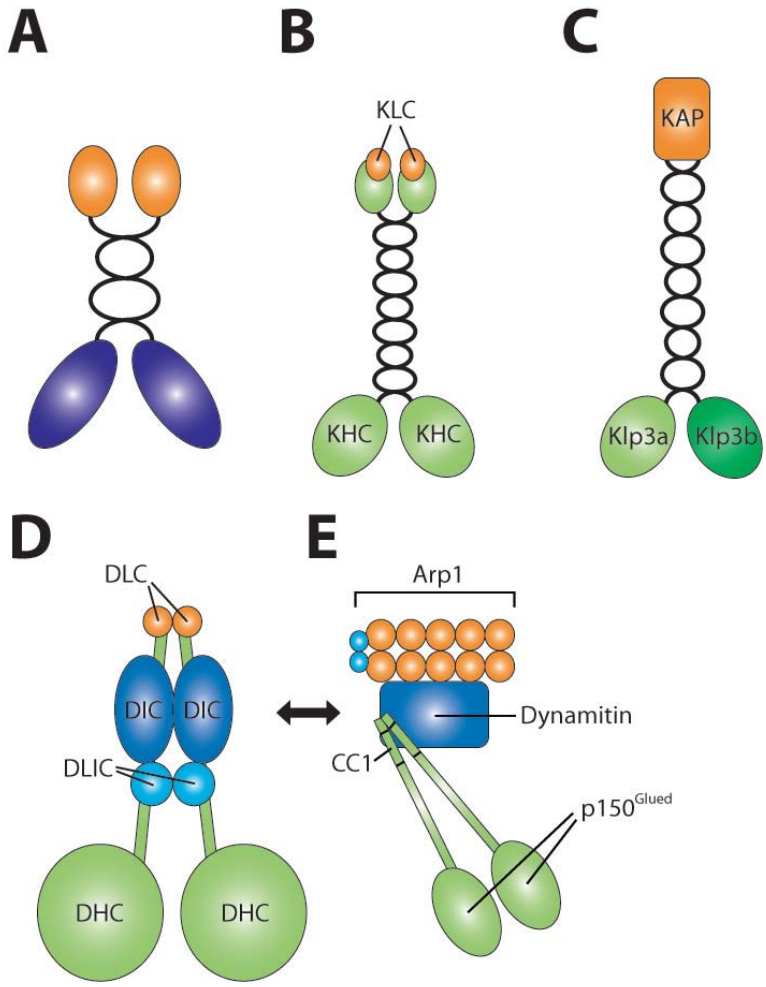

Figure 2. *Molecular Motors.* Cargo domains are labeled in orange, microtubule binding domains in green, and actin binding domains in purple. Some subunits have been omitted for clarity. (A) Dimeric myosin-V. (B) Heterotetrameric kinesin-1. Kinesin Heavy Chains (KHC) and Kinesin Light Chains (KLC) are indicated. (C) Heterotrimeric kinesin-2. Klp3a, Klp3b and Kinesin Associated Protein (KAP) are indicated. (D) Multi subunit cytoplasmic dynein. Dynein Heavy Chains (DHC), Dynein Light Intermediate Chains (DLIC), Dynein Intermediate Chains (DIC) and Dynein Light Chains (DLC) are indicated. (E) The multi subunit dynactin complex. $p150^{Glued}$, the Coiled Coil 1 domain of $p150^{Glued}$ (CC1), dynamitin and Arp1 subunits are indicated.

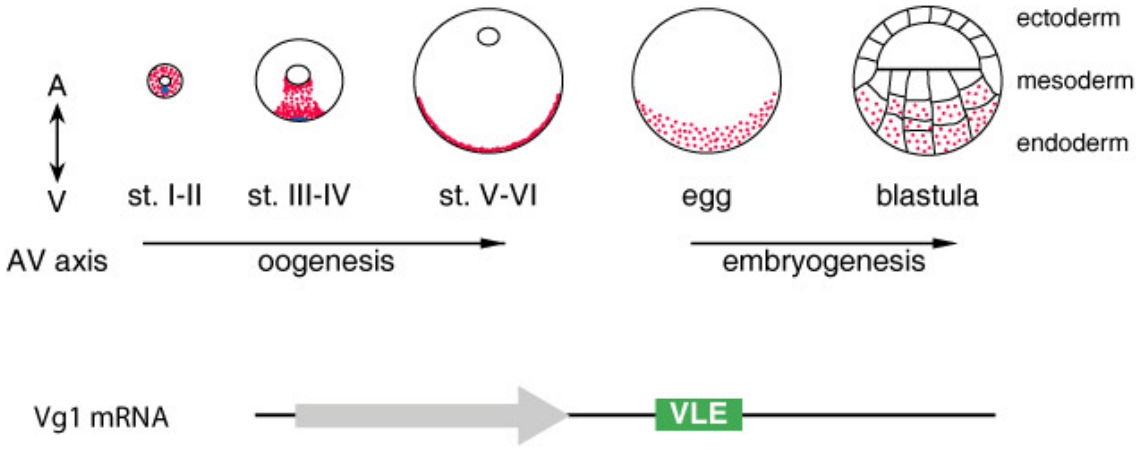

Figure 3. *Vg1 RNA Localization During Oogenesis.* At the beginning of oogenesis (stages I-II), Vg1 mRNA (red dots) is distributed uniformly throughout the oocyte. During mid-oogenesis (stages III-IV), Vg1 mRNA becomes restricted to the vegetal cytoplasm, and by the end of oogenesis (stages V-VI), Vg1 mRNA is tightly anchored at the vegetal cortex. After fertilization, Vg1 mRNA is inherited by only the vegetal-most blastomeres, where its translated protein can direct endodermal and mesodermal fates during embryogenesis. The mitochondrial cloud (blue) is present in the vegetal cytoplasm during early oogenesis, is deposited at the vegetal cortex by stage II of oogenesis. The Vg1 mRNA is diagrammed below, with the Vg1 Localization Element (VLE) indicated in green within the 3' UTR.

Chapter 2: Multiple Kinesin Motors Coordinate Cytoplasmic RNA Transport on a Sub-population of Microtubules in *Xenopus* Oocytes

Timothy J. Messitt, **James A. Gagnon**, Jill A. Kreiling, Catherine A. Pratt, Young J. Yoon and Kimberly L. Mowry: *I contributed to Figure 2.4 and Supplemental Figures 2.S4, 2.S5, S.S7.*

Multiple kinesin motors coordinate cytoplasmic RNA transport on a subpopulation of microtubules in *Xenopus* oocytes.

Messitt TJ, Gagnon JA, Kreiling JA, Pratt CA, Yoon YJ, Mowry KL.

Dev Cell. 2008 Sep;15(3):426-36.

Abstract

RNA localization is a widely conserved mechanism for generating cellular asymmetry. In *Xenopus* oocytes, microtubule-dependent transport of RNAs to the vegetal cortex underlies germ layer patterning. Although kinesin motors have been implicated in this process, the apparent polarity of the microtubule cytoskeleton has pointed instead to roles for minus end-directed motors. To resolve this issue, we have analyzed participation of kinesin motors in vegetal RNA transport and identified a direct role for *Xenopus* kinesin-1. Moreover, *in vivo* interference and biochemical experiments reveal a key function for multiple motors, specifically kinesin-1 and kinesin-2, and suggest that these motors may interact during transport. Critically, we have discovered a sub-population of microtubules with plus ends at the vegetal cortex, supporting roles for these kinesin motors in vegetal RNA transport. These results provide a new mechanistic basis for understanding directed RNA transport within the cytoplasm.

Introduction

Localization of mRNAs within cells is a powerful mechanism for generating cell and developmental polarity (reviewed in Du et al., 2007). In somatic cells, localized mRNAs can influence both cell motility and morphology, as exemplified by localization of β-actin RNA in fibroblasts (reviewed in Condeelis and Singer, 2005). In many organisms, localization of maternal mRNAs in eggs and oocytes provides the basis for embryonic patterning. For example, in *Drosophila melanogaster*, localized mRNAs are necessary for anterior-posterior and dorsal-ventral patterning of the oocyte and developing embryo (reviewed in Minakhina and Steward, 2005). Among vertebrates, Vg1 mRNA is a prominent example of a localized maternal mRNA that plays a role in embryonic patterning (reviewed in King et al., 2005). Vg1 mRNA, which encodes a member of the TGF-β family of growth factors (Weeks and Melton, 1987), is localized to the vegetal hemisphere in oocytes of the frog, *Xenopus laevis*. Spatially appropriate expression of Vg1 is necessary for proper mesoderm and endoderm specification during embryonic development (Birsoy et al., 2006; Dale et al., 1993; Thomsen and Melton, 1993), and transport of Vg1 mRNA to the vegetal hemisphere during oogenesis initiates this process. However, mechanistic insight into the transport process itself is lacking.

Localization of Vg1 mRNA occurs during mid-oogenesis, and relies on a 340-nucleotide element in the 3′ UTR of Vg1 mRNA termed the Vg1 Localization Element (VLE) (Mowry and Melton, 1992). The VLE is sufficient to direct vegetal

RNA localization and associates with specific proteins to form a vegetal ribonucleoprotein (RNP) complex (Cote et al., 1999; Czaplinski and Mattaj, 2006; Deshler et al., 1998; Havin et al., 1998; Kress et al., 2004; Mowry, 1996; Yoon and Mowry, 2004). Notably, one component of the Vg1 RNP, *Xenopus* Staufen, has been shown to interact with the molecular motor kinesin-1 (Yoon and Mowry, 2004). An active transport mechanism for Vg1 mRNA localization was first suggested by pharmacological experiments in which depolymerization of the microtubule cytoskeleton abolished Vg1 localization (Yisraeli et al., 1990). More recently, vegetal localization of Vg1 mRNA was shown to be disrupted by blocking the function of another molecular motor, kinesin-2 (Betley et al., 2004). It is not yet clear whether either of these kinesin motors function directly in vegetal RNA transport.

The kinesins are a large superfamily of motor proteins containing 14 classes (reviewed in Miki et al., 2005). The founding member of the kinesin superfamily, conventional kinesin, or kinesin-1, consists of two identical heavy chains, containing the motor domain responsible for ATP hydrolysis and microtubule binding, and two identical light chains, necessary for cargo binding (Diefenbach et al., 1998; Yang et al., 1989). By contrast, kinesin-2 is a heterotrimeric motor protein, containing two non-identical motor subunits and a single non-motor accessory protein (Cole et al., 1993; Wedaman et al., 1996).

Kinesin function has been implicated in RNA transport in diverse systems, from oocytes to neurons (reviewed in Bullock, 2007; Hirokawa, 2006). For kinesin-1, specific examples include transport of CaMKIIα, Arc, and Tau RNAs in mammalian neurons (Aronov et al., 2002; Kanai et al., 2004; Ohashi et al., 2002), localization of myelin basic protein mRNA in oligodendrocytes (Carson et al., 1997), and transport of oskar mRNA in the *Drosophila* oocyte (Brendza et al., 2000). However, direct roles for kinesin motors are, in many cases, still unclear. In the *Drosophila* oocyte for example, kinesin has been suggested to play an indirect role through regulating cytoplasmic flows or exclusion of RNA from the oocyte cortex (Cha et al., 2002; Glotzer et al., 1997; Palacios and St Johnston, 2002). In addition, kinesin could act in RNA localization through interactions with other motor proteins (Duncan and Warrior, 2002; Januschke et al., 2002; Mische et al., 2007).

Microtubules in the *Xenopus* oocyte are largely oriented with their minus ends towards the cell periphery (Pfeiffer and Gard, 1999). Thus, the oocyte cortex is rich in minus ends, and roles for minus end-directed motors in vegetal RNA transport have been postulated (Kloc and Etkin, 2005; Palacios, 2007; St Johnston, 2005). Both kinesin-1 and kinesin-2 are plus end-directed motors (reviewed in Vale, 2003), complicating models for vegetal RNA transport that rely on direct participation by such motors.

We have investigated the function of kinesin motors in vegetal RNA transport in the *Xenopus* oocyte. We show that kinesin-1 interacts with VLE RNA *in vivo* and *in vitro*, and that interfering with kinesin-1 function *in vivo* blocks VLE RNA localization, suggesting a direct role for kinesin-1 in vegetal RNA localization. Our results also demonstrate that kinesin-1 interacts with kinesin-2 and that these motors carry out overlapping functions in RNA transport. Moreover, using expression of specific kinesin-1 and kinesin-2 mutants we have uncovered a previously unidentified step in the vegetal RNA localization pathway. Finally, using markers for microtubule polarity we have discovered a population of microtubules with plus ends directed toward the vegetal cortex, providing new mechanistic insight into this motor-driven RNA transport process.

Results

Kinesin-1 Interacts with Localized RNA

Kinesin-1 is implicated in vegetal RNA transport in *Xenopus* oocytes by virtue of association with at least one critical component of a vegetally localized ribonucleoprotein (RNP) complex (Yoon and Mowry, 2004). As a test of a direct role for kinesin-1 in vegetal RNA transport, we asked if kinesin-1 associates with RNAs during transport (Fig. 2.1). We injected stage (st.) III oocytes with fluorescently labeled VLE RNA and cultured to allow localization. We then immunostained with SUK4 antibodies, which specifically recognize kinesin-1 heavy chain (KHC) in a variety of organisms, including *Xenopus* (Lane and Allan, 1999; Tuma et al., 1998; Wright et al., 1993). Confocal microscopy revealed that while kinesin-1 is located throughout the perinuclear region of the oocyte, the protein is largely absent from the outer ring of the cytoplasm and cortex (Fig. 2.1A). Only the vegetal cortical region of the oocyte shows enrichment of kinesin-1, precisely coincident with the localization of VLE RNA (Fig. 2.1A-B). Thus, endogenous kinesin-1 is colocalized with RNA undergoing localization *in vivo*.

We further tested the interaction of kinesin-1 with both injected VLE and endogenous Vg1 RNAs biochemically. VLE RNA was injected into st. III oocytes for localization *in vivo*. Control oocytes were injected with *Xenopus* β-globin RNA (XβM), which does not localize (Mowry and Melton, 1992). Immunoprecipitation with SUK4 antibodies from oocyte lysates captured complexes containing kinesin-1, and bound RNAs were detected by RT-PCR. Both Vg1 and VLE RNAs

are specifically immunoprecipitated with kinesin-1 (Figs. 2.1C, 2.1D; lanes 3); the interaction cannot be detected with non-relevant antibodies (lanes 2), or with unlocalized control RNAs, XβM (1C, lane 6) and EF1α (1D, lane 6). Taken together, these results indicate that kinesin-1 is associated with vegetally localized RNP complexes.

Xenopus Kinesin-1 is Necessary for Vegetal RNA Localization

To probe the functional relevance of the interaction between kinesin-1 and VLE RNA, we used *in vivo* interference. We again used SUK4 antibodies, which recognize the motor domain of KHC and effectively block kinesin-1 function (Ingold et al., 1988). We injected these antibodies into st. III oocytes, followed by injection of fluorescently labeled VLE RNA to determine the phenotypic effects of kinesin-1 inhibition on vegetal RNA localization (Fig. 2.2). Control oocytes were injected with either mouse IgG or SUK2 antibodies, which recognize kinesin-1 but do not block function (Wright et al., 1991). In control oocytes, RNA in the process of vegetal localization is evident by its enrichment in the vegetal cytoplasm, extending from the nucleus to the vegetal cortex (Fig. 2.2A,B). In the presence of kinesin-1 function-blocking antibodies (SUK4), however, vegetal localization is strongly impaired (Fig. 2.2C). Localization is observed in only 52% of SUK4-injected oocytes (Fig. 2.2D), as compared to control oocytes. These results suggest a necessary role for kinesin-1 in vegetal RNA localization.

As a further step towards testing the function of kinesin-1 in vegetal localization, we cloned the *Xenopus* kinesin-1 heavy chain (XKHC) from oocyte RNA. Sequence analysis of the XKHC cDNA (Fig. 2.S1) confirms XKHC as a member of the kinesin-1 family (Lawrence et al., 2004). *In vitro* translation of recombinant XKHC carrying a C-terminal FLAG epitope tag generates a protein that is detected by both SUK4 and FLAG antibodies (Figs. 2.S2, 2.S3D). When FLAG-tagged XKHC is expressed in st. III oocytes, immunofluorescence using anti-FLAG antibodies reveals an expression pattern that colocalizes with fluorescently labeled VLE RNA (Fig. 2.S3A). Thus, recombinant XKHC is appropriately expressed in the oocyte. We next used the cloned XKHC to interfere with kinesin-1 function *in vivo*.

Kinesin-1 function can be blocked by a rigor–type mutation, which causes the motor domain to bind tightly, but rarely detach from microtubules (Nakata and Hirokawa, 1995). A point mutation (threonine to isoleucine) in the motor domain of mouse KHC inhibits kinesin-1 function in mouse fibroblasts (Nakata and Hirokawa, 1995). We engineered a similar rigor XKHC point mutant designated XKHC-T92I for *in vivo* expression studies. To quantitate kinesin-1 rigor mutant effects on vegetal localization, we injected fluorescently labeled VLE RNA into st. III oocytes expressing either wild-type XKHC, XKHC-T92I, or control oocytes expressing no exogenous protein (Fig. 2.3). VLE RNA localization was assessed by confocal microscopy; oocytes scored as positive for localization exhibited accumulation of VLE RNA in the vegetal cytoplasm (Fig. 2.3A,B,D,E,F). Oocytes

expressing wild-type XKHC displayed normal localization as compared to control oocytes (Figs. 2.3A,B,F). By contrast, oocytes expressing the XKHC-T92I rigor mutant displayed a dramatic inhibition of VLE localization (Figs. 2.3C,F). To test the specificity of the inhibitory effect on VLE localization observed for the kinesin-1 rigor mutation, we engineered and expressed a rigor mutation in another plus end-directed kinesin motor, Eg5. *Xenopus* Eg5 was chosen as a control because it has an established rigor mutation equivalent to that of KHC (Blangy et al., 1998) and is expressed during mid-oogenesis (Houliston et al., 1994). As shown in Fig. 2.3, oocytes expressing either wild-type XEg5 (Fig. 2.3D) or the Eg5 rigor mutant, XEg5-T105N (Fig. 2.3E), at levels equal to XKHC and XKHC-T92I (Fig. 2.S3D), displayed no inhibition of vegetal localization (Fig. 2.3F). The results of this experiment indicate that the effect of the kinesin-1 rigor mutation on vegetal localization is specific and is not a general property of plus end-directed motors, providing further evidence that kinesin-1 is necessary for vegetal RNA transport.

An Intermediate Kinesin-1 Rigor Mutant Phenotype May Provide Mechanistic Insight into Kinesin-1 Function During Vegetal Localization

Although the majority of oocytes expressing the kinesin-1 rigor mutant displayed a complete inhibition of VLE localization, a significant fraction was scored as positive for localization (Fig. 2.3F). Many of these (30-40%) display an intermediate phenotype that is not observed with wild-type kinesin-1 or the Eg5 rigor mutant, and with a frequency that is directly correlated with higher concentrations of injected XKHC-T92I-encoding RNA (Fig. 2.S4A). Typically,

VLE RNA in the process of localization adopts an hourglass-like distribution within the vegetal cytoplasm, with RNA distributed from the vegetal side of the nucleus to the vegetal cortex (Fig. 2.4A). Rather than resembling an hourglass, however, oocytes with this intermediate phenotype resemble a half-hourglass with RNA accumulating only from the middle of the hourglass region to the cortex (Fig. 2.4B). The microtubule cytoskeleton shows no apparent disruption after expression of the XKHC-T92I rigor mutant (Fig. 2.S5), and one possible explanation for the observed RNA distribution is that the rigor mutants could disrupt transport in the upper vegetal cytoplasm. Alternatively, the phenotype could result from inhibition of transport within the lower vegetal cytoplasm due to rigor mutant motors locked onto microtubules while simultaneously bound to RNA transport cargoes. Indeed, the kinesin-1 rigor mutant is colocalized with the aberrantly localized RNA (Fig. 2.S3B).

To further investigate the nature of the kinesin-1 rigor intermediate phenotype, we carried out a temporal analysis of VLE RNA localization, comparing oocytes expressing either wild-type XKHC (Fig. 2.4C) or rigor-XKHC (Fig. 2.4D; XKHC-T92I). After injection of fluorescently-labeled VLE RNA, oocytes were harvested at 2, 4, 6 or 8 hrs., and vegetal RNA localization was analyzed by confocal microscopy. By 4 hrs., a distinct difference is apparent between oocytes expressing wild-type or kinesin-1-rigor. In oocytes expressing wild-type XKHC (Fig. 2.4C) VLE RNA accumulates near the germinal vesicle at 4 hrs., with little accumulation in the lower vegetal cytoplasm. By contrast, in oocytes expressing

kinesin-1 rigor mutant (Fig. 2.4D), RNA is present throughout the vegetal cytoplasm. By 6 hrs. RNA is present throughout the vegetal cytoplasm in control oocytes (Fig. 2.4C), but is restricted to the lower vegetal cytoplasm in oocytes expressing the kinesin-1 rigor mutant (Fig. 2.4D). These results indicate that movement from the upper vegetal cytoplasm is unaffected by the kinesin-1 rigor mutant, suggesting that this step does not rely on kinesin-1.

Our results revealing a role for kinesin-1 in vegetal RNA transport raise the question of whether kinesin-2, also a plus end-directed motor implicated in this process (Betley et al., 2004), might act to promote a step in the vegetal localization pathway that is distinct from that mediated by kinesin-1. Alternatively, these motors could act together to promote vegetal localization, or they could function redundantly. To address whether kinesin-1 and kinesin-2 act at distinct steps in vegetal RNA localization, we exploited the intermediate phenotype that we observed upon expression of the kinesin-1 rigor mutant (Fig. 2.4B). The bottom-half distribution may indicate a function for kinesin-1 in the vegetal-most region of the oocyte, specifically in the vegetal cytoplasm closest to the cortex, where VLE RNA accumulates in oocytes expressing XKHC-T92I (Fig. 2.4B). If kinesin-2 does not function within this region of the oocyte, we would not expect to obtain a bottom-half phenotype in the presence of a kinesin-2 rigor mutant. To test this, we constructed a kinesin-2 rigor mutation. *Xenopus* kinesin-2 is a heterotrimeric motor that contains two different motor subunits termed XKlp3a and XKlp3b (De Marco et al., 2001). We introduced a threonine-to-isoleucine

mutation into the ATP-binding site within the motor domain of XKlp3b (Le Bot et al., 1998) to generate a kinesin-2 rigor mutant, termed XKlp3b-T103I. Using our localization assay we directly compared the phenotypes of oocytes expressing equivalent rigor mutations. As shown in Fig. 2.4F, expression of XKlp3b-T103I, results in the same intermediate phenotype observed with XKHC-T92I (Fig. 2.4B) at similar levels (Fig. 2.S4B), and additive effects are observed when XKHC-T92I and XKlp3b-T103I are co-expressed (Fig. 2.4G). The intermediate phenotype is specific to kinesin-1 and kinesin-2 rigor mutants and is not observed in oocytes expressing either wild-type proteins (Fig. 2.S4B) or the Eg5 rigor mutant (data not shown). Moreover, both kinesin-1 and kinesin-2 rigor-mutant motors colocalize with VLE RNA in the lower vegetal cytoplasm (Fig. 2.S3B,C). These data suggest that kinesin-1 and kinesin-2 mediate RNA localization in the same region of the oocyte.

Kinesin-1 and Kinesin-2 May Coordinate Transport in the Oocyte

Functions for both kinesin-1 and kinesin-2 in the same region of the vegetal cytoplasm may indicate that these motor proteins either act redundantly or have overlapping functions. To test this we constructed a kinesin-1 mutant that lacks the motor domain, termed XKHCΔm. The XKHCΔm mutant is expected to interact with cargo but not microtubules (Berliner et al., 1995; Gelfand et al., 2001) and would thus exert a dominant negative effect by forming heterodimers with endogenous XKHC, thereby reducing levels of active kinesin-1 rather than by locking onto microtubules as with a rigor mutant. As shown in Figure 2.5A,

expression of XKHCΔm inhibits localization to a similar extent as XKHC-rigor (XKHC-T92I). However, in contrast to XKHC-rigor, inhibition of VLE localization by KHCΔm results in lack of detectable vegetal RNA accumulation; no intermediate phenotype is observed. Inhibition of vegetal localization upon reduction of kinesin-1 function with the XKHCΔm mutation indicates that endogenous levels of kinesin-2 are insufficient alone to support vegetal RNA localization, suggesting that function of these motors is not simply redundant. Likewise, Betley *et al.* (2004) demonstrated inhibition of vegetal localization upon over-expression of kinesin-2 heavy chain (XKlp3b) lacking a motor domain. Thus, endogenous levels of kinesin-1 and kinesin-2 cannot rescue the effects of reduction in activity of either kinesin motor, suggesting that kinesin-1 and kinesin-2 do not function redundantly in vegetal RNA localization.

It is possible, however, that kinesin-1 and kinesin-2 may have overlapping functions, as these motors appear to function in the same region of the vegetal cytoplasm. While reduction in kinesin-1 activity cannot be compensated for by endogenous kinesin-2 (Fig. 2.5A,B) and *vice versa* (Fig. 2.5C; Betley *et al.* 2004), over-expression of one motor could potentially rescue loss of the other motor. To test this possibility, we expressed kinesin-1 heavy chain lacking a motor domain (XKHCΔm) and asked whether over-expression of kinesin-2 heavy chain (XKlp3b) could rescue vegetal RNA localization. As shown in Fig. 2.5B, inhibition of vegetal RNA localization by expression of XKHCΔm, can be rescued by the co-expression of kinesin-2 heavy chain (XKHCΔm + XKlp3b). As expected,

rescue is also obtained by co-expression of wild-type kinesin-1 heavy chain (XKHCΔm + XKHC). Likewise (Fig. 2.5C), disruption of vegetal RNA localization caused by expression of kinesin-2 heavy chains lacking a motor domain (Xklp3bΔm) can be rescued by expression of either wild-type kinesin-2 heavy chain (XKlp3bΔm + XKlp3b) or wild-type kinesin-1 (XKlp3bΔm + XKHC). Although reduction of either kinesin-1 or kinesin-2 function can be complemented by expression of the other motor, endogenous levels of those motors are not sufficient for complementation, suggesting overlapping functions for these kinesins in vegetal RNA transport.

Overlapping functions for kinesin-1 and kinesin-2 in vegetal RNA transport in the oocyte predicts that they would be involved in the same steps of the localization pathway. If kinesin-1 and kinesin-2 are operating within the same step of localization it is possible they are interacting with the same cargo. To test this we asked whether these motors could be co-immunoprecipitated. KHC-specific SUK4 antibodies were used to immunoprecipitate kinesin-1 from oocyte lysates. As shown in Figure 2.5D, kinesin-2 is co-immunoprecipitated with kinesin-1, as detected with K2.4 antibodies, which recognize the motor domain of the XKlp3a subunit of kinesin-2 (Cole et al., 1993). To test whether the association between kinesin-1 and kinesin-2 might be due to interaction with Vg1 RNA during transport, we first asked if the co-immunoprecipitation of kinesin-1 and kinesin-2 was sensitive to RNase treatment. As shown in Fig. 2.5E, XKHC is co-immunoprecipicated from oocyte lysates using XKlp3a-specific antibodies (lane

1), but the interaction is abolished upon treatment with RNase (lane 2). Next, we tested whether kinesin-2 is associated with endogenous Vg1 RNA. As shown in Fig. 2.5F, Vg1 RNA is co-immunoprecipitated by XKlp3a-specific antibodies (lane 3). As demonstrated for kinesin-1 (Fig. 2.1D), this interaction is specific; non-relevant antibodies fail to immunoprecipitate Vg1 mRNA (lane 2) and EF1α mRNA is not co-immunoprecipitated with kinesin-2 (lane 6). The results of these experiments suggest that kinesin-1 and kinesin-2 may operate by simultaneously binding the same cargo and coordination of these motor activities may be necessary to transport RNA to the vegetal cortex.

A Sub-Population of Microtubules are Directed with Their Plus Ends Toward the Vegetal Cortex

Delivery of RNA to the vegetal cortex of the oocyte by kinesins 1 and 2 requires microtubules with plus ends oriented toward the oocyte cortex. However, it has been shown that the *Xenopus* oocyte microtubule cytoskeleton is organized with minus ends primarily directed toward the cortex (Pfeiffer and Gard, 1999). This raises the question of how these plus end-directed kinesin motors could be directly involved in vegetal RNA transport if microtubule polarity is opposite to the direction of kinesin movement. To address this issue, we performed immunostaining on st. III oocytes with markers for microtubule polarity. We used antibodies specific for EB1, which has been shown to bind the plus ends of growing microtubules (Mimori-Kiyosue et al., 2000), and γ-tubulin, which is a component of nucleation complexes at the minus ends of microtubules (Stearns

et al., 1991). As shown in Figure 2.6A, EB1 staining is concentrated in the vegetal cortex of the oocyte, indicating an enrichment of plus ends in this region of the oocyte. Analysis of the immunostaining results by 3-D reconstruction reveals that EB1 is concentrated in a disc within the vegetal cortical cytoplasm (Movie S1). As expected, EB1 staining is abolished upon depolymerization of the microtubule cytoskeleton (Fig. 2.S6). Analysis of EB1 and microtubule distribution at high magnification (Fig. 2.6D-F) reveals that EB1 is co-localized with microtubule ends (Fig. 2.6E-F). In contrast to the vegetal cortical enrichment of EB1 staining, visualization of γ-tubulin reveals a slight reduction in concentration of this minus end marker in the vegetal cortex (Fig. 2.6G). These data indicate that while microtubule minus ends appear to be abundant in the vegetal cortex, there is a significant concentration of microtubule plus ends, specifically in the vegetal cortex. Vegetal enrichment of EB1 is not evident at early stages in oogenesis, and is correlated temporally with the onset of Vg1 RNA localization (Fig. 2.S7). Moreover, EB1 that is enriched in the vegetal cortex is co-localized with VLE RNA (Fig. 2.6H,I), and no such colocalization is evident in the animal hemisphere (Fig. 2.6J). These data reveal a sub-population of microtubules in the oocyte that can provide directionality for kinesin-mediated transport of vegetally localized RNAs.

Discussion

We have studied the localization of Vg1 mRNA in the developing *Xenopus* oocyte to gain insight into the mechanisms responsible for transport of mRNA molecules to defined regions of the cell cytoplasm. Our results support roles for two plus end-directed molecular motors, kinesin-1 and kinesin-2, in transport of Vg1 mRNA to the vegetal cortical cytoplasm. We have obtained functional evidence that *Xenopus* kinesin-1 is a necessary component of the vegetal RNA localization machinery (Figs. 2.1-2.3), and that kinesin-1 and kinesin-2 may act together to carry out vegetal RNA transport (Figs. 2.4, 2.5). Previous results (Betley et al., 2004; Yoon and Mowry, 2004) implicating plus end-directed motors in transport of Vg1 mRNA to the vegetal cortical cytoplasm have been viewed with uncertainty (Kloc and Etkin, 2005; Palacios, 2007; St Johnston, 2005), as the polarity of the oocyte cytoskeleton, with microtubule minus ends throughout the oocyte cortex (Pfeiffer and Gard, 1999), was thought to be incompatible with a role for plus end-directed motors in vegetal transport. In this work, we have uncovered a population of microtubule plus ends that are enriched at the vegetal cortex (Fig. 2.6), consistent with a role for plus end motors in vegetal RNA transport. Based on these results, we propose a new model for vegetal RNA transport, as depicted in Figure 2.7. In this model, RNP complexes (red) are bound by both kinesin-1 and kinesin-2 (inset). Although the majority of microtubules in the oocyte (brown) are oriented with minus ends towards the cortex (Pfeiffer and Gard, 1999), directional transport of the RNP cargoes to the

vegetal cortex is facilitated by a sub-population of microtubules (gold) in the vegetal cytoplasm with plus ends directed towards the cortex.

Active transport of mRNAs by molecular motors provides an efficient mechanism to deliver mRNAs to distinct sub-domains within the cell cytoplasm. For large cells, such as the *Xenopus* oocyte, ~300μm in diameter at st. III, motor-driven transport is a particularly attractive model. In this work, we have obtained evidence of a necessary and direct function for *Xenopus* kinesin-1 in vegetal RNA transport. We find that kinesin-1 interacts specifically with VLE and Vg1 RNA, as evidenced by both co-localization and co-immunoprecipitation (Fig. 2.1). Importantly, vegetal RNA localization is inhibited by kinesin-1 function blocking antibodies (Fig. 2.2), and by expression of two distinct kinesin-1 heavy chain (XKHC) mutant constructs (Figs. 2.3-2.5). These results support a direct role for kinesin-1 in vegetal RNA transport. Another kinesin motor, kinesin-2, has been implicated in vegetal RNA localization (Betley et al., 2004), raising the question of how these plus end-directed motors individually contribute to vegetal RNA localization. By comparing the *in vivo* effects of kinesin rigor mutations, we have discovered a previously unidentified step in the RNA transport pathway, mediated by kinesins -1 and -2. Oocytes expressing either kinesin-1 or kinesin-2 rigor mutants display identical phenotypes (Fig. 2.4), in which VLE RNA is restricted to a sub-region of the vegetal cytoplasm lying above the vegetal cortex. Kinesin rigor mutants have been shown to lock onto microtubules (Nakata and Hirokawa, 1995), suggesting that RNA cargoes should collect in the region where

the kinesin motor is acting. Indeed, we find that VLE RNA accumulates in the bottom half of the vegetal cytoplasm in the presence of the kinesin-1 or -2 rigor mutants (Fig. 2.4). Kinesin function in the lower vegetal cytoplasm is further supported by the observation that endogenous kinesin-1 colocalizes with VLE RNA in this same region (Fig. 2.1), as do both kinesin-1 and kinesin-2 rigor-mutant motors (Fig. 2.S3). Importantly, kinesin-1 and kinesin-2 co-immunoprecipitate in an RNA-dependent manner (Fig. 2.5D,E), implying association through a shared RNA cargo. Taken together, these data suggest that these motors function during the same step in RNA localization. This is a particularly intriguing result as it is, to our knowledge, the first indication that kinesin-1 and kinesin-2 interact during cellular transport.

The transport phase of Vg1 RNA localization has long been described as a two-step process, in which vegetally-directed transport is followed by anchoring of the RNA to the vegetal cortical cytoskeleton (Yisraeli et al., 1990). Our data now suggest at least three distinct steps, as transport in the upper and lower vegetal cytoplasm appear mechanistically distinct. The “intermediate” kinesin-1 and kinesin-2 rigor mutant phenotypes (Fig. 2.4) indicate that transport in the upper vegetal cytoplasm can occur in the presence of kinesin-1 and kinesin-2 rigor-mutant motors, suggesting that transport from the germinal vesicle until approximately midway to the vegetal cortex is independent of kinesin-1 and kinesin-2 and may rely on an as yet unidentified motor. Thus, our results suggest that transport to the vegetal cortex consists of a step in the upper vegetal

cytoplasm that is independent of kinesins -1 and -2 and a step in the lower vegetal cytoplasm that relies on these kinesin motors.

These results raise the question of why two different types of plus end-directed kinesin motors are required to coordinate transport to the vegetal cortex. If these motors are simply redundant, loss of either motor should be compensated for by the other motor. Contrary to this expectation, reduction of either kinesin-1 (Figs. 2.3-2.5) or kinesin-2 (Betley et al., 2004) activity disrupts vegetal RNA localization. Thus, kinesin-1 and kinesin-2 do not simply act redundantly in vegetal RNA localization. Further clues can be provided by cross-rescue experiments. We used kinesin mutants carrying motor domain deletions to reduce the levels of active kinesin-1 and kinesin-2 (Fig. 2.5), and showed that kinesin-1 was able to rescue kinesin-2 mutants and *vice versa*. These results suggest that the levels of kinesin motors in the oocyte may be a limiting factor for RNA transport, and that multiple motors may be bound to RNA cargoes to facilitate transport. Much evidence disputes a 1:1 stoichiometry of motor to cargo, with estimates of motors bound to a single cargo ranging between 1 and 11 (Bullock et al., 2006; Levi et al., 2006; Vershinin et al., 2007). One rationale for multiple motors bound to a particle is that increased numbers of bound motors should decrease the likelihood of a cargo detaching from a microtubule. Importantly, mixed polarity of the microtubules in the vegetal oocyte cytoplasm may necessitate multiple motors bound to RNA cargoes. Our results (Fig. 2.6) have revealed a population of microtubules with plus ends at the vegetal cortex,

which is compatible with kinesin-driven transport to the vegetal cortex. However, a significant population of microtubules is also oriented with minus ends directed towards the vegetal cortex (Figs. 2.6G, 2.7; Pfieffer and Gard, 1999). Within this mixed population of microtubules, multiple motors bound to RNA cargoes would ensure that an RNA cargo remains attached to a single microtubule regardless of whether it is oriented toward the vegetal cortex or away. In this light, continued accumulation of RNA in the upper vegetal cytoplasm in wild-type XKHC-expressing oocytes at timepoints after RNA has cleared from the upper vegetal cytoplasm in XKHC-rigor expressing oocytes (Fig. 2.4C,D) is intriguing, and could suggest bi-directional transport in the lower vegetal cytoplasm. In such a model, RNAs could be transported both towards and away from the vegetal cortex, but anchoring of the RNA at the vegetal cortex could bias the flux of RNA transport vegetally. Indeed, Vg1 has been shown to be anchored to the vegetal cortex after transport (Alarcon and Elinson, 2001; Yisraeli et al., 1990). Our model for vegetal RNA transport (Fig. 2.7) incorporates the existence of a sub-population of microtubules with plus ends at the vegetal cortex, along with multiple motors bound to RNA cargoes and anchoring at the vegetal cortex to provide a new mechanistic basis for directional RNA transport in the cytoplasm.

Materials and Methods

In Vitro Transcription

Transcription of VLE and XβM RNA for immunoprecipitation and RT-PCR were performed as in Mowry (1996). Fluorescently labeled VLE RNA was transcribed as above, with inclusion of 1 mM Alexa Fluor 546-14-UTP (Molecular Probes). Transcription of FLAG-tagged RNA was performed using the mMessage mMachine kit (Ambion).

Microinjection and Oocyte Manipulation

Microinjection and culture of *X. laevis* oocytes was performed as in Kress *et al*. (Kress et al., 2004). For RNA localization assays, 0.05 fmol of fluorescently labeled VLE RNA (2 nl at 25 nM) was injected into st. III oocytes and allowed to localize for 8 hr. FLAG-tagged rigor-mutant and control RNAs (4 nl) were injected at concentrations ranging from 62.5-500 nM (as noted in the figure legends) and allowed to express protein for 16 hr. prior to VLE RNA injection. For antibody interference, oocytes were injected with 4 ng of Protein-G purified antibodies and incubated 2 hr. prior to VLE RNA injection. For immunoprecipitation and RT-PCR experiments, oocytes were injected with 2 nl of VLE or XβM RNA at 50 nM.

Cloning

XKHC was amplified from *Xenopus* oocyte RNA using primers designed to the predicted N– and C–termini. The full-length XKHC cDNA (deposited into GenBank; DQ680042) was cloned into pSP64TSN-FLAG (Kress et al., 2004) to

generate pXKHC-FLAG. XEg5 (GenBank# X54002) and XKlp3b (GenBank# AJ009839) were amplified by PCR and cloned into pSP64TSN-FLAG. XKHC-T92I-FLAG, XEg5-T105N-FLAG and XKlp3b-T103I-FLAG were cloned by PCR amplification of fragments corresponding to the N– and C– terminal halves of each protein. All primer sequences are listed in Fig. 2.S8.

Immunoprecipitation

Immunoprecipitations were carried out as in Kress *et al*. (2004), except that S10 lysates were prepared and immunoprecipitated using WB [10mM HEPES pH 7.4, 10mM KOAc, 3mM $Mg(OAc)_2$, 5mM EGTA, 0.05% NP-40, 1mM DTT, 0.1μg/ml leupeptin (MP Biomedicals), 0.1μg/ml antipain (MP Biomedicals), 0.1μg/ml trypsin inhibitor (MP Biomedicals), 0.4mM pefabloc (Roche), 1U/ml rRNasin (Promega), 34g/l sucrose] at 0.5 μl/oocyte. Either 25 μl (for RT-PCR) or 125 μl (for co-IP) of lysate, was mixed with Protein G-purified antibodies [SUK4 (DSHB), K2.4 (Covance)]; purified mouse IgG (Sigma) was used as a control. XKHC and XKlp3a were detected by immunoblotting using SUK4 or K2.4 antibodies at dilutions of 1:500 or 1:50, respectively. RNA isolation and RT-PCR were performed as in Kress *et al*. (2004), using primers specific for Vg1, EF1α, VLE or XβM RNAs (Fig. 2.S8).

Immunolocalization and Imaging

For immunolocalization, performed as in Yoon and Mowry (2004), αSUK4 (DSHB), αFLAG (Sigma), and anti-α-Tubulin (Sigma) were used at 1:250, and γ-

Tubulin antibodies (Sigma) were used at 1:150. Monoclonal EB1 antibodies (BD Biosciences) were used at 1:50,and polyclonal EB1 antibodies (a kind gift of E. Karsenti; (Niethammer et al., 2007) were used at 1:250. Alexa-546, Alexa-633, Alexa-647 and Alexa-546 antibodies (Molecular Probes) were used at 1:500. Oocytes were imaged by confocal microscopy using either a Leica TCS SP2 or a Zeiss LSM 510 META.

Acknowledgments

This work was supported by Public Health Service grant GM071049 from the National Institute of General Medicine to K.L.M. T.J.M. and J.A.G. were pre-doctoral trainees, supported in part by grant T32-GM07601. We thank A. DeLong, M. McKeown, T. Serio and G. Wessel for critical reading of the manuscript, and to R. Lesiak for illustration. We are grateful to M. Feldbrügge, E. Houliston W. Theurkauf and T. Wood for helpful advice and discussions and to J. Deshler and E. Karsenti for generously sharing reagents.

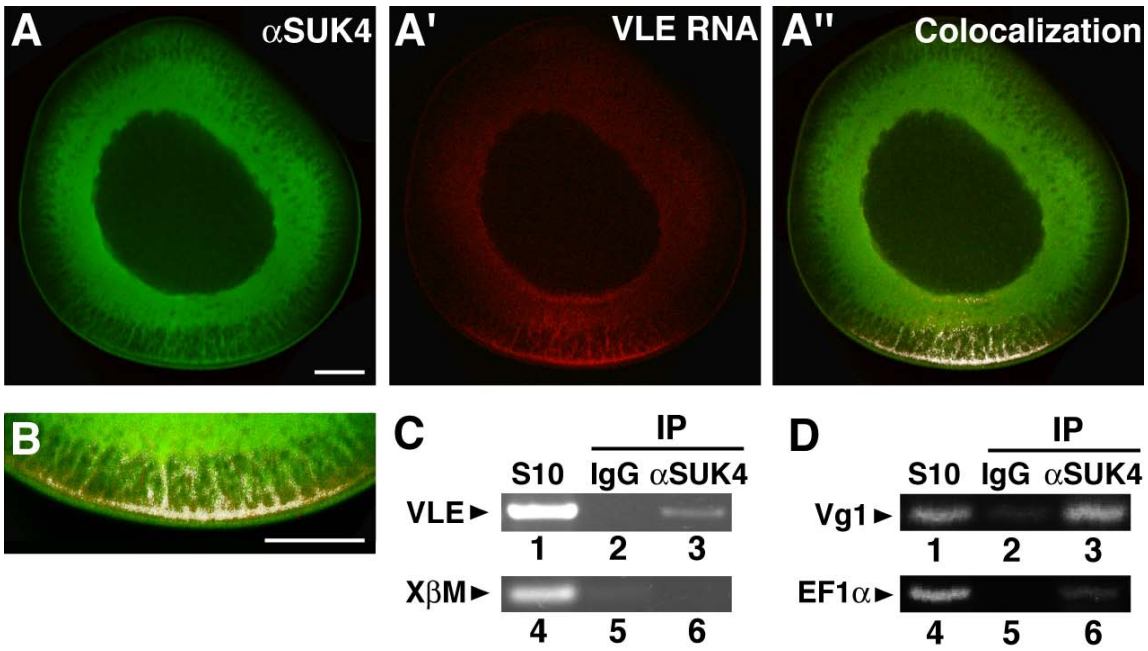

Figure 2.1. *Kinesin-1 Interacts with VLE RNA.* (A-B) Immunofluorescence was carried out using SUK4 antibodies on st. III oocytes injected with fluorescently labeled VLE RNA. Shown is a confocal section with kinesin-1 shown in green (A; αSUK4) and VLE RNA in red (A′); the overlap of VLE RNA and SUK4 staining (A′′) is shown in white. (B) Higher magnification view of VLE RNA and KHC colocalization (white) in the vegetal oocyte cytoplasm. For A-B, scale=50 μm. (C) S10 lysates from oocytes injected with VLE or XβM RNA (lanes 1 and 4 show 10% of total) were immunoprecipitated with mouse IgG (lanes 2, 5) or αSUK4 (lanes 3, 6). Bound RNAs were detected by RT-PCR using primers for VLE (lanes 1-3) or XβM (lanes 4-6). (D) S10 lysates from uninjected oocytes were immunoprecipitated with mouse IgG (lanes 2, 5) or αSUK4 (lanes 3, 6). Bound RNAs were detected by RT-PCR using primers for Vg1 (lanes 1-3) or EF1α (lanes 4-6). Lanes 1 and 4 show 20% of total input RNA.

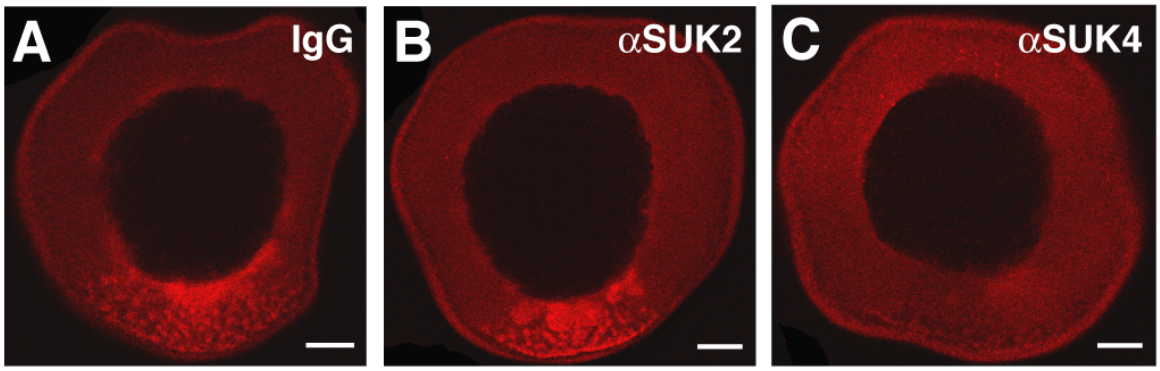

D

Injection	Localization (%)	*n*
IgG	100	62
αSUK2	102	36
αSUK4	52	53

Figure 2.2. *Kinesin-1 Has a Role in Vegetal RNA Transport.* (A-C) Confocal images of representative oocytes injected with fluorescently labeled VLE RNA following injection with (A) IgG (control), (B) αSUK2 (non-function-blocking αKHC) or (C) αSUK4 (function blocking αKHC) antibodies. Scale=50 μm. (D) Quantification of antibody interference results. Oocytes were analyzed for VLE RNA localization by confocal microscopy, with percent of oocytes exhibiting localization scored relative to the IgG control, which was set to 100%.

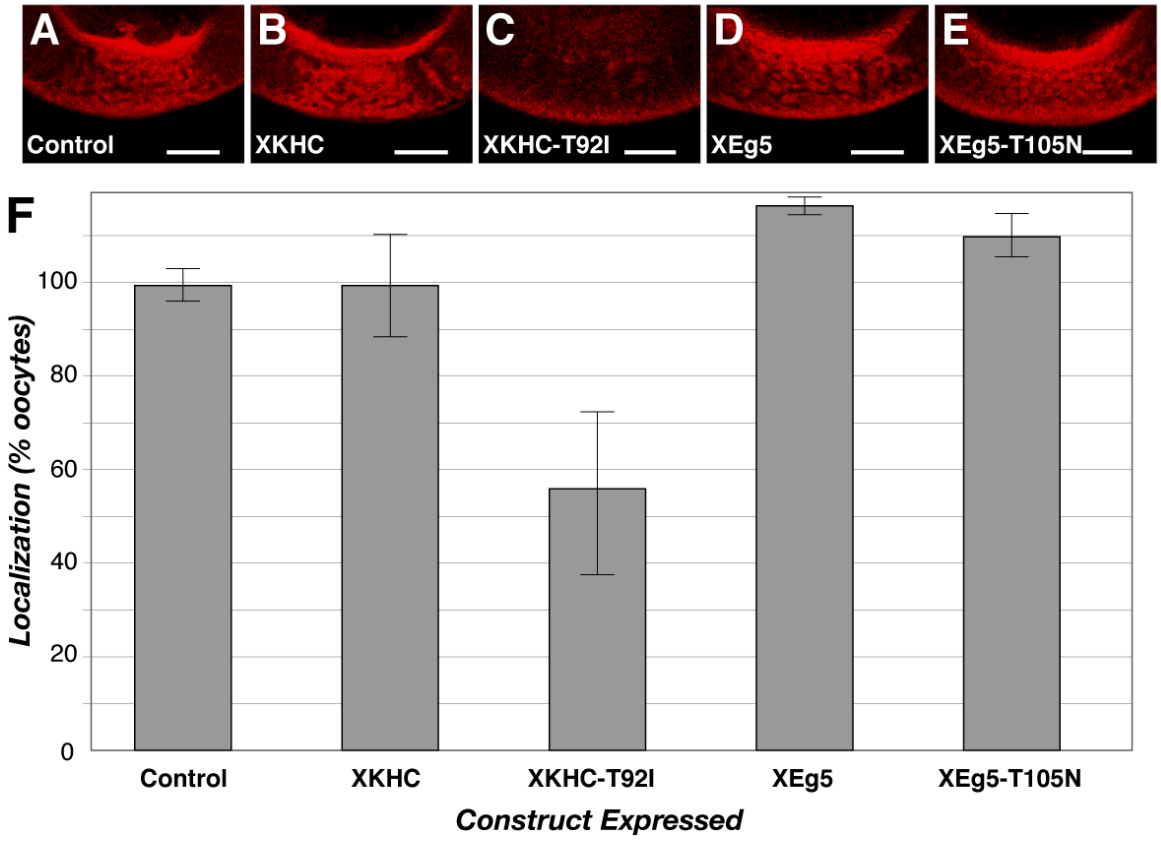

Figure 2.3. *Kinesin-1 Rigor Mutation Disrupts Vegetal RNA Transport.* (A-E) Alexa-546 labeled VLE RNA was injected into oocytes expressing (A) no exogenous protein (control, *n*=311), (B) kinesin-1 heavy chain (XKHC, *n*=253), (C) kinesin-1 rigor mutant (XKHC-T92I, *n*=260), (D) Eg5 (XEg5, *n*=116), or (E) Eg5 rigor mutant (XEg5-T105N, *n*=123), all injected at 500 nM. Representative confocal images of the vegetal hemisphere cytoplasm are shown; scale=50 μm. (F) Comparison of the percentage of oocytes (gray bars, ± st. dev.) exhibiting vegetal localization scored relative to the average for control oocytes (A), which was set to 100%.

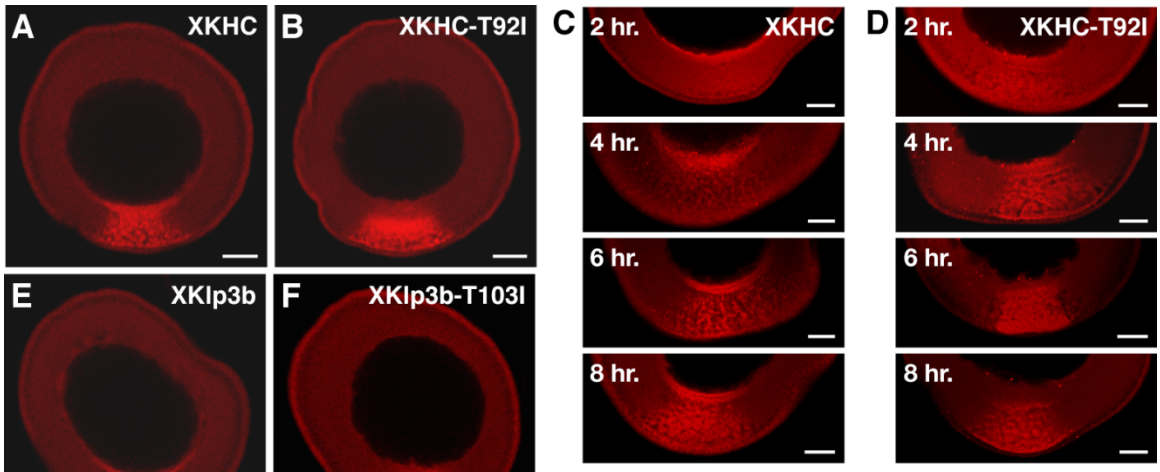

G

	Control	XKHC-T92I	XKlp3b-T103I	XKHC-T92I + XKlp3b-T103I
% Intermediate Phenotype	0	16	26	43
n	61	71	71	75

Figure 2.4. *The Kinesin-1 Rigor Mutation Has an Intermediate Phenotype that may Provide Insight into Kinesin-1 Function.* (A-B) Oocytes were injected with either (A) XKHC-FLAG or (B) XKHC-T92I-FLAG at 125 nM. After 16 hr. expression, fluorescently labeled VLE RNA was injected, and localization was assayed after 8 hrs. by confocal microscopy. Representative images are shown for the "normal" phenotype (A) and "intermediate" phenotype (B), with the vegetal hemisphere towards the bottom. (C-D) Oocytes were injected with either (C) XKHC- or (D) XKHC-T92I-encoding RNAs at 500 nM, followed by injection of fluorescently labeled VLE RNA. Oocytes were harvested at 2, 4, 6, and 8 hrs., and localization was assayed as above. Representative images of the vegetal cytoplasm are shown. (E-F) Oocytes were injected with (E) XKlp3b- or (F) XKlp3b-T103I-encoding RNAs at 125 nM, and assayed for VLE localization as in A-B. For A-F, scale=50 μm. (G) Oocytes (from A,B,E,F) were scored for localization by confocal microscopy, and the percentage that exhibited the

"intermediate" rigor phenotype is indicated, along with the number of oocytes (*n*) assayed.

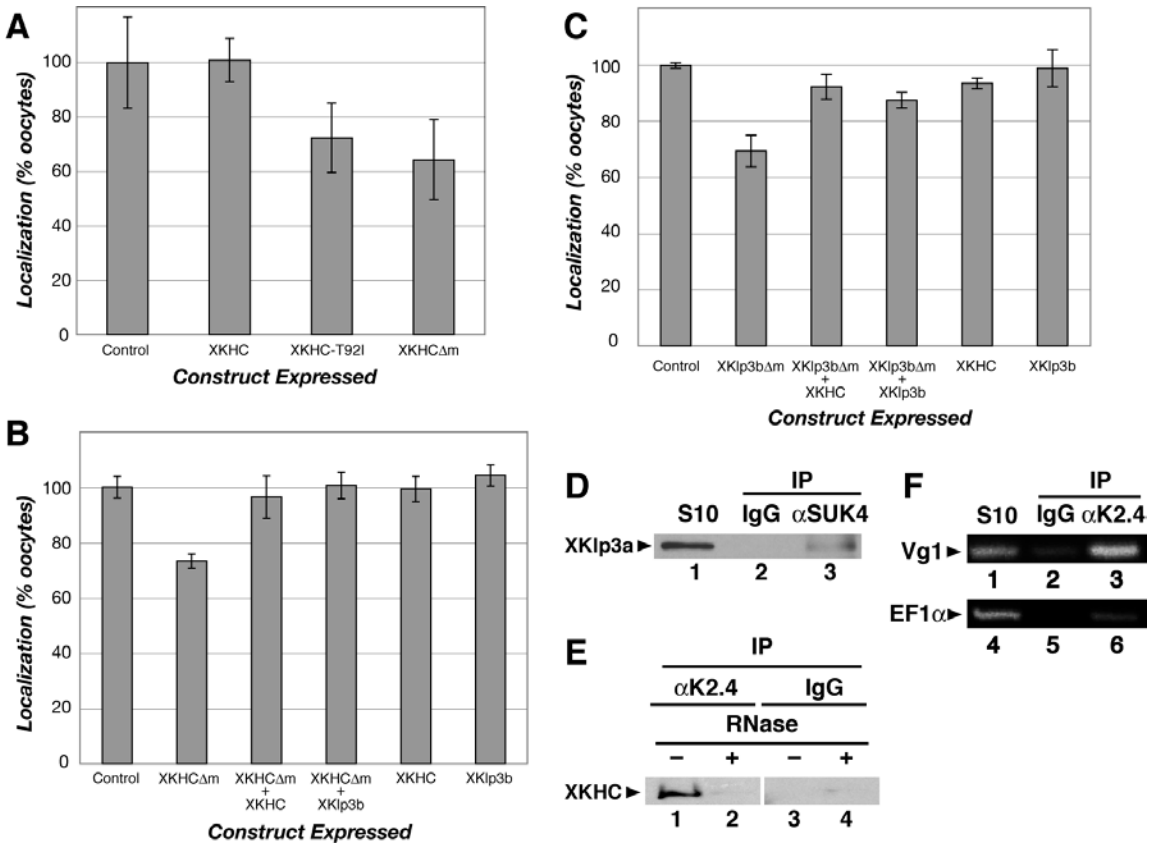

Figure 2.5. *Kinesin-1 and Kinesin-2 Have Overlapping Functions.* (A) Oocytes were injected with RNAs encoding kinesin-1 heavy chain (XKHC, *n*=168), kinesin-1 rigor mutant (XKHC-T92I, *n*=155) or kinesin-1 mutant lacking the motor domain (XKHCΔm, *n*=164), all at 125 nM; control oocytes expressed no exogenous protein (Control, *n*=158). Vegetal ocalization was assayed after injection of Alexa-546 labeled VLE RNA. The percentage of oocytes (± st. dev.) exhibiting accumulation of the injected RNA in the vegetal hemisphere is indicated by gray bars, with the average of control oocytes set to 100%. (B) Oocytes injected with RNA encoding kinesin-1 mutant lacking the motor domain (XKHCΔm *n*=160) at 50 nM were rescued by co-expression of either XKHC (XKHCΔm+XKHC *n*=168) or XKlp3b (XKHCΔm+XKlp3b *n*=165) at 125 nM.

Control oocytes expressed no exogenous protein (Control *n*=161); additional controls expressed XKHC (XKHC *n*=150) or XKlp3b (XKlp3b *n*=157) alone. Vegetal RNA localization was assayed as in A. The percentage of oocytes (± st. dev.) exhibiting vegetal localization is shown by gray bars, with the control average set to 100%. (C) Oocytes injected with RNA encoding kinesin-2 mutant lacking the motor domain (XKlp3bΔm *n*=160) were rescued by co-injection of XKHC (XKlp3bΔm+XKHC, *n*=155) or XKlp3b (XKlp3bΔm+XKlp3b, *n*=155) all at 125 nM. Control oocytes expressed no exogenous protein (Control, *n*=154); additional controls expressed XKHC (XKHC, *n*=153) or Xklp3b (XKlp3b, *n*=160) alone. Vegetal RNA localization was assessed and presented as in B. (D) Immunoprecipitation was carried out from oocyte S10 lysates (lane 1) using SUK4 (lane 3), or control IgG antibodies (lane 2). After SDS-PAGE, immunoblotting was carried out with αK2.4. (E) S10 lysate, prepared from st. III oocytes, was treated with either RNase A (+) or RNasin (-), and immunoprecipitation was carried out using K2.4 (lanes 1-2) or control IgG antibodies (lanes 3-4). After SDS-PAGE, immunoblotting was carried out using SUK4 antibodies. (F) Immunoprecipitation from oocyte S10 lysates was carried out using K2.4 (lanes 3 and 6) or control IgG antibodies (lanes 2 and 5). Bound RNAs were detected by RT-PCR using primers for Vg1 (lanes 1-3) or EF1α (lanes 4-6) mRNAs. Lanes 1 and 4 show 20% of total input RNA.

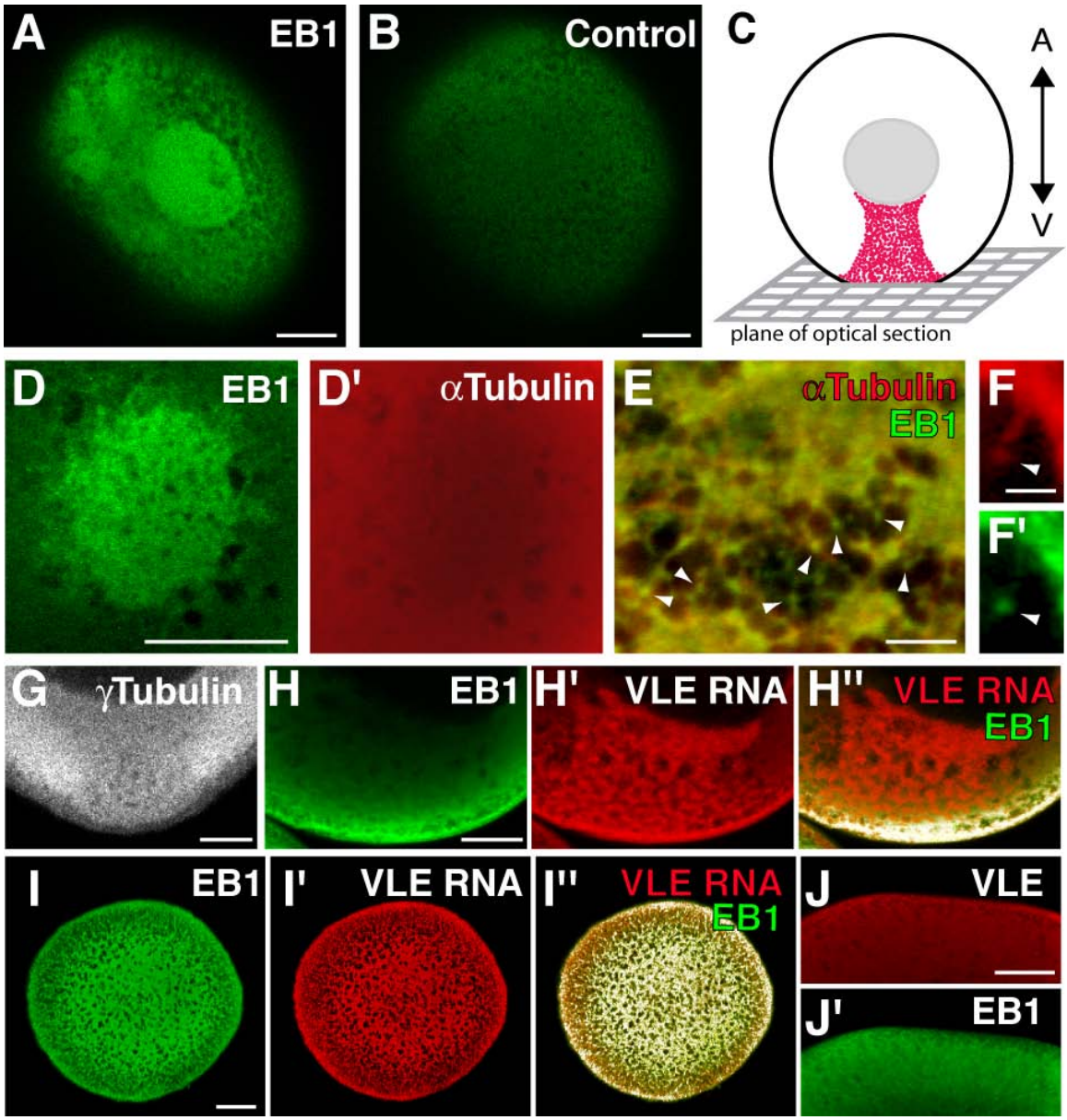

Figure 2.6. *Markers of Microtubule Polarity Reveal a Vegetal Population of Plus Ends.* (A-B) Immunofluorescence was performed on st. III oocytes using: (A) EB1 antibodies or (B) no primary antibody. (C) Depiction of vegetal views shown in A,B,D,E,I. The optical section, ~10-25 μm from the vegetal pole, is depicted as a gray grid relative to oocyte A/V axis. (D-F) Immunofluorescence was performed on st. III oocytes using both EB1 and α-Tubulin antibodies. (D) An optical section

shows EB1 in green (D) and α-Tubulin in red (D′). (E) Colocalization of EB1 (green) and microtubules (red), viewed at high magnification (scale=5μm). Arrowheads point to examples of microtubule ends colocalized with EB1. (F) An optical section, with the vegetal pole oriented towards the bottom, shows α-Tubulin in red (F) and EB1 in green (F′). Arrowhead points to a microtubule end colocalized with EB1; scale=2μm. (G) Immunofluorescence was performed on st. III oocytes using γ-Tubulin antibodies. A cross section through the vegetal cytoplasm is shown, with the vegetal pole at the bottom. (H) Immunofluorescence was performed on Alexa-546 VLE-injected oocytes using EB1 antibodies. An optical cross section of the vegetal cytoplasm is shown, with the vegetal pole at the bottom. EB1 is shown in green (H), VLE RNA is shown in red (H′) and the overlap of VLE RNA and EB1 is visualized as white (H′′). (I) Vegetal view (as in C) of EB1 and VLE colocalization in a st. III oocyte. EB1 is shown in green (I), VLE RNA is shown in red (I′); VLE RNA and EB1 overlap is shown in white (I′′). (J) An optical cross section of the animal hemisphere from (H) is shown, with VLE RNA as red (J) and EB1 as green (J′). Scale bars represent 50μm (A-B,D,G-J), 5μm (E) or 2μm (F).

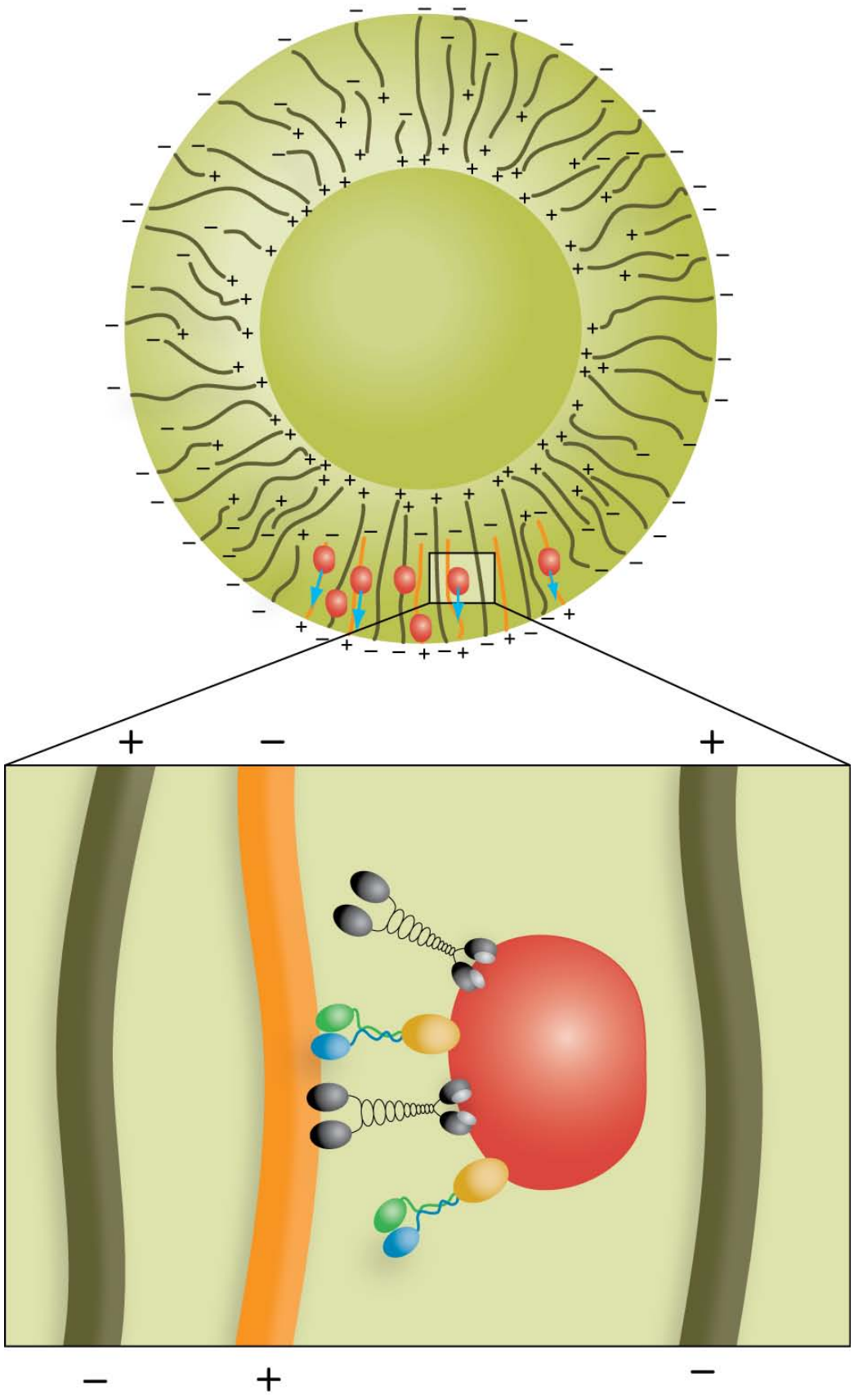

Figure 2.7. *Model for Vegetal RNA Localization.* A depiction of a st. III oocyte is shown, with the majority of microtubules (shown in brown) oriented with minus ends directed towards the vegetal cortex (bottom). A sub-population of microtubules (shown as gold) is present in the vegetal cytoplasm, with plus ends oriented towards the vegetal cortex. RNA-protein complexes (RNPs) transported to the vegetal cortex are shown in red. Vegetally transported RNPs are bound (see inset) by both kinesin-1 (black) and kinesin-2 (blue/green) motors. Anchoring of the RNA at the vegetal cortex is not depicted.

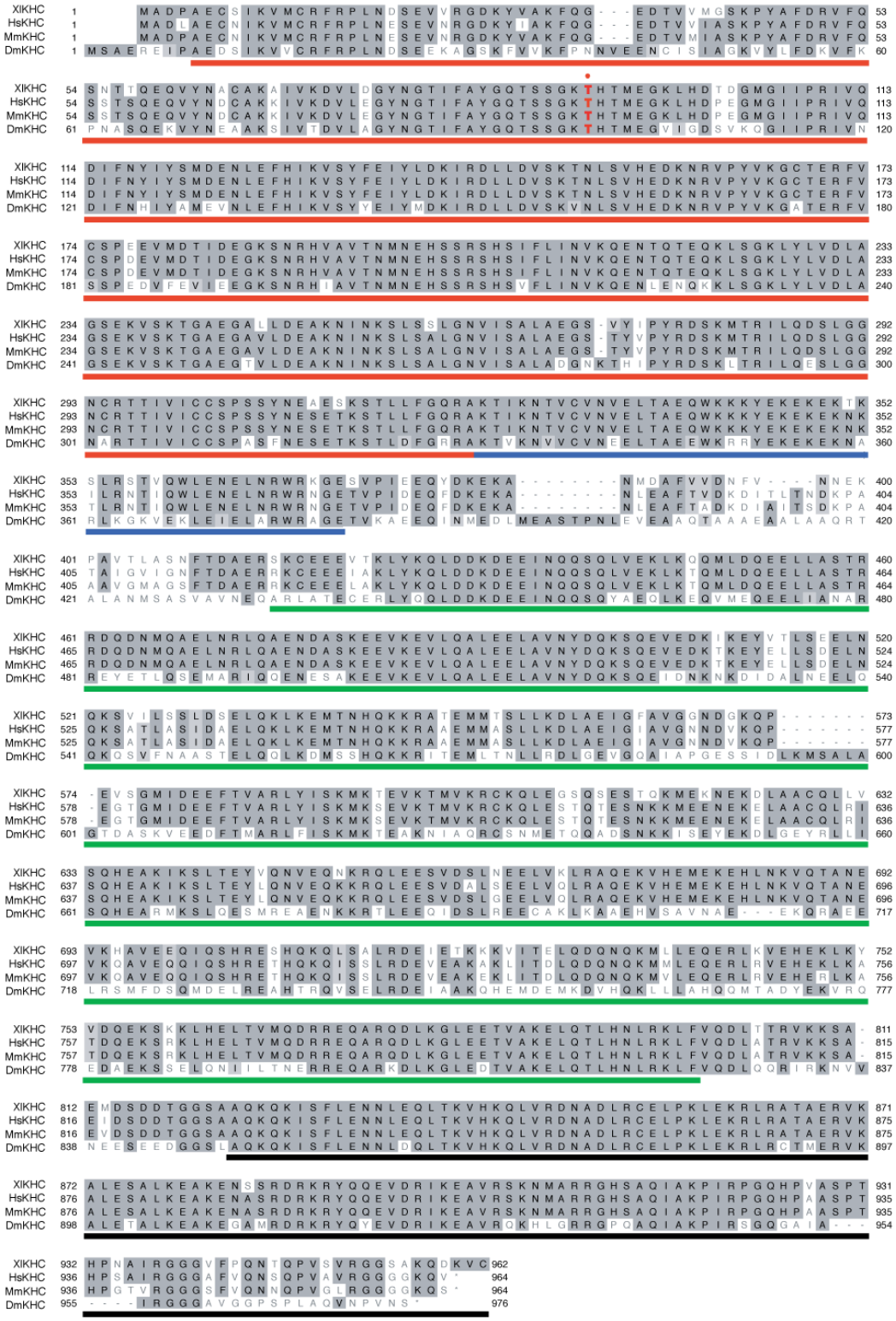
XlKHC
HsKHC
MmKHC
DmKHC

Figure 2.S1. *Cloning of Xenopus kinesin-1 heavy chain.* The complete open reading frame for the XKHC cDNA encodes a protein of 962 amino acids with a predicted molecular weight of 110 kDa. Alignment of *Xenopus* kinesin heavy chain (XlKHC) (GenBank Accession Number DQ680042) with human (HsKHC; Navone et al., 1992), mouse (MmKHC; Gudkov et al., 1994), and fly sequences (DmKHC; Yang et al., 1989). Below the aligned sequences are lines representing head (red), neck (blue), stalk (green), and tail (black) domains of KHC. Comparison with mammalian sequences shows that XKHC shares 94%, 90%, 87% and 91% amino acid identity, within the N-terminal motor, neck, stalk and tail domains, respectively. For the *Drosophila* sequence, XKHC shares 75%, 66%, 50%, and 89% sequence identity with these domains, respectively. Within the motor domain the threonine residue that is mutated to isoleucine to generate a kinesin-1 rigor mutation is shown in red.

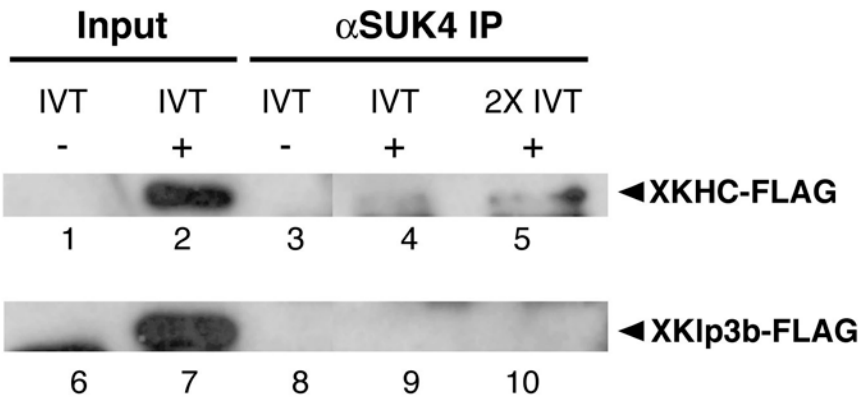

Figure 2.S2. *SUK4 antibodies specifically recognize recombinant XKHC.* SUK4 antibodies specifically immunoprecipitate recombinant XKHC (top), but not kinesin-2 subunit XKlp3b (bottom). XKHC-FLAG (top) or XKlp3b-FLAG (bottom) RNAs were added (+; lanes 2,4-6,9,10) to rabbit reticulocyte lysate (Promega) for *in vitro* translation (IVT). Mock reactions contained no added RNA (-; lanes 1,3,6,8). 20% (lanes 3,4,8,9) or 40% (2X; lanes 5,10) of the IVT reactions were immunoprecipitated with SUK4 (DSHB) antibodies. Input represents 5% of IVT. After SDS-PAGE, translated proteins were detected by immunoblotting for the C-terminal FLAG epitope using FLAG antibodies (Sigma) at 1:1000.

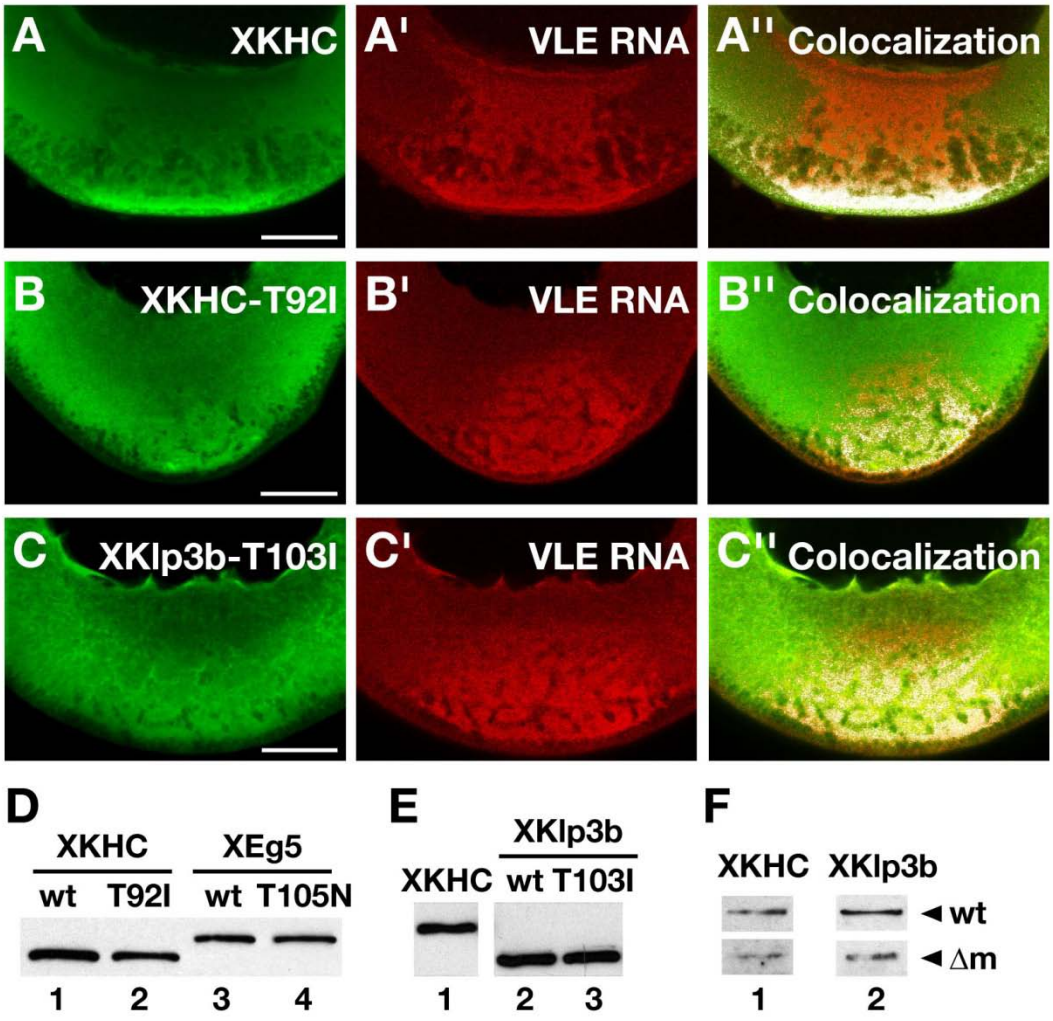

Figure 2.S3. *Expressed FLAG-tagged wild-type and mutant kinesin motor proteins colocalize with VLE RNA.* (A-C) RNAs encoding (A) XKHC-FLAG, (B) XKHC-T92I-FLAG or (C) XKlp3b-T103I-FLAG were injected into st. III oocytes and incubated overnight to allow protein expression. Oocytes were then injected with fluorescently labeled VLE RNA and cultured for 8 hr. Immunofluorescence was performed with FLAG (Sigma) and Alexa-633 (Molecular Probes) antibodies, and confocal images were obtained using a Zeiss LSM 510 META. Expressed FLAG-tagged protein is shown in green (A-C), VLE RNA is shown in red (A′-C′),

and overlap of FLAG-tagged kinesin motor proteins and VLE RNA is in white (A′′-C′′). Cross-sections through the vegetal hemisphere are shown, with the vegetal cortex oriented towards the bottom. Scale=50 μm. (D-F) Immunoblotting was performed on lysates prepared from oocytes expressing (D) XKHC-FLAG (lane 1), XKHC-T92I-FLAG (lane 2), XEg5-FLAG (lane 3), or XEg5-T105N-FLAG (lane 4); (E) XKHC-FLAG (lane 1), XKlp3b-FLAG (lane 2) or XKlp3b-T103I (lane 3); (F) XKHCΔm-FLAG (lane 1) or HA-XKlp3bΔm (lane 2). Blots were probed with (D-E) αFLAG (Sigma), (F) αSUK4 (lane 1; DHSB) or αK2.4 (lane 2; Covance) at 1:500 dilution.

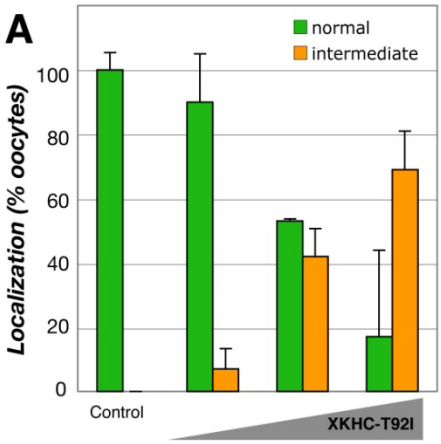

B

Construct	Localization Phenotype (%) Normal	Intermediate	None	*n*
XKHC	93	0	7	62
XKHC-T92I	49	35	16	49
XKlp3b	76	0	24	55
XKlp3b-T103I	33	32	35	51

Figure 2.S4. *The intermediate phenotype results from expression of rigor-mutant kinesin motor proteins.* (A) Alexa-546 labeled VLE RNA was injected into oocytes expressing either no exogenous protein (Control, *n*=102), 62.5 nM XKHC-T92I-FLAG RNA (*n*=75), 125 nM XKHC-T92I-FLAG RNA (*n*=102) or 500 nM XKHC-T92I-FLAG RNA (*n*=87). After incubation for 8 hr., localization was scored by confocal microscopy. The graph shows the percentage of oocytes that exhibited normal localization (green) and the percentage showing the rigor "intermediate" phenotype (orange). The average normal localization observed for the control oocytes was set to 100%. (B) Oocytes expressing XHKC-FLAG, XKHC-T92I-FLAG, XKlp3b-FLAG or XKlp3B-T103I were assayed and scored for localization as above (A), and the percentage that exhibited normal localization (normal), the intermediate rigor phenotype (intermediate), or no detectable localization (none) is shown in the table. The number of oocytes (*n*) is indicated on the right.

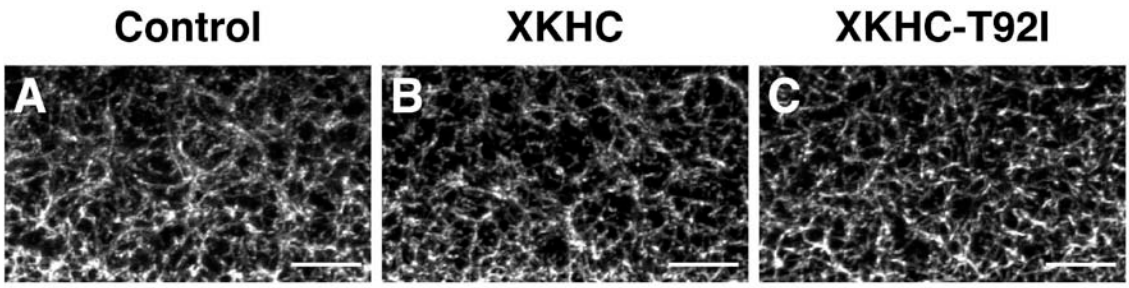

Figure 2.S5. *Microtubules are not disrupted in the presence of the kinesin-1 rigor mutant XKHC-T92I.* Microtubules in st. III oocytes expressing (A) no exogenous protein (Control), (B) XKHC-FLAG or (C) the kinesin-1 rigor mutant (XKHC-T92I) were labeled with antibodies directed toward α-Tubulin (Sigma; 1:150). Alexa-546 anti-rabbit secondary antibodies were used at 1:500 and oocytes were imaged by confocal microscopy using a Zeiss LSM 510 META. Optical cross-sections of the vegetal cytoplasm are shown, with the vegetal hemisphere towards the bottom. Scale=10 μm.

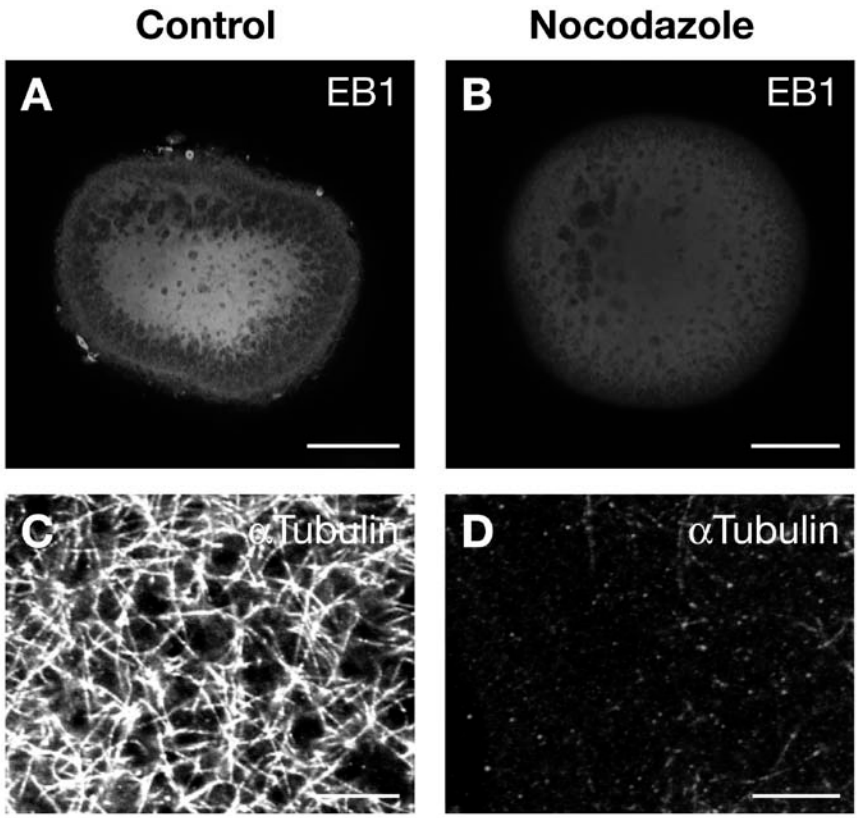

Figure 2.S6. *Depolymerization of microtubules abolishes EB1 staining.* Stage III oocytes were incubated in the presence of 10 µg/ml nocodazole to depolymerize microtubules. Immunofluorescence was performed using (A,B) EB1 antibodies (BD Biosciences) at 1:50 and (C, D) α-Tubulin antibodies (Sigma) at 1:250. Enrichment of EB1 in the vegetal cortex observed in control oocytes (A), is abolished by treatment with nocodazole (B). Vegetal views (as in Fig. 2.6C) are shown for A-B, and Alexa-633 (Molecular Probes) anti-mouse secondary antibodies were used at 1:500. Scale=50 µm. The filamentous network of microtubules evident in control oocytes (C) is depolymerized upon nocodazole treatment (D). Optical cross-sections are shown for C-D, and Alexa-546 anti-rabbit secondary antibodies were used at 1:500. Imaging was performed on a Zeiss LSM 510 META. Scale=10 µm.

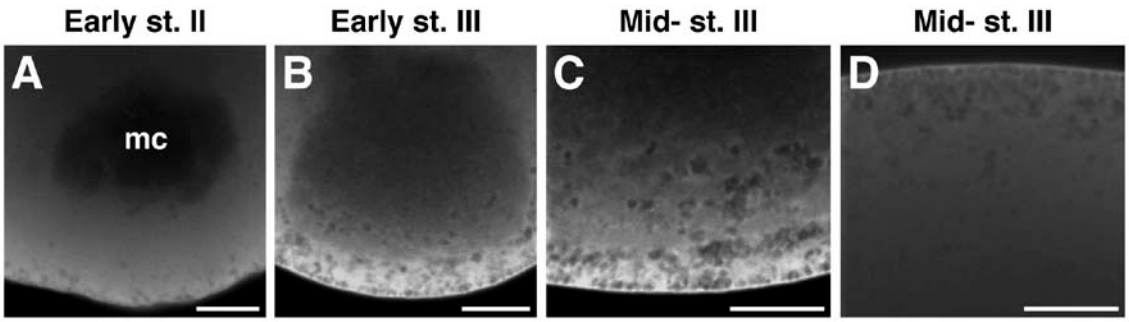

Figure 2.S7. *EB1 accumulates at the vegetal cortex during early stage III of oogenesis.* Immunofluorescence was performed with anti-EB1 antibodies (Niethammer et al., 2007) on (A) early st. II, (B) early st. III, or (C-D) mid-st. III oocytes. Anti-rabbit Alexa-546 secondary antibodies were used at 1:500, and oocytes were imaged by confocal microscopy using a Zeiss LSM 510 META. The mitochondrial cloud (mc) is apparent as a dark area in the early st. II oocyte (A), but no evidence of cortical EB1 enrichment is evident. In the early st. III oocyte (B), the mc is in the process of breaking down towards the vegetal hemisphere, and accumulation of EB1 is evident at the vegetal cortex. By mid-st. III (C,D), the disc of EB1 enrichment in the vegetal cortex is larger (C; compare also, vegetal views in Fig. 2.6A [early st. III] and 2.6I [mid-st. III]), and no EB1 accumulation is evident in the animal hemisphere cortex (D). Oocyte stages are as in Dumont (1972). Oocytes are oriented with the vegetal hemisphere towards the bottom; scale =20 μm.

Amplicon	Forward Primer	Reverse Primer
XKHC	GAGAACCAGATCTATG GCGGACCCGGCGGAG	GAACCCTCGA GAGGCAGACT TTGTCCTGTTT AGC
N- XKHC-T92I	GAGAACCAGATCTATG GCGGACCCGGCGGAG	TTCCCTCCATG GTATGGATTTT TCCTGATGATG T
C- XKHC-T92I	GGCATCCCATGGAGGG AAAACTCCATG	GAACCCTCGA GAGGCAGACT TTGTCCTGTTT AGC
XEg5	GCCATCTCGAGCATGG CCAGCAAGAAGGAGG	GAACCCTCGA GGAGTTCTGC ATTCGCAGGG GAAG
N- XEg5-T105N	GCCATCTCGAGCATGG CCAGCAAGAAGGAGG	CATAGTAAAGT TCTTGCCGGTA CCAGTCTGCC C
C- XEg5-T105N	TGCGTATGGGCAGACT GGTACCGGCAAGAACT TTAC	GAACCCTCGA GGAGTTCTGC ATTCGCAGGG GAAG
XKlp3B	GCGAGCGGAGATCTAT GTCCAAGTCTAAGAGCT CGG	GCGAGCTCGA GGATTTGGGT ACCAGGCCTC GTG
N-XKlp3B-T103I	GCGAGCGGAGATCTAT GTCCAAGTCTAAGAGCT CGG	CTTTTCTGGAT CCCCACGCAC TCCCTCCATTG TGTAAATTTTT CC
C-XKlp3B-T103I	GCGTGGGGATCCAGAA AAGAGAGG	GCGAGCTCGA GGATTTGGGT ACCAGGCCTC GTG
VLE RNA	CGATGACATCCACCCAA CAC	GAGGGTCACA GTCAGCAAGG

XβM RNA	GCAGAAGCTCAGAATAAACGC	GCACATAGTTTGCCCCAGG
Vg1 mRNA	CGATGACATCCACCCAACAC	ATAGGTGTTCTGGCTGAACC
EF1α mRNA	CAGATTGGTGCTGGATATGC	ACTGCCTTGATGACTCCTAG

Figure 2.S8. *PCR Primer Sequences.* All primer sequences are listed 5′-3′. PCR was performed using Platinum Taq (Invitrogen), according to the manufacturer's instructions.

Chapter 3: Directional Transport Mediated by a Dynein-Dependent Step in an RNA Localization Pathway

James A. Gagnon, Jill A. Kreiling, and Kimberly L. Mowry

Abstract

Cytoplasmic RNA localization is a key mechanism for establishing cell polarity in a variety of organisms and cell types (reviewed in Holt and Bullock, 2009; Martin and Ephrussi, 2009). However, the mechanisms that control directionality during asymmetric RNA transport are not yet clear. To gain insight into this crucial process, we have analyzed the mechanisms directing polarized transport of RNA to the vegetal cortex in *Xenopus* oocytes. Using a novel approach to measure directionality of mRNA transport in live oocytes, we observe discrete domains of unidirectional and bidirectional transport that are dependent on distinct molecular motors. Specifically, both dynein and kinesin motors mediate steps in the vegetal RNA transport pathway, with dynein acting prior to kinesin. Moreover, dynein, but not kinesin-1, promotes unidirectional transport of RNA towards the vegetal cortex. Thus, vegetal RNA transport occurs through a multi-step pathway, providing a new framework for understanding the mechanistic basis of cell polarity.

Results and Discussion

Motor-driven RNA transport underlies cell and developmental polarity in many organisms including *Xenopus* oocytes, where localization of Vg1 mRNA to the vegetal cortex during oogenesis is essential for proper germ layer patterning during embryogenesis (Birsoy et al., 2006). Vegetal transport of Vg1 RNA is directed by a vegetal localization element (VLE), which can itself be correctly localized after microinjection into immature oocytes (Mowry and Melton, 1992) (Figure 1a). Kinesin molecular motors and cytoskeletal polarity have been implicated in transport of Vg1 mRNA to the vegetal cortex of the oocyte (Messitt et al., 2008). However, kinesin-1 and kinesin-2 have been shown to mediate transport only in the lower half of the vegetal cytoplasm (Messitt et al., 2008), near the RNA's final destination. These results suggest that directional RNA transport could require additional steps and rely on multiple microtubule motors; however, other motors or mechanisms directing transport in other regions of the oocyte cytoplasm have not yet been identified. Therefore, we investigated a role for dynein in vegetal transport in *Xenopus* oocytes. The dynein protein complex transports diverse cargoes, including RNAs (reviewed in Tekotte and Davis, 2002), on microtubule networks within the cytoplasm of all eukaryotic cells (reviewed in Kardon and Vale, 2009). Dynein is coupled to its cargos by dynactin, a distinct protein complex that specifically targets and adapts vesicles, organelles, spindles, peroxisomes, and mRNAs for dynein-dependent transport (reviewed in Schroer, 2004).

To disrupt dynein function *in vivo*, we used three approaches that have been previously shown to block cargo binding by disrupting interactions between dynein and dynactin (Burkhardt et al., 1997; Compton, 1998; Quintyne et al., 1999). Two approaches relied on overexpression of dynactin components, either the CC1 domain of $p150^{Glued}$ (Figure 3.1b) or dynamitin (Figure 3.1c), and the third used microinjection of a function blocking dynein antibody (Figure 3.S1). After disrupting dynein function, we microinjected fluorescently labeled VLE RNA to assess effects on mRNA localization (Gagnon and Mowry, 2010; Mowry and Melton, 1992). In untreated control oocytes, VLE RNA undergoing localization adopts a characteristic distribution in the vegetal cytoplasm, typified by a cup of RNA on the vegetal side of the nucleus and a crescent of RNA at the vegetal cortex, with the RNA in the process of localization evident in the vegetal cytoplasm between the cup and cortex (Figure 3.1a). Disruption of dynein function using all three approaches caused a strong enrichment of VLE RNA in a cup-like region on the vegetal side of the oocyte nucleus and significant loss of RNA accumulation in the lower vegetal cytoplasm and cortex (Figure 3.1b,c), relative to VLE RNA localization in control oocytes (Figure 3.1 a,d). The observed loss of VLE localization after disruption of dynein function reveals a critical function for dynein in vegetal RNA localization.

To address whether dynein plays a direct role in vegetal RNA transport, we tested whether dynein is specifically associated with Vg1 RNA. We first performed immunofluorescence for dynein in oocytes that were microinjected

with fluorescent VLE RNA. Dynein (Figure 3.1e) is co-localized with VLE RNA (Figure 3.1e′) at the cortex and throughout the vegetal cytoplasm, but not in the cup region (Figures 3.1e′′, 3.1f). In addition, immunoprecipitation of dynein complexes using a cytoplasmic dynein intermediate chain (cDIC) antibody specifically recovered Vg1 mRNA but not a highly abundant control RNA, EF1α (Figure 3.1g). Moreover, immunoprecipitation of dynein complexes also recovered known components of the Vg1 mRNP (Lewis and Mowry, 2007), including PTB, Vera and Staufen, but not a non-relevant RNA-binding protein, ribosomal protein S6 (Figure 3.1h). Together, these data support a direct role for dynein in vegetal RNA transport.

The phenotype observed upon dynein disruption (Figures 3.1b,c) is quite distinct from that previously observed upon expression of a dominant negative kinesin-1 rigor mutant (Messitt et al., 2008) (Figure 3.2a). Dynein interference leads to accumulation of VLE RNA in the cup region on the vegetal side of the nucleus (Figures 3.1b-c, 3.2b), while kinesin-1 disruption with the rigor mutant, which locks cargo onto microtubules at the site of kinesin binding (Messitt et al., 2008; Nakata and Hirokawa, 1995), results in accumulation of VLE RNA in the lower vegetal cytoplasm (Figure 3.2a). The RNA is absent from the cup region and the upper vegetal cytoplasm. These results suggest that dynein and kinesin mediate distinct, possibly sequential, steps in vegetal RNA transport. To order these motors in the RNA transport pathway we performed molecular epistasis experiments by disrupting the function of both motors simultaneously in oocytes

and monitoring localization of microinjected VLE RNA. We observed that accumulation of VLE RNA in the perinuclear cup after disruption of dynein function by CC1 overexpression was unaffected by kinesin-1 rigor expression while the kinesin-1 rigor phenotype was significantly reduced (Figure 3.2c,d). Because the dynein-disruption phenotype of accumulation in the perinuclear cup region is predominant upon simultaneous disruption of dynein and kinesin-1 function, these results indicate that dynein functions upstream of kinesin-1 in the transport pathway.

Because dynein and kinesin have been reported to act together in transport of some cargos (Hendricks et al., 2010; Kural et al., 2005; Ling et al., 2004), we next asked whether both motors were present on a single ribonucleoprotein particle (RNP). Alternatively, these two motors might traffic RNPs independently, presumably in opposite directions along microtubules. To test this, we imaged endogenous dynein and kinesin molecular motors using immunofluorescence in oocytes injected with fluorescently labeled VLE RNA. Strong co-localization (Figure 3.2e) between VLE RNA (Figure 3.2e′), dynein (Figure 3.2e′′), and kinesin-1 (Figure 3.2e′′′) is evident in the vegetal cytoplasm. At higher magnification (Figure 3.2f), numerous RNP particles are apparent, which contain both dynein and kinesin-1. Quantification of particle co-localization (Figure 3.2g) reveals significant colocalization of dynein RNP particles with kinesin. Notably, co-localization with kinesin is greater in the lower vegetal cytoplasm, indicating that kinesin may be recruited to the dynein-RNP in that region. These results

further suggest that both motors can be bound to single RNP particles during vegetal localization. Our data support a model in which dynein controls vegetal RNA transport in the upper vegetal cytoplasm, while kinesin motors mediate RNA transport in the lower vegetal cytoplasm. Yet, dynein is colocalized with VLE RNA at the vegetal cortex (Figures 3.1f, 3.2e). Clearly, an understanding of vegetal RNA transport dynamics is impossible to attain using standard fixed cell imaging techniques.

To define specific roles for molecular motors in directional RNA transport, we developed a live imaging system for *Xenopus* oocytes by adapting a method first established for imaging RNA transport in yeast (Bertrand et al., 1998). Briefly, a fluorescent protein, mCherry (Shaner et al., 2004) (mCh) in this case, is tethered to the RNA of interest by exploiting a strong binding interaction between the MS2 bacteriophage coat protein (MCP) and a 21-nucleotide RNA hairpin (Coller and Wickens, 2007) (Figure 3.3a). In live *Xenopus* oocytes, injection of a non-localized RNA tagged with MS2 hairpins (βG-MS2) into oocytes expressing mCh-MCP produced a signal that was uniform throughout the cytoplasm (Figure 3.3b). By contrast, oocytes expressing mCh-MCP injected with VLE-MS2 RNA exhibited a strong signal at the vegetal pole (Figure 3.3c), demonstrating that tethering multiple fluorescent proteins to RNA can be used to monitor RNA localization in live *Xenopus* oocytes.

As a first approach to measure RNA transport *in vivo*, we used Fluorescence Recovery After Photobleaching (FRAP) (Sprague and McNally, 2005). The large size of the *Xenopus* oocyte (~300 μm diameter at stage III (Dumont, 1972)) provides a unique opportunity to assess RNA mobility in multiple regions of the vegetal cytoplasm: adjacent to the nucleus (Figure 3.3d, Region 1), in the upper vegetal cytoplasm (Figure 3.3d, Region 2), and in the lower vegetal cytoplasm (Figure 3.3d, Region 3). FRAP analysis showed the mobility of VLE-MS2 RNA in both the upper and lower vegetal cytoplasm ($t_{1/2}$ (sec) = 86.7 ± 6.72) to be significantly lower than that of a non-localizing RNA βG-MS2 ($t_{1/2}$ (sec) = 16.6 ± 1.92). Yet, the mobility of VLE-MS2 RNA outside of the vegetal cytoplasm (Figure 3.3d, Region 4) is similar ($t_{1/2}$ (sec) = 16.4 ± 0.97) to that of non-localizing βG-MS2, suggesting that VLE RNA can diffuse freely outside of the vegetal cytoplasm. The behavior of VLE RNA in the vegetal cytoplasm is dependent on microtubules, as VLE RNA mobility is similar to βG-MS2 RNA after nocodazole treatment to disrupt microtubules ($t_{1/2}$ (sec) = 16.2 ± 2.13). Because the FRAP experiments assess the mobility of the entire population of MS2-tagged RNAs in a given region, these results indicate that the majority of VLE-MS2 RNAs in the vegetal cytoplasm are not moving rapidly at any particular time. Moreover, the reduced mobility of VLE RNA in the vegetal cytoplasm is likely due to interaction of the RNA with the microtubule cytoskeleton, presumably through interaction with molecular motors.

To assess the effects of dynein disruption in live oocytes, we performed FRAP in the vegetal cytoplasm in oocytes expressing dynamitin and in control oocytes. We carried out FRAP in regions 1 and 3, but not region 2, due to enlargement of the cup region in oocytes expressing dynamitin (Figure 3.1b), which made measurements in region 2 unreliable. As shown in Figure 3.3e, we discovered that dynein disruption significantly slows RNA mobility in the cup (Region 1), but had no effect on mobility in Region 3. These results suggest that dynein is required to move RNA out of the cup region towards the vegetal cortex and further indicate that RNA movement in the lower vegetal cytoplasm may not depend on dynein. Taken together, our live-imaging results support a model in which dynein is responsible for RNA transport in the upper vegetal cytoplasm, while kinesin motors carry out transport in the lower vegetal cytoplasm.

Directionality is crucial to understanding the mechanisms controlling asymmetric RNA transport, and roles for motors that move in opposing directions on microtubules complicate this issue. We have previously described a subpopulation of microtubules, present at the vegetal pole during mid-oogenesis, which are oriented with plus ends at the cortex (Messitt et al., 2008). This sub-population is superimposed over a microtubule network present throughout the oocyte cytoplasm, which is oriented with minus ends towards the cortex (Gard, 1994). Thus, microtubules are polarized with plus ends at the nucleus and minus ends pointed towards the cortex in the upper vegetal cytoplasm, while in the lower vegetal cytoplasm the microtubule array is mixed, with microtubules

oriented in both directions (Messitt et al., 2008). Since vegetal RNA transport is dependent on microtubule-based molecular motors with opposing polarities, transport directionality might differ between these regions, with unidirectional transport in the upper vegetal cytoplasm and bidirectional transport in the lower vegetal cytoplasm. To assess transport directionality, we extended our live imaging system by incorporating a photoactivatable form of mCherry (Subach et al., 2009) (PA-mCh-MCP), which is non-fluorescent until laser stimulation at 405 nm. Thus, activation of the fluorophore, attached to VLE-MS2 RNA, in specific regions of the oocyte allows RNP transport directionality to be tracked in defined regions of the cytoplasm. Expressed *in vivo*, PA-mCh-MCP was non-fluorescent (Figure 3.4a, t=0) until activated by a six-second laser pulse, after which we observed robust activation (Figure 3.4a′, t=7 sec). To discern any potential asymmetry in transport, we then tracked RNA transport at timepoints after activation (Figure 3.4a′-a′′′) by measuring the fluorescence in four collection quadrants- left (L), right (R), animal (A) and vegetal (V)- surrounding the activation point (Figure 3.4a′′′, white circles). To quantify transport directionality in the animal/vegetal axis, we determined the ratio of intensities in the vegetal *vs.* animal collection quadrants over time (see Methods for details). Ratios at or near 1 indicate no bias in transport directionality, while values greater than 1 represent vegetally-directed transport. After activation in the upper vegetal cytoplasm (Region 2, Figure 3.4b), the ratio of vegetal- over animal-quadrant signal intensity (blue) is greater than 1 and increases over time, indicating directional transport towards the vegetal pole; no bias in left/right transport (red)

is detectable. Similarly, the averaged ratios of vegetal to animal intensities after eight minutes of RNA transport (Figure 3.4c) demonstrates significant bias of vegetal versus animal hemisphere transport (64:36, vegetal:animal; p=0.00001), again supporting a significant bias towards vegetal transport in the upper vegetal cytoplasm (Region 2). In striking contrast, activation in the lower vegetal cytoplasm (Region 3) exhibits no trend in either direction over time (Figure 3.4c), and no bias between vegetal and animal transport (Figure 3.4e, 47:53, vegetal:animal; p=0.16), indicating bidirectional transport in the lower vegetal cytoplasm. Control experiments show no transport bias in the animal hemisphere (Region 4, Figure 3.4f) or in the upper vegetal cytoplasm following microtubule disruption (Figure 3.4g). These results support a model for vegetal RNA transport in which kinesin-dependent transport in the lower vegetal cytoplasm is bidirectional, while dynein-dependent transport in the upper vegetal cytoplasm is strongly biased towards the vegetal cortex.

We have presented biochemical and *in vivo* interference data that demonstrate a direct role for dynein in transport of Vg1 mRNA and have allowed us to define distinct steps in the RNA transport pathway. Although molecular motors are known to play important roles in RNA transport, ordering individual steps into a coherent pathway has been impossible until now. The complementary phenotypes we obtained upon dynein and kinesin-1 disruption indicate roles for these motors in distinct transport steps (Figure 3.2). Moreover, the predominance of the dynein cup phenotype upon simultaneous disruption of

those motors, demonstrates that dynein functions upstream of kinesin in the transport pathway. Although dynein does not function in the lower vegetal cytoplasm, as evidenced by FRAP experiments showing that dynein disruption does not affect RNA mobility in that region (Figure 3.3f), dynein is colocalized with VLE RNA in the lower vegetal cytoplasm and at the oocyte cortex (Figures 3.1f, 3.S2). These results raise the intriguing possibility that in *Xenopus* oocytes, dynein may function not only in the first transport step, but may participate in anchoring as well. Although the mechanisms and machinery responsible for anchoring at the vegetal cortex are poorly understood, studies in *Drosophila* oocytes suggest that dynein may transition from a role in mRNA transport to a new role as a static anchor at the oocyte cortex (Delanoue et al., 2007). Taken together, these results suggest a transport pathway in which dynein is responsible for transport from the perinuclear region through the upper vegetal cytoplasm, followed by kinesin-mediated transport to the vegetal cortex, and ultimately anchoring of the RNA at the cortex.

Directionality is key to achieving polarized transport, and our live imaging experiments have revealed domains of RNA transport directionality that are under control of distinct molecular motors. Our results contrast with a recent study of *oskar* mRNA localization in *Drosophila* oocytes, which uncovered only a slight directionality bias in transport (Zimyanin et al., 2008). Our proposed vegetal RNA localization pathway, in which dynein-dependent transport in the upper vegetal cytoplasm precedes kinesin-dependent transport in the lower vegetal

cytoplasm, raises important questions regarding directionality, given the previously-described mixed microtubule polarity in the lower vegetal cytoplasm (Messitt et al., 2008). We gained insight into transport directionality by exploiting a photoactivatable version of mCherry (PA-mCh-MCP) (Subach et al., 2009). These experiments (Figure 3.4) revealed that transport in the upper vegetal cytoplasm is strongly biased towards the vegetal cortex, while transport in the lower vegetal cytoplasm is bidirectional. These results support a model in which bidirectional kinesin-dependent transport in the lower vegetal cytoplasm traffics on microtubules with plus-ends both away from and towards the vegetal cortex (Messitt et al., 2008). Most importantly, transport in the upper vegetal cytoplasm is strongly biased towards the vegetal cortex, providing a directional cue for vegetal transport. This represents a new model for the establishment of directional transport of cargo by coordinated functions of motors with opposing activity, which takes into account the inherent polarity of the cytoskeleton.

Methods

Fluorescent RNA synthesis and microinjection. Fluorescent RNA was transcribed and microinjected into *Xenopus* oocytes as previously described (Messitt et al., 2008). Briefly, 1 µg of linear template DNA was incubated for 2-4 hrs in a T7 RNA polymerase reaction (Gagnon and Mowry, 2010) supplemented with 50 µM Chromatide Alexa Fluor 546-14-UTP (Invitrogen). Labeled RNA was diluted to 50 nM and microinjected into stage III *Xenopus* oocytes. Oocytes were cultured, as previously described (Gagnon and Mowry, 2010), at 18˚ C for 8 - 16 hrs.

Cloning. The CC1 domain of chicken p150^{Glued} (a gift from T. Schroer (Quintyne et al., 1999), GenBank #NM_001031367), mouse p50/dynamitin (a gift from R. Vallee (Burkhardt et al., 1997), GenBank #NM_027151), mCherry (a gift from R. Tsien (Shaner et al., 2004), GenBank #AY678264), PAmCherry1 (a gift from V. Verkushka (Subach et al., 2009), GenBank #3KCT_A), and MS2 Coat Protein (a gift from R. Singer (Bertrand et al., 1998), GenBank #NP_040648) were amplified and subcloned into pSP64TSN (Kress et al., 2004) to create pSP64TSN-CC1, pSP64TSN-Dynamitin, pSP64TSN-mCherry, pSP64TSN-MCP-mCherry, and pSP64TSN-MCP-PAmCherry1 for *in vitro* transcription. Chimeric VLE-MS2 and βG-MS2 constructs were prepared by subcloning VLE (Mowry and Melton, 1992) or *Xenopus* β-globin (Krieg and Melton, 1984) sequences with 24 multimerized MS2 binding sites (a gift from R. Singer (Bertrand et al., 1998)) into pSP73 to create pSP73-βG-MS2 and pSP73-VLE-MS2.

In vivo interference. Kinesin-1 rigor (Messitt et al., 2008), p50-dynamitin and CC1 RNAs were transcribed using mMESSAGE mMACHINE (Ambion) and diluted to 250-500 nM for microinjection. Oocytes were microinjected with dominant negative RNAs or purified control IgG (Sigma) or anti-dynein function blocking antibodies (Abcam), followed by injection with VLE RNA, and cultured as described above.

Immunohistochemistry and confocal microscopy. Oocytes microinjected with fluorescently labeled VLE RNA were permeabilized with 50 µg/ml proteinase K for 3 - 6 minutes, fixed in 3.7% formaldehyde for an hour, blocked in 2% BSA and 2% goat serum and incubated overnight with purified mouse anti-kinesin (SUK4 antibody, DSHB) and/or anti-dynein (DIC 74.1, Abcam), both at 1:100 dilution. Oocytes were then washed with PBT and incubated overnight with isotype specific mouse Alexa-633 and Alexa-594 fluorescent secondary antibodies (Invitrogen), washed with PBT, dehydrated and stored in anhydrous methanol at -20˚ C. Oocytes were imaged on either a Zeiss LSM510 or LSM710 confocal microscope as previously described (Gagnon and Mowry, 2010). VLE localization in each oocyte was scored as "wildtype," enriched in the "cup" on the vegetal side of the nucleus, enriched in the "lower half" of the vegetal cytoplasm, or "no localization." Oocytes were treated with 10 µg/ml nocodazole (Sigma-Aldrich) as previously described (Messitt et al., 2008).

Particle counting. Oocytes were imaged using a 63x oil immersion objective taking a single high resolution image through the vegetal pole. Particles containing both dynein and VLE RNA particles were identified by co-localization in the upper half (Region 2) and lower half (Region 3) of the vegetal cytoplasm for each oocyte. Each particle was subsequently scored for co-localization with kinesin.

Live cell imaging. After screening a panel of fluorescent proteins, mCherry ((mCh, Shaner et al., 2004) was chosen as the best candidate for live cell imaging in *Xenopus* oocytes because of its strong emission at 610 nm, where the autofluorescence of the oocyte cytoplasm is minimal (data not shown). Stage III albino oocytes were injected with 2 nl of either 250 nM mCh-MCP mRNA or 250 nM PA-mCh-MCP mRNA and incubated overnight in oocyte culture medium (OCM, 50% L15 medium (Sigma-Aldrich), 15 mM HEPES (pH 7.6), 1 mg/ml insulin (Sigma-Aldrich), 100 mg/ml gentamicin (Gibco), 50 U/ml nystatin (Gibco), 50 U/ml penicillin (Gibco), 50 mg/ml streptomycin (Gibco)) to allow protein expression. Oocytes in some cases were incubated in 10 µg/ml nocodazole and subsequently injected with 2 nl of either 250 nM WT-MS2 RNA or βG–MS2 RNA. For imaging, oocytes were mounted in fluorodishes (WPI Inc.) in OCM containing 1% low melting temperature agarose (Sigma-Aldrich) to orient each oocyte for imaging in desired regions (Regions 1-4).

Fluorescence recovery after photobleaching. FRAP analyses were carried out using a Zeiss LSM 510 Meta Confocal Laser Scanning Microscope equipped with a 40x water correction C-Apochromat objective. A 5 µm circular region of interest (ROI) was bleached using the 405, 488, 561, and 633 laser lines at 100%. Four iterations of the laser during the bleach pulse lasted 9.5 seconds. Fluorescence recovery was monitored using the 561 laser line at 5-second intervals to track WT-MS2 recovery and 1-second intervals for βG-MS2.

FRAP Statistical analysis and curve fitting. FRAP data were fit to a single exponential rise to maximum model (1) using SigmaPlot 11 software.

$$y=a(1-e^{-bx})$$

where: a = end value of the recovered intensities, b = rate constant.

Half times of recovery were calculated using the previously determined rate constant (b) in the following equation:

$$t_{1/2} = \frac{\ln 2}{b}$$

Live cell photoactivation. A Zeiss LSM 710 Confocal Laser Scanning Microscope equipped with a 40x water correction C-Apochromat objective was used to acquire images. PA-mCh-MCP was activated by focusing the 405 laser on a 0.8 µm diameter circular ROI for 6 seconds at 100% power. Mobility of activated PA-mCh-MCP tethered to RNA was monitored in four 10 µm diameter ROIs surrounding the activation region of interest (animal, vegetal, left and right of the

activation ROI) using the 561 laser line at 2 second intervals for approximately eight minutes.

Statistical analysis of directionality. Only oocytes that exhibited at least a three-fold increase in fluorescence in the activation ROI after photoactivation were included in further statistical analyses. For each collection quadrant surrounding the activation ROI, a pre-activation background value was subtracted from the raw intensity value to give a Calculated Activation Value (CAV). These CAVs were then evaluated to deduce transport directionality. Transport bias for each oocyte in the vegetal/animal axis were generated by calculating a ratio of the vegetal collection quadrant CAV : animal collection quadrant CAV for each timepoint (*t*), and plotting the A:V ratio over time.

Likewise, transport bias for each oocyte in the left/right axis were generated by calculating a ratio of the left collection quadrant CAV : right collection quadrant CAV for each timepoint (*t*), and plotting the L:R ratio over time.

Endpoint transport directionality was calculated by taking CAVs at the last twenty timepoints (40 seconds of a 480 second timecourse), averaging them, and calculating intensity in each quadrant as a percentage of total intensity (100%) for each axis. These percentages were then averaged across all oocytes for each condition. P-values were generated using an unpaired Student's *t*-test.

Immunoprecipitation and protein blotting. Oocyte cell lysates were made in WozGold buffer (10 mM HEPES pH 7.4, 100 mM potassium acetate, 10 mM magnesium acetate, 5 mM EGTA, 0.1 M sucrose, 1 mM DTT, 0.4 mM Pefabloc SC (Sigma-Aldrich), 0.1% NP-40, 1 U/mL RNasin (Promega), 0.1 µg/mL leupeptin, 0.1 µg/mL antipain, 0.1 µg/mL trypsin inhibitor), centrifuged at 10 Kg for 10 minutes to remove organelles and membranes and pre-cleared with mouse IgG-agarose beads (Sigma) before overnight incubation with mouse IgG (Sigma) or mouse DIC 74.1 antibody (Abcam) pre-bound to Protein A-Sepharose beads (Millipore). After washes, bound samples were reserved for protein blotting, or samples were sequentially treated with DNase and proteinase K before RT-PCR as previously described (Messitt et al., 2008). Antibodies and concentrations for protein blotting were as follows: mouse anti-DIC - 1:1000 (Abcam), rabbit anti-PTB - 1:1000 , rabbit anti-Vera 1:1000, rabbit anti-Staufen 1:1000, rabbit anti-rS6 1:1000 (Santa Cruz).

Acknowledgements

This work was supported by Public Health Service grant GM071049 from the National Institute of General Medicine to K.L.M. J.A.G. was a predoctoral trainee supported in part by grant T32-GM07601. We thank our colleagues, M. Johnson, M. McKeown, C. Pratt, E. Powrie and T. Serio, for critical review of the manuscript, R. Creton, M. Feldbrügge, P. Hung, T. Messitt, C. Pratt, G. Williams and T. Wood for advice, discussions and technical support, and E. Gavis, T. Schroer, R. Singer, R. Tsien, R. Vallee and V. Verkhusha for generously providing reagents.

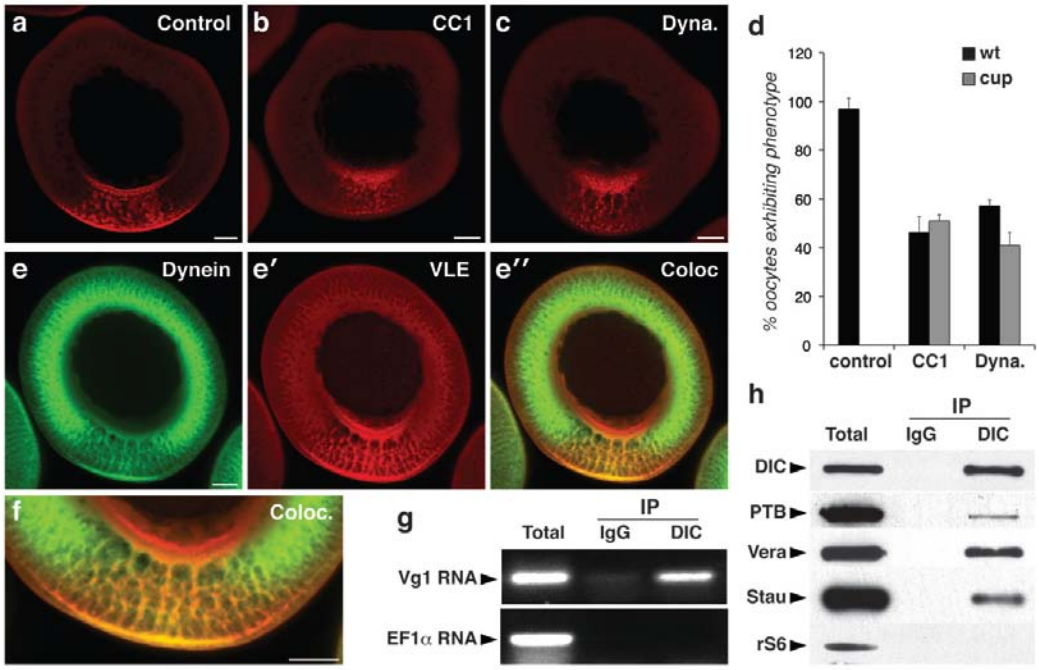

Figure 3.1: Dynein is in a complex with Vg1 RNA and is required for vegetal RNA localization.

(a-c) Fluorescently labeled VLE RNA was microinjected into oocytes expressing (a) no exogenous protein, (b) $p150^{Glued}$ CC1 domain, or (c) p50-dynamitin. Representative confocal images are shown, with the vegetal pole oriented towards the bottom. Scale bar = 50 μm. (d) Quantification of *in vivo* interference results (control [control, *n*=69], $p150^{Glued}$ CC1 [CC1, *n*=97], p50-dynamitin [Dyna., *n*=98]). Oocytes were scored for VLE RNA localization by confocal microscopy according to the phenotypes described in the Methods, with percent of oocytes exhibiting localization scored relative to the control. Error bars indicate standard deviation. (e) Oocytes microinjected with fluorescently labeled VLE RNA were probed with anti-dynein (DIC) and imaged by confocal microscopy. Dynein (e) is shown in green, VLE RNA (e′) is in red and co-localization (e′′) is in yellow. The

vegetal pole is towards the bottom and the scale bar = 50 μm. (f) Zoomed view of (e'') showing the vegetal cytoplasm. (g) Oocyte lysates were immunoprecipitated with non-specific mouse IgG or mouse anti-dynein (DIC). Bound RNAs were detected by RT-PCR using primers for Vg1 or EF1α as previously described (Messitt et al., 2008). (h) Oocyte lysates were immunoprecipitated as in (g) and probed with antibodies for dynein (DIC), hnRNP I/PTB (PTB), Vg1RBP/Vera (Vera), Staufen (Stau), or ribosomal protein S6 (rS6).

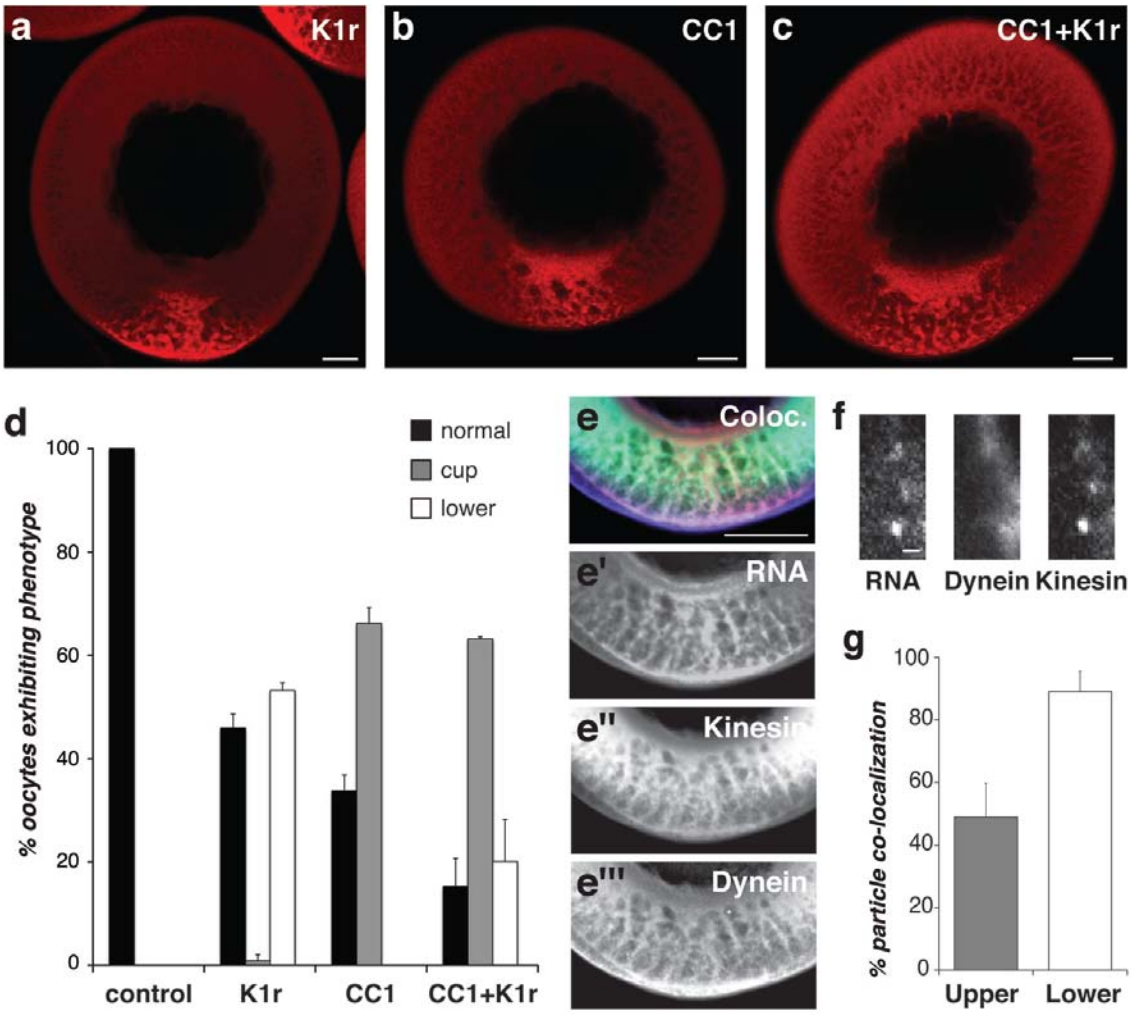

Figure 3.2: Dynein and Kinesin Cooperate to Transport Vg1 RNA

(a-c) Fluorescently labeled VLE RNA was microinjected into oocytes expressing (a) kinesin-1 rigor mutant (K1r), (b) $p150^{Glued}$ CC1 (CC1), or (c) both kinesin-1 rigor mutant and $p150^{Glued}$ CC1 (K1r+CC1). Representative oocytes are shown, with the vegetal pole towards the bottom. Scale bar = 50 μm. (d) Quantification of *in vivo* interference results for oocytes expressing no exogenous protein (control, *n*=167), kinesin-1 rigor (K1r, *n*=159), CC1 domain of $p150^{Glued}$ (CC1, *n*=209), both kinesin-1 rigor and CC1 (CC1+K1r, *n*=208). (e) Oocytes microinjected with fluorescently labeled VLE RNA were probed with anti-dynein

(DIC) and anti-kinesin-1 (SUK4). A confocal image of the vegetal cytoplasm is shown: (e) VLE RNA, (e') dynein, (e'') kinesin-1. For co-localization (e'''), VLE RNA is in red, dynein is green, and kinesin-1 is blue. Scale bar = 50 μm. (f) RNP particles are shown at high magnification: (f') VLE RNA, (f'') dynein, (f''') kinesin-1. Scale bar = 1 μm. (g) Quantification of dynein/VLE RNA particle co-localization with kinesin-1 in the upper and lower half of the vegetal cytoplasm, *n*=5 oocytes, 200 particles. All error bars indicate standard deviation.

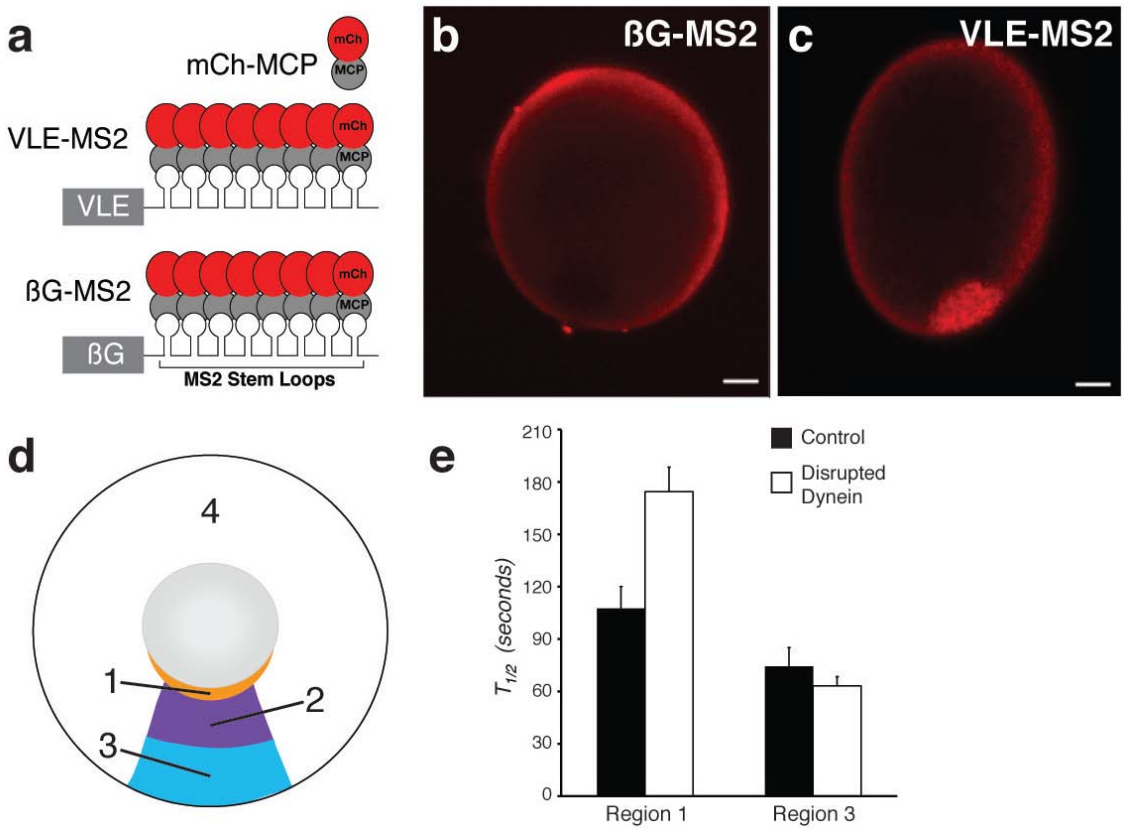

Figure 3.3: Live Imaging of RNA Localization Reveals Transport Dynamics

(a) Diagram of VLE RNA (VLE-MS2) and non-localizing β-globin RNA (βG-MS2) tagged with multimerized MS2 binding sites (Bertrand et al., 1998), which recruit MS2 coat protein fused to mCherry (mCh-MCP). (b) Oocytes expressing mCh-MCP and injected with βG-MS2 RNA exhibit uniform cytoplasmic fluorescence. (c) Oocytes expressing mCh-MCP and injected with VLE-MS2 RNA exhibit strong vegetal fluorescence. (b-c) The vegetal pole is towards the bottom and scale bars = 20 μm. (d) Diagram of oocyte showing regions used for analysis: immediately adjacent to the nucleus on the vegetal side (Region 1), the upper vegetal cytoplasm (Region 2), the lower vegetal cytoplasm (Region 3), and the animal hemisphere (Region 4). (e) Averaged FRAP recovery times for regions

shown in (e) in control oocytes (black bars) or oocytes expressing p50-dynamitin to disrupt dynein function (white bars). Control (Region 1, *n*=10; Region 3, *n*=10), Disrupted dynein (Region 1, *n*=21; Region 3, *n*=22). Error bars indicate S.E.M.

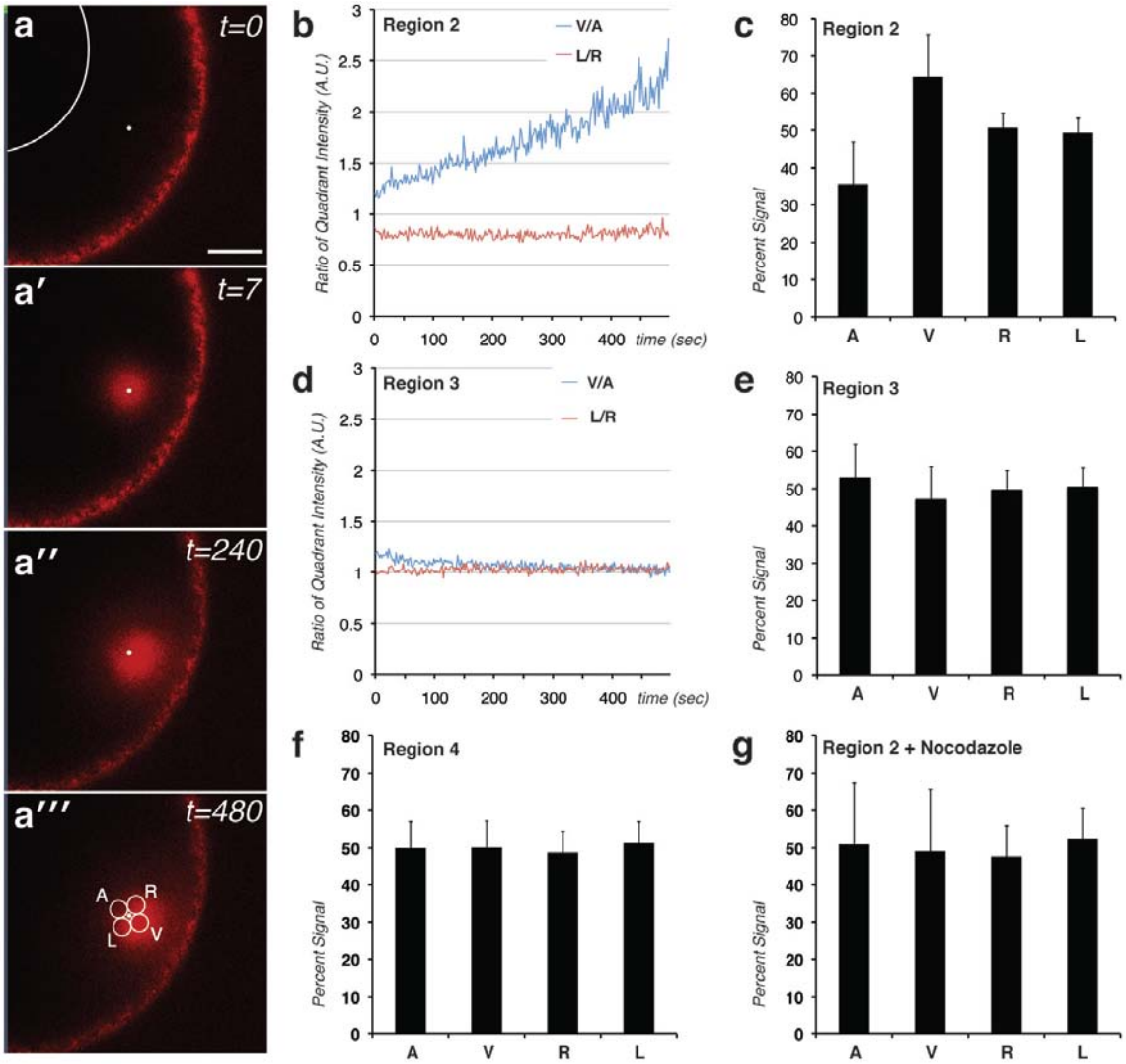

Figure 3.4: Distinct Regions of RNA Transport Directionality

(a) Prior to activation of (PA-mCh-MCP) in *Xenopus* oocytes (t=0), minimal fluorescence is observed. The activation point is shown by the small white dot and the oocyte nucleus outlined by a white line. Scale bar = 20 μm. (a′) 7 sec. after activation of PA-mCh-MCP, robust fluorescence (red) is evident at and around the activation point (white dot). (a″-a‴) By 240-480 sec. after activation, PA-mCh-MCP tethered to RNA can be visualized asymmetrically around the activation point. (a‴) The four collection windows are indicated by white circles

surrounding the activation point: V indicates the collection window on the vegetal side of the activation point and A shows the collection window on the animal side. L and R show the collection windows on the left and right sides, respectively. (b) After activation of PA-mCh-MCP in the upper vegetal cytoplasm (Region 2, Figure 3.3d), the ratio of V/A (red) and L/R (blue) intensities was plotted over time for a representative oocyte. (c) The endpoint intensities eight minutes after activation in the upper vegetal cytoplasm were determined in the four quadrants (A=animal, V=vegetal, L=left, R=right); *n*=10 oocytes. (d) After activation of PA-mCh-MCP in the lower vegetal cytoplasm (Region 3, Figure 3.3d), the ratio of V/A (red) and L/R (blue) intensities was plotted over time for a representative oocyte. (e) The endpoint intensities eight minutes after activation in the lower vegetal cytoplasm were determined in the four quadrants (A=animal, V=vegetal, L=left, R=right); *n*=10 oocytes. (f-g) Endpoint intensities eight minutes after activation in the animal hemisphere cytoplasm (f, *n*=19), and in nocodazole treated oocytes activated in the vegetal cytoplasm (g, *n*=12). All error bars indicate standard deviation.

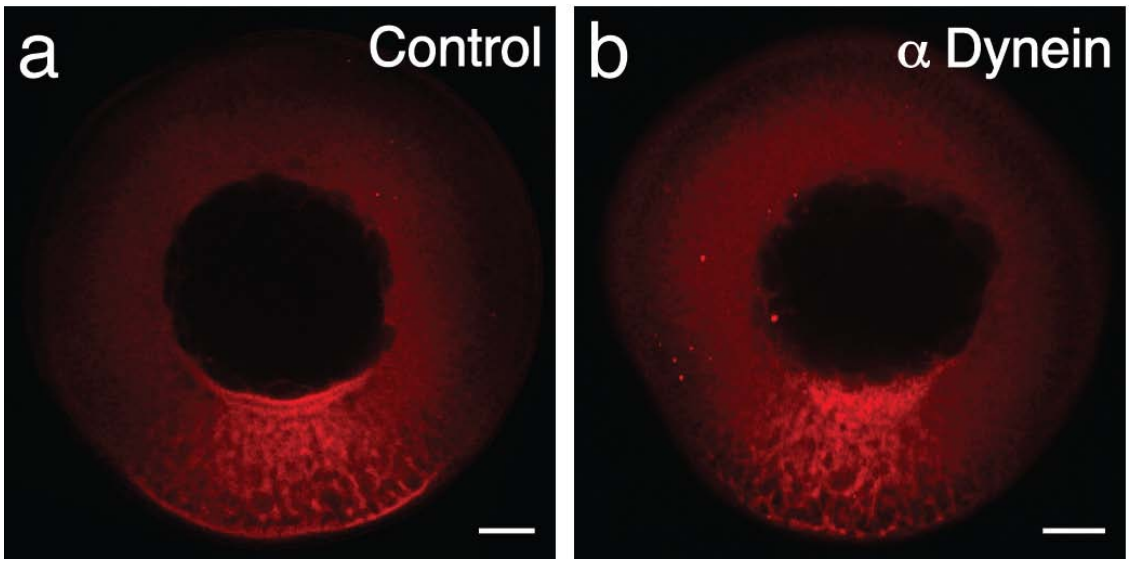

Figure 3.S1: A Role for Dynein Revealed by Antibody Interference

Oocytes injected with control (a) or function blocking DIC antibodies (b) were subsequently injected with fluorescently labeled VLE RNA. Representative confocal images are shown, scale bars = 50 μm.

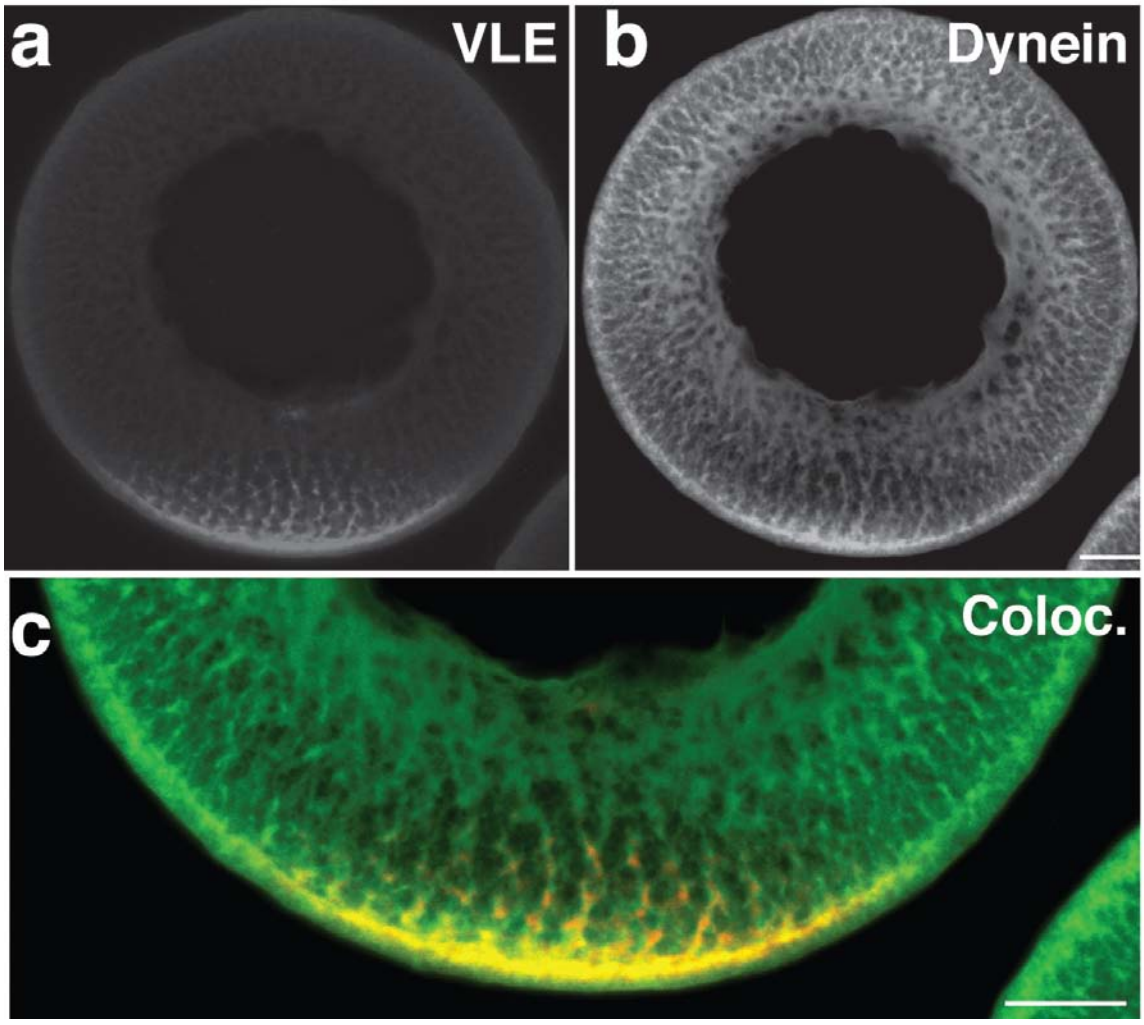

Figure 3.S2: Dynein Remains Co-Localized with VLE RNA After Localization

Oocytes injected with VLE RNA were incubated for 24 hours to allow the majority of localization to complete, then probed sequentially for dynein using DIC and fluorescent secondary antibodies before confocal microscopy. VLE RNA is shown in the red channel (a) and dynein is shown in the green channel (b). (c) A cropped and zoomed view shows co-localization in the vegetal cytoplasm, with VLE RNA in red, dynein in green, and co-localization in yellow. Scale bars = 50 μm.

Chapter 4: Visualization of mRNA Localization in *Xenopus* Oocytes

James A. Gagnon and Kimberly L. Mowry

Visualization of RNA Localization in *Xenopus* Oocytes.
Gagnon JA, Mowry KL.

Methods in Molecular Biology (In Press)

Abstract

Visualization of *in vivo* mRNA localization provides a tool for understanding steps in the mechanism of transport. Here we detail a method of fluorescently labeling mRNA transcripts and microinjecting them into *Xenopus* laevis oocytes followed with imaging by confocal microscopy. This technique overcomes a significant hurdle of imaging RNA in the frog oocyte while providing a rapid method of visualizing mRNA localization in high resolution.

Introduction

RNA localization is a conserved mechanism of establishing cell polarity in a variety of cell types and organisms. Such spatial regulation of gene expression can define specialized regions of the cell, and prominent examples include germ layer specification during vertebrate development and cytoskeletal rearrangements involved in cell motility (King et al., 2005; Shav-Tal and Singer, 2005; St Johnston, 2005).

Visualization of RNA distribution patterns has provided valuable insights into RNA transport steps and mechanisms. A number of techniques have been developed to visualize subcellular RNA localization, including in situ hybridization with digoxigenin- and fluorescently-labeled probes (Cote et al., 1999; Forristall et al., 1995; Kloc and Etkin, 1995), molecular beacons (Bratu et al., 2003), and fluorescent protein tethering (Bertrand et al., 1998; Forrest and Gavis, 2003).

RNA localization has been studied extensively in *Xenopus* laevis oocytes, where RNAs are localized during oogenesis and underlie patterning along the animal-vegetal axis (Cote et al., 1999; Czaplinski et al., 2005; Deshler et al., 1997; Forristall et al., 1995; Havin et al., 1998; Houston and King, 2000; King et al., 2005; Kloc and Etkin, 1995; Messitt et al., 2008; Mowry and Melton, 1992; Yisraeli et al., 1990; Yoon and Mowry, 2004; Zhang et al., 1998). The *Xenopus* oocyte offers several significant advantages for studies of RNA transport. First, oocytes are easily obtained through non-lethal surgery. Each surgery can yield

thousands of oocytes, making the system amenable to biochemical analyses. Second, oocytes are large in size, easily visible in detail under standard light microscopes, offering facile microinjection of RNA, proteins, DNA, and antibodies, which can be targeted into the nucleus or cytoplasm. Third, isolated oocytes are amenable to culture outside of the frog (Wallace et al., 1980; Yisraeli and Melton, 1988). However, one disadvantage is increasing opacity as yolk protein accumulates during oogenesis, complicating imaging approaches. Here we describe a method of visualizing RNA localization in *Xenopus* oocytes that overcomes this issue while providing striking, high-resolution images of in vivo RNA transport.

Materials

2.1 Reagents for in vitro RNA transcription

1. DEPC-treated deionized H_2O (DEPC-H_2O): Add 1-2 drops DEPC (Sigma-Aldrich) per 100 ml deionized H_2O. Incubate for 30 minutes at room temperature. Autoclave.
2. 10× Transcription Buffer (10× Tx): 60mM $MgCl_2$, 400 mM Tris-HCl (pH 7.5), 20 mM spermidine-HCl. Store as 1 ml aliquots at -20˚C.
3. 20x cap/NTP mix: 10 mM CTP, 10 mM ATP, 9 mM UTP, 2 mM GTP, 20 mM G(ppp)G Cap Analog (New England Biolabs # S1407L). Store as 25 µl aliquots at -20˚C.
4. Fluorescent nucleotides: Chromatide Alexa Fluor 488-5-UTP or 546-14-UTP (Invitrogen # C11403 and # C11404, see note 6).
5. G-50 solution: Hydrate 5 g Sephadex G-50 beads (Sigma Aldrich) in 100 ml deionized H_2O. DEPC-treat as detailed above (see Materials 2.1.1). Before use, add the following: 0.5 ml 0.2 M EDTA, 1 ml 1 M Tris pH 8.0, 0.5 ml 20% SDS (all solutions must be RNase-free). Store at 4˚ C.
6. G-50 column: Remove and discard the plunger from a 3 ml syringe (BD Biosciences) and place the barrel of the syringe into a 15 ml conical tube (Corning). Plug the syringe with a small amount of glass wool (a plug about half the size of a penny). Swirl the G-50 solution (see Materials 2.1.5) to resuspend beads. Add 2 ml G-50 solution to the empty column. Spin for 1 minute at 1,000 × *g* in benchtop centrifuge. Add 200 µl DEPC-H_2O to each

column. Spin. Repeat wash twice more for a total of three washes. Remove the column to a fresh 15 ml conical tube prior to use.

2.2 Oocyte microinjection

1. Needles: To make beveled glass needles with an outer diameter of ~0.05 mm, we pull 3.5 inch capillaries (Drummond Scientific item # 3-000-203-G/X) using a Sutter Instrument Co. micropipette puller. Needles are beveled to an angle of 40˚ using a Narishige Co. EG-4 micropipette grinder.
2. Microinjection Apparatus: Harvard Apparatus model # PLI-100.
3. Injection dish: We line a small plastic dish with 1/8th inch thick black foam rubber, cut to fit and secured to the dish with double-sided tape. The white oocytes stand out against the black foam background.
4. MBSH buffer: 88 mM NaCl, 1 mM KCl, 2.4 mM $NaHCO_3$, 0.82 mM $MgSO_4 \cdot 7H_2O$, 0.33 mM $Ca(NO_3)_2 \cdot 4H_2O$, 0.41 mM $CaCl_2 \cdot 6H_2O$, 10 mM HEPES (pH 7.6).

2.3 Oocyte culture

1. Collagenase Solution: 3 mg/ml collagenase (Sigma-Aldrich # C0130), 0.1 M KPO_3^+ (pH 7.4).
2. 24 well plates (Sigma-Aldrich #CLS 3527).
3. Antibiotic Stocks: Nystatin (10,000 U/ml, Gibco, store in 1 ml aliquots at -20˚C). Penicillin/Streptomycin (10,000 U/ml, 10 mg/ml, Gibco, store in 100 µl aliquots at -20˚C). Gentamicin (10 mg/ml, Gibco, store at 4˚ C).

4. Incomplete Oocyte Culture Medium (In-OCM): 50% L-15 medium (Sigma-Aldrich), 15 mM HEPES (pH 7.6), 1 mg/ml insulin (Sigma-Aldrich). We typically make a 50 ml stock, which can be stored at 4°C for up to two months.
5. Complete Oocyte Culture Medium (OCM): 980 µl In-OCM, 5 µl nystatin stock, 10 µl gentamicin stock, 5 µl penicillin/streptomycin stock. Sterilize using a 0.22 µm syringe filter (Millipore # SLGP033RS). Make fresh, do not store.

2.4 Oocyte fixation and immunofluorescence

1. Glass vials for fixation (Fisher # 03-339-26B).
2. 10x MEM Stock: 1 M MOPS (pH 7.4), 20 mM EGTA, 10 mM $MgSO_4$. Store at room temperature.
3. MEMFA: 1 ml 10x MEM, 1 ml 37% formaldehyde, 8 ml deionized H_2O. Prepare fresh for each use.
4. Methanol: Anhydrous methanol (Alfa Aesar # 41467), must be fresh.
5. Proteinase K Solution: 0.1 M Tris pH 7.5, 10 mM EDTA, 50 µg/ml Proteinase K (Sigma-Aldrich). Prepare fresh for each use.
6. PBT: PBS (pH 7.4), 0.2 % BSA, 0.1 % Triton X-100 (Roche).
7. Alexa Fluor 633 - coupled secondary antibodies (Invitrogen # A21070 [goat anti-rabbit IgG] or # A21050 [goat anti-mouse IgG], see Note 6).

2.5 Confocal Microscopy

1. Murray's Clearing Medium: 2 parts benzyl benzoate (MD Biomedicals), 1 part benzyl alcohol (Fisher). Store at room temperature.
2. Imaging dishes: FluoroDish (WPI Inc. # FD3510-100).

Methods

3.1 Preparation of fluorescently labeled RNA by in vitro transcription

1. Linearize plasmid DNA containing the relevant sequence and upstream promoter sites for transcription by T7, SP6, or T3 RNA polymerase.
2. Resuspend DNA at 1 µg/µl with DEPC-H_2O (see Materials 2.1.1).
3. Add the following reagents, in order, to a sterile 1.5 ml tube:

2 µl 10× Tx buffer (see Materials 2.1.2)

1 µl 20x cap/NTP mix (see Materials 2.1.3)

11 µl DEPC-H_2O (see Materials 2.1.1)

1 µl 0.2 M DTT

1 µl RNasin (Promega)

1 µl linearized DNA template (see Methods 3.1.1)

1 µl 1 mM Alexa Fluor 546-14-UTP (see Materials 2.1.4)

1 µl [α-^{32}P]UTP (1 µCi/µl, Perkin Elmer)

1 µl RNA Polymerase (Promega)

4. Mix reagents gently and centrifuge briefly (10 sec. in a microcentrifuge).
5. Incubate for 2-4 hours at 37° C, covering the tube with aluminum foil to prevent photobleaching of fluorophore.
6. Add 1 µl 1 mg/ml RNase-free DNase (Promega) to degrade template DNA.
7. Incubate 15 minutes at 37° C.
8. Add 79 µl 20 mM EDTA (pH 8.0) to stop the reaction.
9. Remove 1 µl to a separate tube, labeled as “input” and save.

10. Spin reaction through a 1 ml G50 column (see Materials 2.1.6), which will retain unincorporated nucleotides while excluding full length mRNA.

11. Concentrate the RNA by ethanol precipitation:

a. Add 250 µl 100% ethanol, 10 µl 7M ammonium acetate, 1 µl carrier RNA (yeast tRNA at 10 µg/µl) or 1 µl glycogen (20 mg/ml).

b. Mix well and freeze until solid on dry ice or at -80°C for ~30 minutes.

c. Spin at maximum speed in microcentrifuge for 15 minutes. Remove the supernatant. Wash the pellet with 150 µl of cold 75% ethanol.

d. Spin for 3 minutes at maximum speed in microcentrifuge. Remove supernatant and allow the pellet to dry for 3 minutes, at 37°C.

12. Resuspend RNA in 11 µl DEPC-H_2O. Remove 1 µl to a separate tube, labeled as “incorporated”.

13. Determine the percent incorporation (see Note 1) and bring the RNA to a final concentration of 50 nM in DEPC-H_2O (see Note 2 for troubleshooting RNA yield).

14. The RNA should be frozen in 5 µl aliquots, for single use (to avoid freeze/thaw cycles), and can be stored for several months at -80°C.

3.2 Oocyte microinjection

1. RNA preparation: Thaw an aliquot of RNA (50 nM), and denature the RNA at 70° C for 3-5 minutes. Spin for 10 minutes at maximum speed in microcentrifuge to remove particulates, remove to a fresh tube and keep on ice.

2. Oocyte preparation: Surgically remove oocytes from albino *Xenopus* laevis females (Nasco) and defolliculate by incubation in Collagenase Solution (see Materials 2.3.1) for 15 minutes, gently shaking (~200 rpm) at 18˚C. Check to ensure ovary has released the defolliculated oocytes (see Note 4). Wash the oocytes three times with MBSH buffer (see Materials 2.2.4). Manually sort stage III/IV oocytes (Dumont, 1972), which are 250-400 μm in diameter.
3. Oocyte microinjection:
    a. Calibrate needle with DEPC-H_2O to deliver 2 nl per injection.
    b. Load RNA into needle.
    c. Place sorted oocytes in injection dish (see Materials 2.2.3) in MBSH buffer.
    d. Carefully inject each oocyte with 2 nl of RNA at 50 nM.
    e. Expel RNA, rinse needle with DEPC-H_2O, and load the next RNA for injection (see Note 3).

3.3 Oocyte culture

1. Place injected oocytes in a well of a sterile 24 well plate.
2. Remove buffer and replace with 400 μl OCM (see Materials 2.3.5) per well.
3. Incubate oocytes at 18° C for time points ranging between 8 and 48 hours.
4. After culture, remove any dead oocytes; we routinely observe >90% survival.

3.4 Oocyte fixation and immunofluorescence

1. Place cultured oocytes in glass vials (see Materials 2.4.1) and rinse with MBSH (see Materials 2.2.1).
2. If you are co-imaging RNA and protein distribution, skip to Methods 3.4.3. If you are imaging RNA alone, fix oocytes as follows:
    a. Remove MBSH and replace with 1 ml MEMFA (see Materials 2.4.3, Note 5).
    b. Rock for 20 minutes at room temperature.
    c. Wash oocytes once with 1 ml MBSH. Skip to Methods 3.4.4.
3. For immunofluorescence, treat the oocytes with Proteinase K, followed by fixation and antibody incubation, as follows:
    a. Remove MBSH and add Proteinase K solution (see Materials 2.4.5). Incubate for three minutes at room temperature.
    b. Remove Proteinase K solution and wash twice with 1 ml MEMFA (see Materials 2.4.3, Note 5).
    c. Rock vials for one hour at room temperature in 1 ml MEMFA.
    d. Remove MEMFA and add 1 ml PBT (see Materials 2.4.6), rock at room temperature for 15 minutes. Repeat PBT wash twice, for a total of three washes.
    e. Replace PBT with 500 µl of fresh PBT plus 2% BSA and 2% goat serum and rock for two hours at room temperature.
    f. Replace solution with 500 µl PBT plus 2% BSA, 2% goat serum, and the appropriate dilution of primary antibody. (You may use 250 µl, if antibody is limiting.) Rock vials overnight at 4˚ C.

g. Replace the primary antibody solution with 500 µl PBT and rock at room temperature for 1.5 hours. Wash twice more with PBT, for a total of three washes.

h. Replace PBT with 500 µl PBT plus 2% BSA, 2% goat serum, and the appropriate dilution of the secondary antibody. Rock vials overnight at 4˚C.

i. Replace solution with 500 µl PBT and rock at room temperature for 1.5 hours. Wash twice more with PBT, for a total of three washes.

4. Dehydrate oocytes as follows:

a. Remove half of the volume of buffer (MBSH or PBT), and replace with an equal volume of anhydrous methanol (see Materials 2.4.4).

b. Remove half of the buffer/methanol solution and replace with an equal volume of anhydrous methanol. Repeat.

c. Remove all of the solution, replace with anhydrous methanol.

d. Wash once with anhydrous methanol.

5. Oocytes can be stored in methanol at -20° C until ready to image.

3.4 Imaging of RNA and protein distribution by confocal microscopy

1. Place Murray's Clearing Medium (see Materials 2.5.1) into a Fluorodish (see Materials 2.5.2).

2. Transfer oocytes from glass vials to an imaging dish, taking care to transfer as little methanol as possible.

3. Wait for several minutes for the oocytes to become optically clear. The oocytes should also sink to the bottom of the imaging dish. If not, gently tap the oocytes with forceps to break surface tension.
4. Image oocytes using an inverted confocal microscope. The entire field of oocytes can first be imaged using a 10× objective, which facilitates scoring localization for entire batches of oocytes. For high-resolution imaging of individual oocytes, a 20× or 63× objective should be used. (See also, Note 8.)
5. Examples of RNAs visualized using this protocol are shown in Figure 4.1. An example of RNA and protein co-localization is shown in Figure 4.2.

Notes

1. To calculate RNA yield, first determine cpm in "input" (see 3.1.9) and "incorporated" (see 3.1.12) samples using a standard scintillation counter (note that the "input" represents 1% of the sample, while the "incorporated" represents 10% of the sample).

$$\% \text{ incorporation} = \frac{\text{“incorporated”}}{10 \times \text{“input”}} \times 100$$

Since 2.64 µg is maximum yield of RNA for a 20 µl transcription reaction where GTP, the limiting nucleotide, is 0.1 mM. The yield of RNA (in µg) is calculated as:

RNA yield = % incorporation × 2.64 µg × 0.01

Typical reaction yields are in the range of 50-100 µl of RNA at 50 nM.

2. Problems with low RNA yield could be due to one or more of the following issues:

a. Low template DNA concentration: Quantify template concentration to ensure addition of 1 µg of linear DNA per transcription reaction.

b. Non-linear template DNA: Run a sample of template on an agarose gel to confirm complete linearization of plasmid DNA.

c. Impurity of template DNA: After linearization of the template DNA, treat with proteinase K, followed by phenol extraction to ensure removal of any contaminating protein. After ethanol precipitation, wash the DNA pellet with 75% ethanol to remove residual salts.

d. Loss of RNA during precipitation: Be careful to completely freeze precipitation reaction as described in Methods 3.3.11.b. Do not phenol extract the RNA.

e. RNase contamination: Verify that all enzymes are RNase-free; DEPC-treat all solutions as described in Materials 2.1.1.

3. The steps below can help to prevent problems with needle clogging during microinjection:

    a. Always centrifuge the RNA and carefully place on ice before loading into the needle. Centrifugation removes large particulate matter that quickly clogs the needle.

    b. Ensure slight outward pressure in the needle. This will prevent viscous cytoplasm from entering the needle upon piercing the oocyte.

    c. Keep the tip of the needle immersed in liquid whenever possible. If you have to take the needle out of liquid, quickly expel a drop to cover the tip. RNA can dry rapidly and clog the needle.

4. Problems with oocyte viability generally stem from extended collagenase treatment during oocyte isolation or non-sterile conditions during oocyte culture. The following precautions are necessary:

    a. Careful collagenase treatment is essential when isolating oocytes. Ovary should be cut with scissors before placing in collagenase solution. Defoliculation is complete when the majority of ovary chunks have completely released individual oocytes. Incubation should be closely monitored especially when using a new batch of collagenase for the first time; lots can vary greatly in activity. Some lots may take up to 25 minutes to reduce ovary to defolliculated oocytes. However, other lots may complete this task in half the time. Buffer pH is also extremely critical; if defolliculation takes an abnormally long time the buffer pH should be checked.

    b. OCM quality must be maintained to successfully culture oocytes. In-OCM should be a bright red/pink color. Any other color indicates that the pH has deviated from normal and the In-OCM should be discarded. Store In-OCM no longer than two months at 4˚ C. We always make complete OCM fresh immediately before use to culture oocytes. Some antibiotics lose their efficacy after repeated freeze / thaw cycles, resulting in bacterial or fungal contamination. We avoid this issue by aliquoting the anti-microbial stock solutions in small volumes, as described in Materials 2.3.3.

c. Successfully cultured oocytes maintain their spherical shape and do not stick to the bottom of the plate well during culture. Microinjection is a stressful procedure for oocytes, approximately 10% of oocytes will not survive even under the best conditions. Greater than 30% oocyte death after culture should be a warning sign that oocytes are not healthy and the experiment may be jeopardized.

5. The 10x MEM stock is good for several months as long as it remains colorless; store at room temperature wrapped in aluminum foil. 20 minutes is the minimum time for fixation; however, we can also fix for several hours without negatively affecting oocyte quality.

6. Autofluorescence of yolk proteins in the oocyte places limitations on the choice of fluorescent nucleotides and secondary antibodies. If possible, fluorescent nucleotides and secondary antibodies giving emission at longer wavelengths (e.g., 546 nm, 633 nm) should be used, as autofluorescence is significant at shorter wavelengths (e.g., 488 nm).

7. Problems with signal detection can occur, and may arise from a number of sources:

   a. No RNA signal/no localization: Adequate controls are critical to dissect issues with RNA signal. Negative controls include both uninjected oocytes (see Fig. 4.1C), and injection of a non-localizing control RNA (such as β-globin, see Fib. 4.1B), which should be uniformly distributed in the oocyte cytoplasm. Additionally, a positive control RNA that is known to exhibit localization (see Fig. 4.1C) is also critical. If both the

non-localizing RNA and the positive control show no fluorescence increase over background, there may be problems in synthesis of fluorescently labeled RNA. If, however, fluorescence of the positive control RNA is evident throughout the cytoplasm, the oocyte quality may be insufficient to support localization, and the experiment must be repeated.

b. No immunofluorescence (IF) signal: Antibody selection is crucial. The optimal antibody to use is one previously shown to work for IF in *Xenopus* oocytes or tissues. However, many antibodies have been shown to work for IF in other systems, but have not been tested in *Xenopus*. We have had success using such antibodies; however, when using an antibody that has not been tested for IF in any system, a series of careful controls must be used to ensure useful data. One essential negative control is the secondary only control, which is treated in an identically to the experiment oocytes but without incubation with primary antibody. A useful positive control when testing unknown antibodies is a proven antibody that works for IF in *Xenopus* oocytes. Finally, the blocking solution should use serum from the animal that the secondary was made; we routinely use goat serum and goat secondary antibodies.

c. Uncleared oocytes: Problems with oocyte clearing can result in residual opacity and inability to visualize signal deep into the oocyte. Often the nucleus cannot be visualized at all. This can be avoided by

carefully dehydrating the oocytes into anhydrous methanol during fixation. Fresh anhydrous methanol and multiple washes are required for dehydration, as even trace amounts of water will prevent clearing. Also, when transferring oocytes from methanol to Murray's Clearing Medium, great care should be taken to minimize the amount of methanol transferred with the single drop containing the oocytes. This ensures that the Murray's Clear penetrates the oocytes without being diluted with methanol.

8. Additional imaging tips: We generally image with a fairly open pinhole (>1 Airy Unit), as fluorescence intensity can be quite weak. However, results may vary from batch to batch of ooytes. Additionally, some autofluorescent subcellular structures may be visualized in the 488 nm (green channel), which can be useful for orienting oocytes along the animal/vegetal axis.

Acknowledgements

We would like to thank Mowry lab members past and present, who helped to develop these methods. This work was supported by NIH grant # R01GM071049 to KLM.

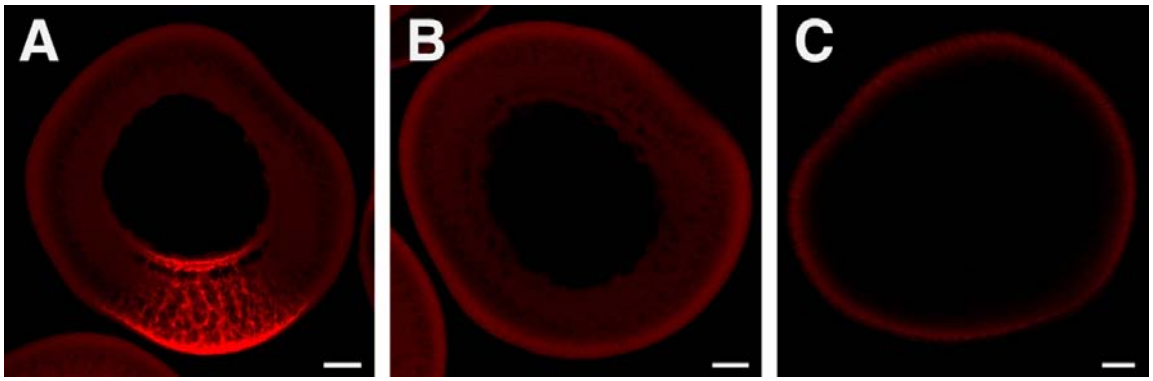

Figure 4.1: Vegetal RNA Localization in *Xenopus* Oocytes. Stage III oocytes were injected with Alexa-546-labeled VLE RNA (**A**) or Alexa-546-labeled vector control RNA (**B**) and cultured to allow localization. Control oocytes were uninjected (**C**). The VLE (Vg1 Localization Element; Mowry and Melton, 1992) directs RNA localization to the vegetal cortex, bottom, while the vector control RNA (of similar length, synthesized from pSP73) is uniformly distributed throughout the oocyte cytoplasm. Scale bar = 50 μm.

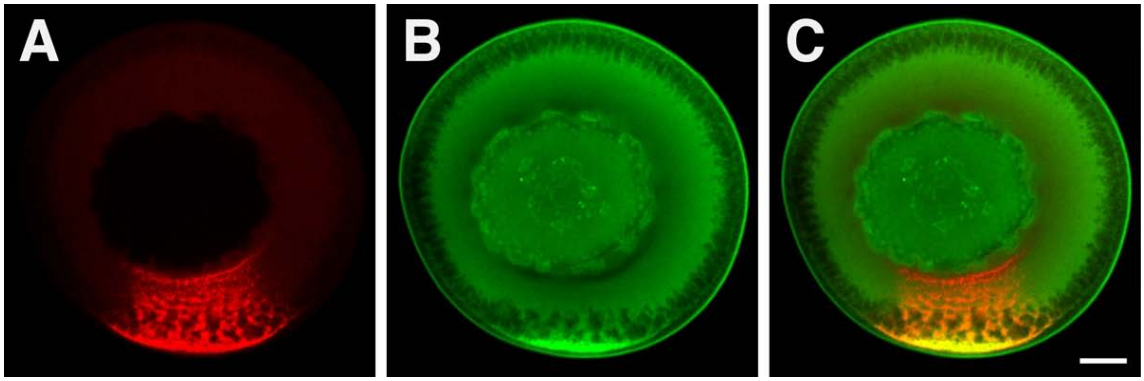

Figure 4.2: RNA and Protein Colocalization in *Xenopus* Oocytes. Stage III oocytes were injected with Alexa-546-labeled VLE RNA and cultured to allow localization of the injected RNA. Immunofluorescence was subsequently performed using antibodies directed against PTB/hnRNP I, an RNA binding protein that associates with VLE RNA and is required for VLE RNA localization (Cote et al., 1999). Vegetal localization of VLE RNA is shown in the red channel (**A**), and PTB distribution is visualized in the green channel (**B**). Co-localization of VLE RNA and PTB protein is evident in the overlay of the red and green channels, and is shown in yellow (**C**). Scale bar = 50 μm.

Chapter 5: RNA Localization *In Ovo*: Simultaneous Visualization of Two RNAs

James A. Gagnon and Kimberly L. Mowry

VISIONS: the art of science.
Gagnon JA, Mowry KL.
Mol Reprod Dev. 2009 Dec;76(12):1115.

Summary

RNA localization is a conserved mechanism of establishing cell polarity. In oocytes of the frog *Xenopus laevis*, Vg1 mRNA localizes to the vegetal pole during oogenesis and spatially restricted expression of Vg1 protein, a secreted growth factor, is required for germ layer specification in the developing embryo. Localization of Vg1 mRNA requires RNA sequence elements collectively known as a zipcode, which are sufficient to direct transport.

We are able to fluorescently label the Vg1 mRNA zipcode (green, Alexa Fluor 488) and a non-localized RNA (red, Alexa Fluor 546) and microinject these transcripts together into the nucleus of individual oocytes. The zipcode-containing RNA is exported and actively transported to the vegetal pole of the oocyte, while the control transcripts lacking the zipcode remain either in the nucleus or evenly distributed throughout the cytoplasm.

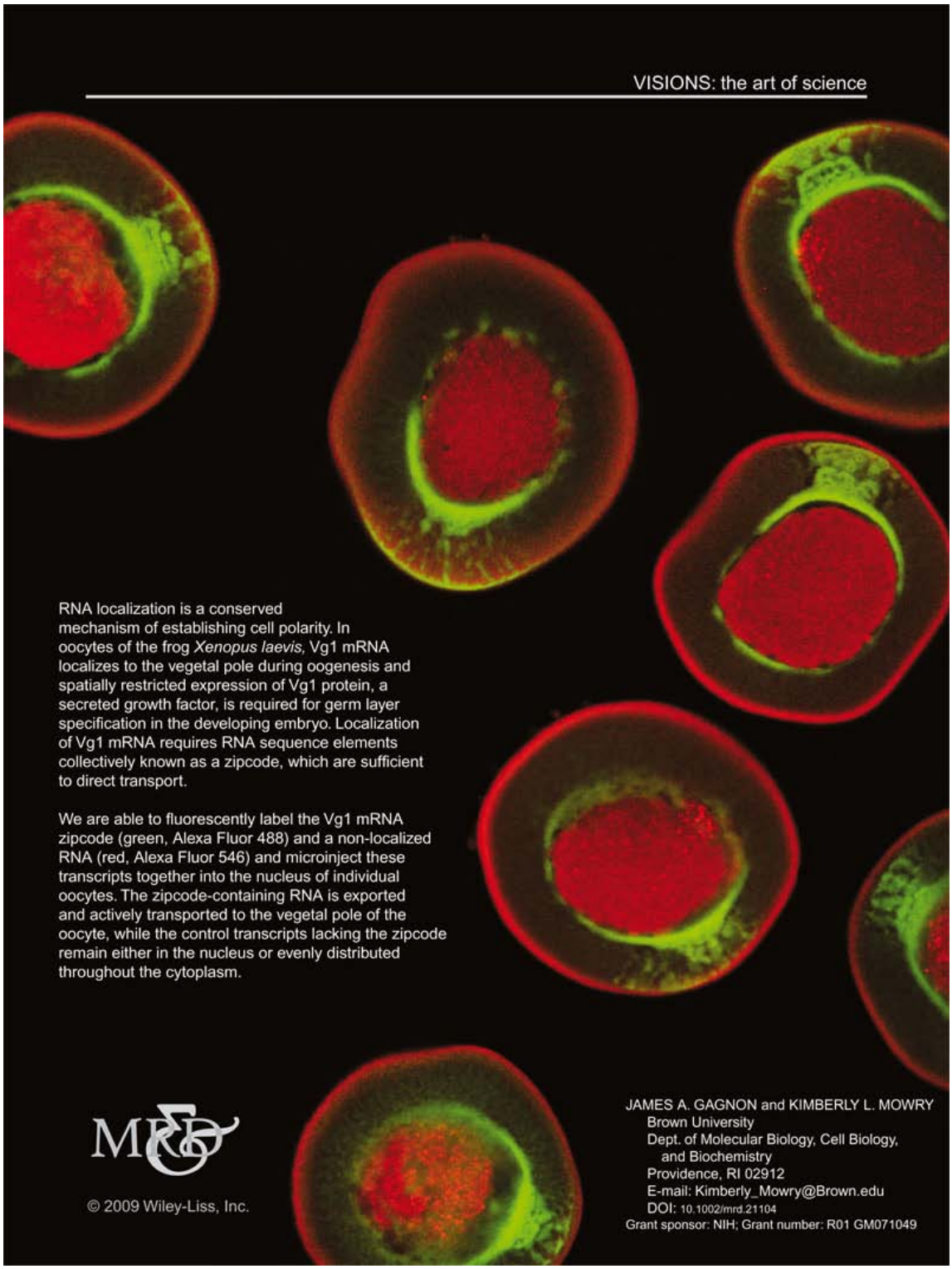

Figure 5.1. Simultaneous Visualization of Two RNAs.

Chapter 6: Conclusions and Future Directions

Vg1 is required for mesoderm and endoderm specification in the *Xenopus* embryo (Birsoy et al., 2006). Over the last fifteen years, we have learned much about the cis- and trans- factors required for spatial control of appropriate expression of Vg1. We have characterized much of the RNA localization machinery, and begun to unveil crucial aspects of the cytoskeleton that control Vg1 mRNA transport and anchoring. My work has focused on defining the factors and mechanisms that mediate active transport of Vg1 mRNA, and has advanced our understanding in several important ways.

First, we have demonstrated direct and distinct roles for kinesin and dynein molecular motors in Vg1 transport. Both types of motors co-localize with VLE RNA (Figures 2.1, 3.1). *In vivo* interference of kinesin-1 and kinesin-2 using rigor mutants interferes with VLE-directed localization, and supports a role for kinesin motors in transport of Vg1 mRNA in the lower vegetal cytoplasm (Figures 2.2, 2.4). Interference with dynein motor activity also blocks VLE-directed localization, but with a different phenotype (Figure 3.1). Interference with dynein function causes accumulation of VLE RNA in the cup, while interference with kinesin function causes accumulation at the midpoint of the vegetal cytoplasm. A molecular epistasis experiment in which we disrupted both kinesin and dynein function demonstrated that the disrupted dynein phenotype predominates (Figure 3.2), indicating that dynein functions upstream of kinesin in transport of VLE RNA.

Second, we have defined a developmentally timed reorganization of the cytoskeleton that generates a subpopulation of microtubules in the vegetal cytoplasm with plus ends at the vegetal cortex. Using EB1 immunofluorescence as a marker of microtubule plus ends over a timecourse of oogenesis, we demonstrated the emergence of plus ends at the vegetal cortex at the beginning of stage III (Figures 2.6, 2.S6). This coincides with localization of Vg1 and other late pathway RNAs (reviewed in King et al., 2005), and correlates with the requirement for plus end directed kinesin motors in transport of Vg1.

Third, we used a novel live imaging approach to define regions of unidirectional and bidirectional transport of Vg1 mRNA. We adapted a live imaging approach developed in yeast (Bertrand et al., 1998), and also applied in flies and tissue culture cells (Forrest and Gavis, 2003; Fusco et al., 2003) to track RNA mobility in the *Xenopus* oocyte for the first time (Figure 3.3). We demonstrated that VLE mRNA mobility is consistent with diffusion outside of the vegetal cytoplasm, and that the mobility of the RNA is dramatically reduced in the vegetal cytoplasm. We infer that only a small fraction of VLE mRNA is motile at any given moment, which may explain why localization takes such a long time to occur. We then modified this live imaging system to determine directionality of transport in different regions of the oocyte (Figure 3.4). We found that RNAs in the lower vegetal cytoplasm were transported bidirectionally (Figure 3.4), consistent with the mixed microtubule population in this region (Figure 2.6). In contrast, we found a strong bias towards directional transport in the upper vegetal cytoplasm

(Figure 3.4). Here, we do not observe mixed microtubule polarity and anticipate microtubules with plus ends at the germinal vesicle. Additionally, transport in this region appears to be dependent only on the dynein molecular motor (Figure 2.4). These data support a model in which dynein directs transport of Vg1 in the vegetal direction on an appropriately polarized microtubule network in the upper vegetal cytoplasm.

These findings integrate into a new model of Vg1 RNA localization in which transport mechanisms are distinct between the upper and lower vegetal cytoplasm. In the upper vegetal cytoplasm, dynein mediates transport in the vegetal direction, providing a directional source of RNA. In the lower vegetal cytoplasm, kinesin motors and potentially dynein cooperate to transport RNA bidirectionally. In this new model, an anchoring mechanism at the vegetal cortex is responsible for ensuring accumulation of Vg1 mRNA at its final destination. However, many features of this model remain to be addressed. Here I will discuss some of the new questions that emerge from this work.

Why so many motors?

Molecular motors from all three families (kinesin, dynein, myosin) are present and play essential roles in eukaryotes as diverse as yeast and man, indicating that motor-based transport on the cytoskeleton probably evolved long ago in simple eukaryotic organisms (reviewed in Hook and Vallee, 2006; Kirchner et al., 1999; Richards and Cavalier-Smith, 2005; Vale and Milligan, 2000). Perhaps as

cells became larger, more complex and polarized, different motor activities became coordinated to ensure cargo delivery over a complex cytoskeleton in a processive manner.

The oocyte cytoplasm, packed with yolk and other factors, represents a viscous and dynamic environment that complicates transport. Microtubule networks in the oocyte are not organized into highly organized and polarized bundles as in neurons; instead, they represent a complex network with subcompartments within domains of the cell (Gard, 1994; Messitt et al., 2008; Pfeiffer and Gard, 1999). The *Xenopus* oocyte is also a massive cell, approximately 300-400 μm in diameter at the stages we study (Dumont, 1972). Multiple motors could be required to coordinate directed transport of cargos over long distances across complex cytoskeletal networks.

The simple concept of a single motor protein being responsible for transport of cargo is increasingly being replaced with a more sophisticated model in which multiple molecules of motor proteins are bound to a single cargo, making transport more processive and continuous (reviewed in Holzbaur and Goldman, 2010). This new model may be applicable to Vg1 mRNA localization, since we and others have identified roles for three distinct molecular motors in transport (Betley et al., 2004; Chapter 2; Chapter 3; Messitt et al., 2008).

How is cytoskeletal reorganization controlled developmentally?

We observe the emergence of a subpopulation of microtubules during mid-oogenesis (Figure 2.6), but how this population is initiated or maintained is unknown. Microtubule organizing centers (MTOCs) nucleate microtubule growth with gamma-tubulin (Stearns and Kirschner, 1994). Recent evidence has suggested that MTOCs could be more dynamic and prevalent than previously thought (reviewed in Luders and Stearns, 2007). Gamma-tubulin at the midpoint of the vegetal cytoplasm could initiate a subpopulation of microtubules with plus ends towards the vegetal cortex. Indeed, the mitochondrial cloud contains gamma-tubulin, and could initiate this subpopulation before it breaks down at stage II of oogenesis (Kloc and Etkin, 1998). There is some evidence that gamma tubulin does accumulate at the midpoint of the vegetal cytoplasm in stage III oocytes (T.Messitt, personal communication).

Many factors are known to mediate microtubule dynamics. Microtubule-associated proteins (MAPs) are thought to be the main modulators of microtubule growth and stability (reviewed in Hirokawa, 1994). These factors could also be involved in developing and maintaining the subpopulation of microtubules in the vegetal cytoplasm. Additionally, microtubules can be altered by many post-translational modifications. Post-translational modifications of tubulin include phosphorylation, acetylation, tyrosination, polyglutamylation and polyglycylation (reviewed in Redeker, 2010). Although the functional consequences of these modifications are largely unknown, in some cases they have been shown to modify microtubule function (reviewed in Westermann and Weber, 2003) and can

be spatially restricted to subcellular regions (Janke and Kneussel, 2010). Modifications to microtubules could modulate interactions with molecular motors, providing a signal for transport, or could preferentially stabilize a subpopulation of microtubules.

Although microtubule polarity has been studied in some depth in the *Xenopus* oocyte (Messitt et al., 2008; Pfeiffer and Gard, 1999), we know little about MTOCs, MAPs, and patterns of post-translation modification. Applying new tools and reagents to the *Xenopus* oocyte could unveil mechanisms that control cytoskeletal reorganization that are relevant to studies of localized RNAs. First, new microscopes offer higher sensitivity and spatial resolution to probe the cytoskeleton in fixed and living cells. Second, new reagents have been developed to analyze the cytoskeleton. We and others have used the EB1 protein to monitor microtubule plus ends in fixed cells. By expressing a form of EB1 tagged with a fluorescent protein, we could use this same approach in living cells. Many groups have used tagged versions of tubulin subunits to monitor microtubule growth in live cells, an approach which could also uncover changes in microtubule polarity in the *Xenopus* oocyte (Andresen et al., 2004; Keppler et al., 2004; Stearns, 1995). Additionally, antibodies exist for some post-translationally modified tubulin subunits and could be used in a screen for modifications enriched in the vegetal cytoplasm. Broad profiling experiments such as the ones described above will pave the way for future investigation into mechanistic links between the cytoskeleton and RNA localization.

How do localized RNAs signal to the cellular machinery to be transported in different directions?

RNAs are localized in the *Xenopus* oocyte at multiple stages of oogenesis and to distinct locations. RNAs appear to localize through early and late pathways by different mechanisms (reviewed in King et al., 2005). RNAs localize to both the vegetal pole and the animal pole of *Xenopus* oocytes, and RNAs are also localized to the mitotic spindle in eggs (Blower et al., 2007; King et al., 2005). Genome-wide analyses of asymmetrically distributed RNAs promise to expand these lists. However, it is unknown how cis- and trans- factors signal to the cellular machinery for transport to these different locations. It is also poorly understood whether RNAs targeted to the same location contain similar cis-elements and are bound by the same trans- factors, or whether these RNAs are transported together in heterogeneous RNP granules.

Our work has developed a number of tools and approaches that could begin to dissect mechanisms of RNA transport to different destinations. Dominant negative approaches have defined roles for kinesin and dynein motors in transport of Vg1 mRNA. The same approach could be used to probe roles for these motors in transport of mRNAs to other locations, and at other times during oogenesis. It is also unclear what role the cytoskeleton plays in directing transport to the animal pole. We and others have used the microtubule disrupting drug nocodazole to demonstrate a role for microtubules in transport of

Vg1 mRNA (Chapter 2; Chapter 3; Messitt et al., 2008; Yisraeli et al., 1990). It will be informative to test roles for kinesin, dynein and the cytoskeleton in transport to the animal pole.

The development of techniques such as fluorescent labeling and microinjection of RNAs (Chapter 4) provides a quick and scaleable method of imaging *in vivo* RNA localization for any transcript. The imaging approach could be expanded to include the live imaging system developed in Chapter 3, which would provide information on transport dynamics and directionality. Localization of RNA is often directed by elements in the 3' UTR. Bioinformatic analysis of the 3' UTRs of transcripts localized by similar mechanisms has revealed similar cis- elements that direct common transport machinery (Andken et al., 2007; Betley et al., 2002; Choo et al., 2005; Lewis et al., 2004). New computational and biochemical tools for analyzing RNA secondary structure are becoming available (Ding et al., 2006; Hamada et al., 2009; Kertesz et al., 2010). By broadening these techniques to investigate more motifs in localized mRNAs, we could uncover transport mechanisms conserved between localized RNAs delivered to similar and different locations.

How and where are localized RNPs recognized as cargo and attached to molecular motors?

Both kinesin and dynein motors bind to their cargos through adapter proteins or complexes (reviewed in Hirokawa et al., 2009; Kardon and Vale, 2009). Staufen is thought to be an adapter protein for coupling several RNAs to the kinesin-1 motor (Brendza et al., 2000; Yoon and Mowry, 2004), but Staufen has little RNA-binding specificity, and it has not yet been shown that Staufen is required for interaction between cargo and motor in any system.

Similarly, several factors have been proposed to be required for dynein-mediated RNA transport. Two proteins, Bicaudal-D (BicD) and egalitarian (Egl), are required for transport of mRNAs by dynein in the *Drosophila* oocyte and embryo. While they were required for transport, neither protein had been shown to have RNA-binding activity. Recent work from the Bullock lab has shown that Egl is indeed an RNA-binding protein that specifically recognizes several RNAs localized by dynein (Dienstbier et al., 2009). The authors build a new model in which Egl recognizes and binds target RNAs, interacts directly with BicD, and binds to dynein or dynactin for transport. This represents an exciting and complete link between the cis-elements of a localized RNA and the transport machinery in a metazoan system. It remains to be seen how this model applies to dynein- directed transport outside of the fly.

Staufen has been shown by dominant negative interference experiments to be required for Vg1 RNA transport in the *Xenopus* oocyte (Yoon and Mowry, 2004). To our knowledge, BicD and Egl remain untested for roles in Vg1 RNA transport,

though *Xenopus* homologs exist. We have begun to develop tools that could be used to test these hypotheses directly in the *Xenopus* oocyte. We have adapted the MS2 tethering system to tether factors other than fluorescent proteins (P. Hung, J. Gagnon, personal communication). We could tether Staufen or Egl to fluorescently labeled non-localizing RNAs, and test whether the association of these factors with RNA is sufficient to produce transport by kinesin or dynein, respectively. These gain-of-function experiments could be supplemented with loss-of-function experiments using dominant negative interference.

What are the mechanisms that control RNA anchoring at the vegetal cortex? How do RNPs transition from active transport to anchored static particles?

The mechanisms that govern RNA anchoring at the final destination of localization remain mysterious in many systems. Vg1 mRNA anchoring appears to involve a non-coding RNA, the actin and tubulin cytoskeleton, and perhaps members of the Vg1 RNP (Kloc and Etkin, 1994; Yisraeli et al., 1990; Zhao et al., 2001). The mechanisms that mediate RNA anchoring can now be addressed using a live cell imaging system. Using a FRAP approach, it will be possible to examine how the dynamics of Vg1 mRNA transport are altered at the vegetal cortex. By using inhibitory drugs, antisense RNAs, and dominant negative proteins, we can probe the role of proposed factors in anchoring Vg1 mRNA. This approach is particularly amenable to studies of RNA anchoring because imaging at the cortex of the oocyte avoids issues related to the opacity of the deeper oocyte cytoplasm, which dims fluorescence signal significantly. New

tools are available to image the actin cytoskeleton. The LifeAct reagent is a small peptide derived from an actin binding protein, and can be used in live cells to image the actin cytoskeleton while avoiding toxicity issues related to other actin probes (Riedl et al., 2008). This reagent could be used in combination with the live imaging system to study interaction between actively transport RNPs and the actin network at the vegetal cortex.

It is also unknown if the transport machinery shares a molecular link with the anchoring mechanism. As previously discussed, dynein transitions from an active molecular motor to a static anchor in transport of *gurken* and pair rule transcripts (Delanoue and Davis, 2005; Delanoue et al., 2007). This provides the first demonstration of a molecular connection between the transport machinery and the anchoring apparatus. Perhaps this model applies just to RNA localization in the *Drosophila* oocyte and embryo, but it is tempting to apply this model elsewhere. Using our new tools and techniques, we can probe a role for dynein in anchoring Vg1 mRNA. For example, we could allow fluorescently labeled Vg1 mRNA to fully localize and become anchored, then disrupt interactions between dynein and Vg1 by overexpressing CC1 or dynamitin, and investigate whether we see release of Vg1 from the vegetal cortex. If so, this would suggest a conserved role for dynein in connecting the transport and anchoring steps of Vg1 mRNA localization.

What mechanisms control transport or enrichment of Vg1 mRNA at the cup?

Before Vg1 mRNA is transported vegetally, it becomes enriched from the bulk cytoplasm in a structure called the cup (Lewis et al., 2008). We hypothesize that the cup represents an important and distinct stage in Vg1 RNA localization for several reasons. In the absence of dynein and kinesin function, Vg1 mRNA is still able to accumulate in the cup (Figure 3.2). Careful examination of kinesin and dynein localization suggests that both motors are excluded from the cup region (Figure 3.2). Also, Vg1 mRNA outside of the vegetal cytoplasm is mobile at rates consistent with diffusion (Figure 3.3). I hypothesize that Vg1 mRNA diffuses in the bulk cytoplasm and accumulates at the cup through an entrapment mechanism. Another possibility is that Vg1 mRNA is directionally exported from the nucleus and feeds into the cup, though this model must be tempered by the fact that much maternal Vg1 mRNA is already diffuse in the cytoplasm before active transport, and thus directional export cannot entirely account for Vg1 mRNA in the cup. The factors that govern the process of accumulation in the cup are unknown; in fact, nothing is known about the composition of the cup or its role in Vg1 mRNA transport.

Conclusions

Much has been discovered about the factors that govern developmental processes such as RNA localization. This thesis presents several advances in our understanding of the mechanisms that govern RNA localization. As tools and

techniques become more sophisticated, so has our understanding of the mechanisms that govern these previously mysterious processes. However, many open questions remain. Further detailed analyses of the processes of recognition, directional transport and anchoring of localized RNAs will require complex and new biochemical, cell biological and imaging approaches - no easy task - but promise tantalizing and invaluable insight into the spatial and temporal organization of early development.

Appendix A: PTB/hnRNP I is Required for RNP Remodeling during RNA Localization in *Xenopus* Oocytes

Raymond A. Lewis, **James A. Gagnon** and Kimberly L. Mowry: *I contributed to Figure A.5.*

PTB/hnRNP I is required for RNP remodeling during RNA localization in *Xenopus* oocytes.
Lewis RA, Gagnon JA, Mowry KL.
Mol Cell Biol. 2008 Jan;28(2):678-86.

Abstract

Transport of specific mRNAs to defined regions within the cell cytoplasm is a fundamental mechanism for regulating cell and developmental polarity. In the *Xenopus* oocyte, Vg1 RNA is transported to the vegetal cytoplasm where localized expression of the encoded protein is critical for embryonic polarity. The Vg1 localization pathway is directed by interactions between key motifs within Vg1 RNA and protein factors recognizing those RNA sequences. We have investigated how RNA–protein interactions could be modulated to trigger distinct steps in the localization pathway, and found that the Vg1 RNP is remodeled during cytoplasmic RNA transport. Our results implicate two RNA binding proteins with key roles in Vg1 RNA localization, PTB/hnRNP I and Vg1RBP/vera, in this process. We show that PTB/hnRNP I is required for remodeling of the interaction between Vg1 RNA and Vg1RBP/vera. Critically, mutations that block this remodeling event also eliminate vegetal localization of the RNA, suggesting that RNP remodeling is required for localization.

Introduction

RNA localization is a widespread mechanism to generate cell polarity through the spatial restriction of gene expression to a defined subcellular region. Localized RNAs in somatic cells are thought to aid in distinct functions such as motility and structure, while those RNAs localized in germ cells play roles in establishing early developmental axes and act in germline specification (reviewed in Condeelis and Singer, 2005; Czaplinski and Singer, 2006; Gonsalvez et al., 2005; King et al., 2005; Kloc and Etkin, 2005; Kloc et al., 2005; Martin and Zukin, 2006; Minakhina and Steward, 2005). Transport of specific RNAs to defined regions within the cell cytoplasm is initiated by RNA–protein interactions that direct the recognition of the RNA and assembly of a ribonucleoprotein (RNP) transport complex. While RNA localization plays a key role in many cellular functions, the molecular mechanisms directing formation of a localization-competent RNP are not yet understood.

Among vertebrates, Vg1 mRNA is a prominent example of a localized mRNA that plays a role in embryonic patterning (reviewed in King et al., 2005; Minakhina and Steward, 2005). Vg1 mRNA is localized to the vegetal hemisphere cytoplasm in oocytes of the frog, *Xenopus laevis*, and restricted expression of the peptide growth factor encoded by Vg1 RNA is critical for correct patterning of the embryo (Birsoy et al., 2006; Weeks and Melton, 1987). The Vg1 RNA localization pathway initiates in the nucleus, where recognition of Vg1 RNA by RNA binding proteins with roles in localization first occurs (Kress et al., 2004). Upon export of

the early RNP complex from the nucleus to the cytoplasm, additional factors, including molecular motors, are assembled onto the Vg1 RNP (Betley et al., 2004; Kress et al., 2004; Yoon and Mowry, 2004). Although Vg1 RNA is transcribed from the earliest stages of oogenesis, the RNA remains uniformly distributed within the oocyte cytoplasm until mid-oogenesis, when it is transported to the vegetal cortex (Melton, 1987). The molecular events that trigger the active transport step of the localization pathway are not yet known, but may require remodeling of the early RNP complex to facilitate assembly of a transport-competent RNP.

Both *cis*-acting sequences within localized RNAs and *trans*-acting factors that interact with those sequences play important roles in the localization process. Localized RNAs contain sequences directing their localization, which are usually found within their 3′ untranslated regions (UTR) (reviewed in St Johnston, 2005). Transport of Vg1 RNA to the vegetal cortical cytoplasm during *Xenopus* oogenesis relies on a localization element (LE) found within its 3′ UTR (Mowry and Melton, 1992). The Vg1 LE (VLE) contains clusters of short sequence motifs implicated in localization (Bubunenko et al., 2002; Deshler et al., 1997; Gautreau et al., 1997; Kwon et al., 2002). Two of these motifs, termed E2 and VM1 sites, are bound, respectively, by two RNA binding proteins, Vg1RBP/vera and PTB/hnRNP I (Cote et al., 1999; Deshler et al., 1998; Deshler et al., 1997; Lewis et al., 2004). PTB/hnRNP I and Vg1RBP/vera are RNA–binding proteins with diverse roles in posttranscriptional regulation of RNA biogenesis in multiple

systems. PTB/hnRNP I is an hnRNP family member with roles in alternative splicing, polyadenylation, mRNA stability, IRES-mediated translation initiation and mRNA localization (reviewed in Dreyfuss et al., 2002; Gautreau et al., 1997). Vg1RBP/vera is a member of a family of RNA–binding proteins also implicated in multiple posttranscriptional processes such as mRNA localization, mRNA stability and translational regulation; other family members include chick ZBP-1, the mammalian IMPs 1-3 and CRD-BP (reviewed in Yisraeli, 2005). Both PTB/hnRNP I and Vg1RBP/vera first associate with Vg1 RNA in the oocyte nucleus (Kress et al., 2004) and are colocalized with the RNA in the vegetal cortical cytoplasm (Cote et al., 1999; Zhang et al., 1999). Mutations in E2 and VM1 sites within the VLE block binding of Vg1RBP/vera and PTB/hnRNP I, respectively (Cote et al., 1999; Deshler et al., 1998; Deshler et al., 1997; Gautreau et al., 1997), and eliminate localization, supporting essential roles for these RNA binding proteins in vegetal localization. However, how such RNA binding proteins function in RNA localization pathways remains unknown.

In cells, RNAs are present as RNP complexes, a collection of RNA and proteins that define the biogenesis and expression of the RNA. As RNAs mature from transcription to destruction, protein factors are added, removed, modified, or rearranged to control the various steps in RNA metabolism. RNP remodeling during events such as transcription, nuclear export, and degradation have been well documented (reviewed in Lewis and Mowry, 2007; Moore, 2005), but little is known about remodeling during RNA localization. In budding yeast,

rearrangement of the ASH1 mRNA localization complex is required for anchoring of the RNA at its destination (Gonsalvez et al., 2004). Certain RNA helicases are required for proper localization and translational regulation of *oskar* mRNA (Nakamura et al., 2001; Palacios et al., 2004), hinting at a role for remodeling during RNA localization in the *Drosophila* oocyte. During localization of Vg1 RNA, Vg1RBP/vera and PTB/hnRNP I interact with each other and with Vg1 RNA in both the nucleus and cytoplasm but the interactions are distinct in each compartment, suggesting a remodeling step in the *Xenopus* vegetal localization pathway (Kress et al., 2004). Although these results have provided tantalizing clues that RNP remodeling may affect localization, a role for RNP rearrangements during vegetal localization has yet to be shown.

To investigate whether RNP remodeling could promote RNA localization, we have investigated the RNA–protein interactions occurring at distinct time points in the RNA localization pathway. We show that interactions between Vg1RBP/vera and VLE RNA sequences are remodeled during localization. Vg1RBP/vera initially interacts only indirectly with VLE RNA, but is bound directly to the RNA later during localization in the cytoplasm. Moreover, we find that PTB/hnRNP I is required for remodeling of the Vg1RBP/vera-VLE interaction, as mutations within PTB/hnRNP I binding sites that block binding of PTB/hnRNP I to VLE RNA also prevent direct interaction between VLE RNA and Vg1RBP/vera, despite recruitment of Vg1RBP/vera to the RNP. Vegetal localization is blocked by these mutations, suggesting that this remodeling event is critical for localization.

Results

In order to dissect distinct steps in the RNA localization pathway, we first established the time course of localization from the oocyte nucleus to the vegetal cortical cytoplasm. For these experiments, we used a vegetal localization element (VLE) that is comprised of a duplication of the first 135 nucleotides of the Vg1 localization element residing in the 3′ UTR of Vg1 RNA (Gautreau et al., 1997; Lewis et al., 2004). This VLE faithfully directs vegetal localization, yet has reduced sequence complexity relative to other sequences known to carry out vegetal localization by this pathway (Bubunenko et al., 2002; Gautreau et al., 1997; Kwon et al., 2002; Mowry and Melton, 1992). Fluorescently labeled VLE transcripts were microinjected into nuclei of stage III *Xenopus* oocytes, and cultured to allow localization of the injected RNA. Oocytes were fixed at various timepoints and localization was assessed by confocal microscopy. As shown in Fig. A.1A, the injected RNA remained in the oocyte nucleus at early timepoints (1-4 hr.), and was undergoing localization in the cytoplasm by 16 hours post-injection (Fig. A.1B). Transport was complete after 3-6 days, by which time the injected RNA was tightly localized at the vegetal cortex (Fig. A.1C). To gain molecular insight into the localization pathway, we analyzed direct interactions between the VLE and RNA binding proteins by UV crosslinking. Oocytes were microinjected with radiolabeled VLE RNA, and cultured as above. Oocyte lysates were prepared at 1 hour and 16 hours post-injection to distinguish RNA–protein interactions that may occur before or during transport in the cytoplasm. As shown in Fig. A.1D, several RNA–binding proteins bind to VLE RNA both

before (1 hr.) and during (16 hr.) localization. Notably however, the 69 kDa protein is bound to VLE RNA only at times when VLE RNA is undergoing localization in the cytoplasm. Several *Xenopus* RNA binding proteins have been implicated in vegetal localization (Cote et al., 1999; Czaplinski et al., 2005; Deshler et al., 1998; Havin et al., 1998; Kroll et al., 2002; Zhao et al., 2001), and of these, Vg1RBP/vera is of the appropriate molecular mass to represent the 69 kDa protein (Deshler et al., 1998; Havin et al., 1998). Immunoprecipation analysis confirmed the identity of the 69 kDa as Vg1RBP/vera (Fig. A.2 and data not shown).

The lack of Vg1RBP/vera binding to VLE RNA in the nucleus was puzzling, as Vg1RBP/vera, along with PTB/hnRNP I, has been shown to associate with endogenous Vg1 RNA in the nucleus (Kress et al., 2004). A potential explanation for this apparent discrepancy may lie in the nature of the interactions revealed by these earlier experiments. The UV crosslinking experiments shown in Fig. A.1D identify direct RNA–protein interactions, while associations determined by co-immunoprecipitation, as in Kress *et al*., (Kress et al., 2004) are potentially indirect. To test this explicitly, we developed a protocol to compare direct *vs.* potentially indirect interactions in RNP complexes isolated from oocytes. As diagrammed in Fig. A.2A, RNAs encoding FLAG-tagged versions of either Vg1RBP/vera or PTB/hnRNP I were injected into stage III oocytes. After overnight culture to allow expression of the FLAG-tagged proteins, radiolabeled VLE RNA was injected into the oocyte nuclei, and oocyte lysates were prepared

after either 1 hour to assess early interactions or after 16 hours to capture interactions that occur in the cytoplasm during localization. To analyze the RNA–protein interactions occurring at these time points the oocyte lysates were split. In one portion, protein–RNA crosslinks were induced by UV irradiation, followed by immunoprecipitation with anti-FLAG antibodies and RNase treatment. Proteins in direct contact with the VLE RNA were detected after SDS-PAGE and autoradiography (Fig. A.2B) by virtue of covalent attachment of radiolabeled oligoribonucleotides. The other portion of the oocyte lysate was subjected to anti-FLAG immunoprecipitation without crosslinking to isolate RNA associated, either directly or indirectly, with the FLAG-tagged proteins (Fig. A.2C).

As shown in Fig. A.2B, PTB/hnRNP I-FLAG (lane 7), but not Vg1RBP/vera-FLAG (lane 3), was crosslinked to VLE RNA at the 1 hour timepoint, whereas both Vg1RBP/vera-FLAG (lane 4) and, PTB/hnRNP I-FLAG (lane 8) bound directly to VLE RNA at the 16 hour timepoint, when VLE RNA is undergoing localization in the cytoplasm. These results are in agreement with the results obtained with endogenous proteins (Fig. A.1D). By contrast, when RNP complexes containing FLAG-tagged Vg1RBP/vera were captured by immunoprecipitation without crosslinking, VLE RNA associated with Vg1RBP/vera-FLAG at both the 1 hour (Fig. A.2C, lane 2) and 16 hour (lane 3) timepoints, as did PTB/hnRNP I-FLAG (lanes 5, 6). As controls, we performed anti-FLAG immunoprecipitations from oocytes that had not been injected with RNAs encoding FLAG-tagged proteins (lanes 11, 12) and from oocytes expressing XStau-FLAG (lanes 9, 10), a double-

stranded RNA–binding protein that associates with the Vg1 RNP in the cytoplasm (Kress et al., 2004). As expected, VLE RNA only co-immunoprecipitated with XStau at the 16 hour timepoint (lane 9), when the RNA was in the cytoplasm, and was not recovered by anti-FLAG immunoprecipitation from uninjected oocytes (lanes 11, 12). These results suggest that Vg1RBP/vera is recruited to the VLE RNP in the nucleus, but does not contact the RNA directly at this early step (compare Figs. A.2B, lane 3 and A.2C, lane 2). Only later, when VLE RNA is undergoing localization in the cytoplasm, does Vg1RBP/vera associate directly with VLE RNA (Fig. A.2B, lane 4). Thus, it is possible that rearrangement of the RNP complex to facilitate direct contact between Vg1RBP/vera and VLE RNA is required for vegetal transport.

Vg1RBP/vera has been shown to bind directly to RNA sequence elements, termed E2 motifs, *in vitro* (Deshler et al., 1998), and mutation or deletion of E2 motifs disrupts VLE localization *in vivo* (Bubunenko et al., 2002; Deshler et al., 1998; Deshler et al., 1997; Kwon et al., 2002). However, our results (Figs. A.1D, A.2B) suggest that E2 motifs alone are not sufficient to mediate direct VLE RNA binding by Vg1RBP/vera in oocytes. The VLE contains two copies of the E2 motif, yet Vg1RBP/vera is not bound directly to the RNA at early timepoints in the localization pathway. A possible explanation for this result is that other factors may act either to block VLE RNA binding by Vg1RBP/vera in the nucleus or to facilitate RNA binding in the cytoplasm. A candidate for such a factor is PTB/hnRNP I, as Vg1RBP/vera and PTB/hnRNP I have been shown to interact

with one another in both the nucleus and in the cytoplasm, and the interaction differs between the two compartments, such that the interaction is RNA-dependent in the cytoplasm, but not in the nucleus .

As a first test of whether PTB/hnRNP I might modulate interactions between Vg1RBP/vera and VLE RNA, we systematically mutated both the PTB/hnRNP I binding sites (VM1 motifs) and the E2 motifs within the VLE. As shown in Fig. A.3A, the VLE (top), consisting of the duplicated 135-nt Vg1 sequence, contains four VM1 sites (depicted as circles) and two E2 motifs (shown as triangles). The VM1 and E2 sites were mutated by engineering specific point mutations that had previously been shown to block binding of PTB/hnRNP I and Vg1RBP/vera to their respective sites *in vitro* (Cote et al., 1999; Deshler et al., 1998; Kress et al., 2004; Kwon et al., 2002; Lewis et al., 2004). To test for potentially synergistic effects on localization *in vivo*, fluorescently labeled wild-type and mutant RNA transcripts were injected into nuclei of stage III oocytes and cultured to allow transport of the injected RNA. The oocytes were fixed and viewed by confocal microscopy, and localization was scored by comparison to localization of the wild-type VLE, which was set at 100%. Oocytes scored as positive for localization (+) exhibited strong accumulation of the injected RNA in the vegetal cytoplasm (Fig. A.3B, top panel), whereas oocytes showing no detectable asymmetry in RNA distribution were scored as negative (-) for localization (Fig. A.3B, bottom panel). As expected, mutation of all four VM1 sites or both E2 sites disrupted VLE RNA localization *in vivo*, as did mutation of all VM1 and E2 sites

together (Fig. A.3A). Positioning of the VM1 and E2 sites relative to one another dramatically affected localization (Fig. A.3C). A minimum of one E2 site and a pair of VM1 sites was necessary to support vegetal localization, but placement of the sites closer to or farther apart from one another disrupted localization. Synergistic effects were also apparent when different combinations of VM1 and E2 sites were mutated. For example, mutation of the downstream E2 site (Fig. A.3D, top) had only a modest effect on localization, as did mutation of the downstream VM1 site (A.3D, middle). However, when both of these sites are mutated together, localization was abolished (Fig. A.3D, bottom). Similar effects were observed with other combinations of VM1 and E2 mutations (Fig. A.3E and data not shown). As shown in Fig. A.3E, mutation of either the upstream E2 site or the first downstream VM1 site resulted in minimal reduction in localization, while mutation of both those sites eliminated localization. These results indicate that spacing and positioning of VM1 and E2 sites relative to one another is critical for proper VLE function during localization, consistent with the possibility PTB/hnRNP I may influence interactions between Vg1RBP/vera and VLE RNA.

To test explicitly whether PTB/hnRNP I binding to the VLE could affect RNA binding by Vg1RBP/vera, we tested *in vitro* binding of Vg1RBP/vera to RNA transcripts that are unable to bind PTB/hnRNP I. For this, we used VLE transcripts in which all four VM1 sites are mutated (VLE-ΔVM1), but the Vg1RBP/vera binding sites (E2 motifs) are intact. Radiolabeled RNA transcripts were combined with partially purified preparations of Vg1RBP/vera and

PTB/hnRNP I, and RNA–protein interactions were assessed by UV crosslinking (Fig. A.4A). As expected, binding of PTB/hnRNP I to VLE-ΔVM1 RNA was dramatically reduced (Fig. A.4A, lanes 1, 2) as compared to the wild-type VLE RNA (lanes 3, 4). Binding of Vg1RBP/vera to the VM1-mutant RNA (VLE-ΔVM1) was reduced as well (Fig. A.4A, lanes 1, 2), indicating that Vg1RBP/vera-RNA interactions are disrupted by mutations that do not impinge on the Vg1RBP/vera binding site, E2. To assess whether disruption of PTB/hnRNP I binding to VLE RNA similarly blocks RNA binding by Vg1RBP/vera *in vivo*, we next analyzed RNP complexes formed in oocytes. Stage III oocytes were injected with radiolabeled VM1-mutant (VLE-ΔVM1) or wild-type VLE RNAs and cultured for 16 hours to promote localization of the injected RNAs. RNA–protein interactions were examined by UV crosslinking in lysates prepared from the injected oocytes. As shown in Fig. A.4B, Vg1RBP/vera bound poorly to VM1-mutant RNA (lane 1), yet binding to the wild-type VLE RNA (lane 2) was robust. While it was not possible to discern PTB/hnRNP I binding in these crude oocyte lysates, as PTB/hnRNP I is not resolved from the p54/p56 RNA–binding proteins (Lewis et al., 2004; Marello et al., 1991) under these conditions, the results observed for Vg1RBP/vera in Fig. A.4B are identical to those obtained *in vitro* (Fig A.4A). The inability of Vg1RBP/vera to bind to VLE RNA containing intact E2 sites and mutated VM1 sites (Fig. A.4A, B) supports a model in which PTB/hnRNP I may modulate interactions between Vg1RBP/vera and VLE RNA. Importantly, mutation of the VM1 sites blocks localization *in vivo* (Fig. A.3A, Fig. A.4C), and

this could be due, at least in part, to disruption of Vg1RBP/vera-VLE RNA interactions.

Our results have shown that interactions between Vg1RBP/vera and VLE RNA are modulated during localization (Fig. A.1D), as are interactions between Vg1RBP/vera and PTB/hnRNP I (Kress et al., 2004). Thus, the observed defects in RNA binding to VM1-mutant VLE RNA by Vg1RBP/vera may reflect a specific RNP remodeling event that is necessary for the transition from early to later steps in the RNA localization pathway. To test whether the RNP complexes formed with VM1-mutant (ΔVM1) VLE RNA are biochemically similar to those detected early in the normal localization pathway (Fig. A.2 B,C), we again used the experimental approach diagrammed in Fig. A.2A to analyze direct *vs.* indirect RNA–protein interactions using wild-type and ΔVM1 VLE RNAs. As shown in Fig. A.5A, both Vg1RBP/vera (lane 4) and PTB/hnRNP I (lane 8) bound directly to the wild-type (wt) VLE, but neither Vg1RBP/vera (lane 3) nor PTB/hnRNP I (lane 7) bound to the ΔVM1 VLE. These results are in agreement with the *in vitro* and *in vivo* results shown in Fig. A.4 (A, B). To test whether the ΔVM1 VLE RNA was present in RNP complexes containing FLAG-tagged Vg1RBP/vera or PTB/hnRNP I, RNA was isolated from anti-FLAG immunoprecipitates without UV crosslinking (Fig. A.5B). In contrast to the UV crosslinking analyses (Fig. A.4 A, B; Fig. A.5A), ΔVM1 VLE RNA was recovered by anti-FLAG immunoprecipitation from oocyte lysates containing FLAG-tagged Vg1RBP/vera (Fig. A.5B, lane 1). Wild-type VLE RNA was recovered from RNP complexes containing

Vg1RBP/vera (lane 2) and from PTB/hnRNP I RNP complexes (lane 4), but PTB/hnRNP I was not associated with VM1-mutant (ΔVM1) VLE RNA (lane 3). These results indicate that VLE RNA lacking VM1 sites (ΔVM1) does not interact, either directly or indirectly with PTB/hnRNP I, and that while Vg1RBP/vera associates with VM1-mutant VLE RNA (Fig. A.5B, lane 1), it does so only indirectly (Fig. A.5A, lane 3). Thus, PTB/hnRNP I does not appear to be necessary for recruitment of Vg1RBP/vera to VLE RNA, as Vg1RBP/vera is able to associate, albeit indirectly, with VM1-mutant (ΔVM1) VLE RNA. Moreover, the interaction of Vg1RBP/vera with ΔVM1 VLE RNA is indistinguishable from the Vg1RBP/vera-VLE RNA interaction observed at the earliest time points in the localization pathway (Fig. A.2B, lane 3; Fig. A.2C, lane 2), suggesting that PTB/hnRNP I promotes remodeling of interactions between Vg1RBP/vera and VLE RNA during transport in the cytoplasm.

Our results (Figs. A.4A-B, A.5A-B) using VLE RNAs lacking PTB/hnRNP I binding sites (ΔVM1) suggest that interaction between PTB/hnRNP I and VLE RNA is required for Vg1RBP/vera to directly bind VLE RNA. However, the possibility remained that the VM1 site mutations could cause secondary effects, unrelated to their ability to bind PTB/hnRNP I, potentially affecting Vg1RBP/vera–VLE RNA interaction. To address this issue, we sought to investigate Vg1RBP/vera interaction with wild-type VLE RNA under conditions where PTB/hnRNP I activity could be reduced. To reduce PTB/hnRNP I binding activity, we included a molar excess of unlabeled RNA transcripts consisting of

three copies of the PTB/hnRNP I binding site (VM1) in *in vitro* binding reactions prior to UV crosslinking to radiolabeled VLE RNA. The 3×VM1 RNA contains only VM1 sites (no E2 sites) and has been shown to specifically bind PTB/hnRNP I, but not to Vg1RBP/vera (Cote et al., 1999; Lewis et al., 2004). As controls, we also included either nonspecific competitor RNA (nsp.) or RNA transcripts with three mutated VM1 sites (mutVM1), which cannot bind PTB/hnRNP I (Cote et al., 1999). As expected, binding of PTB/hnRNP I to VLE RNA (Fig. A.5C, bottom) is eliminated in the presence of excess VM1 RNA (lane 2) and is unaffected by the excess mutant VM1 RNA (mutVM1, lane 3). Importantly, reduction of PTB/hnRNP I binding activity by inclusion of excess VM1 RNA also affected binding of Vg1RBP/vera binding to VLE RNA (Fig. A.5C, top). Binding of Vg1RBP/vera to VLE RNA was reduced in the presence of excess wild-type (lane 2), but not mutant (lane 3) VM1 RNA. As shown in Fig. A.5D, incubation with excess VM1 RNA reduced the binding of Vg1RBP/vera to VLE RNA by greater than 2-fold relative to the level observed in the presence of nonspecific competitor RNA (nsp.), while only modest effects were detected in the presence of mutant VM1 RNA. As VM1 RNA interacts specifically with PTB/hnRNP I and does not itself bind to Vg1RBP/vera (Cote et al., 1999), the observed effects on binding of Vg1RBP/vera to VLE RNA are likely to be exerted through reduction in binding of PTB/hnRNP I to VLE RNA. These results suggest that binding of PTB/hnRNP I to VLE RNA is required to facilitate direct interactions between Vg1RBP/vera and VLE RNA.

Discussion

RNA localization promotes cell polarity by spatially restricting protein expression. Targeting of mRNA molecules to discrete regions within the cell cytoplasm proceeds through multi-step pathways (Czaplinski and Singer, 2006; St Johnston, 2005), but the molecular mechanisms directing transitions between steps in RNA localization pathways have remained unresolved. Remodeling of RNP complexes is an attractive mechanism to regulate such transitions, and we have found that the Vg1 RNP is remodeled in the cytoplasm during vegetal localization. At an early step in the Vg1 localization pathway, Vg1RBP/vera is recruited to the Vg1 RNP, but does not bind VLE RNA directly. It is only later, when VLE RNA is undergoing transport in the cytoplasm, that Vg1RBP/vera associates directly with VLE RNA. In probing the mechanism of this remodeling event, we have uncovered a requirement for the RNA binding protein, PTB/hnRNP I. Moreover, mutations that prevent recruitment of PTB/hnRNP I to the Vg1 RNP, block both remodeling of the VLE–Vg1RBP/vera interaction and RNA transport, suggesting a functional requirement for RNP remodeling during RNA localization.

Accumulating evidence indicates that RNA localization pathways initiate in the nucleus, as factors that bind to the RNA and assemble an early RNP influence localization of the RNA later in the cytoplasm (reviewed in Giorgi and Moore, 2007). Indeed, PTB/hnRNP I and Vg1RBP/vera associate in RNP complexes with Vg1 RNA in the *Xenopus* oocyte nucleus and cytoplasm, although the

nuclear and cytoplasmic RNP complexes are distinct (Kress et al., 2004). Potentially indirect protein–protein contacts appear to mediate the nuclear interaction between PTB/hnRNP I and Vg1RBP/vera, while in the cytoplasm, their interaction appears to be based on association with a shared target RNA (Kress et al., 2004). These results could suggest a role for PTB/hnRNP I in recruitment of Vg1RBP/vera to the Vg1 RNP, but our results disfavor this idea. Although PTB/hnRNP I appears to be critical for Vg1RBP/vera to gain direct contact with VLE RNA in the cytoplasm, our results show that initial recruitment of Vg1RBP/vera does not require PTB/hnRNP I. Instead, we propose a model (Figure A.6), in which an early step in the localization pathway is recruitment of PTB/hnRNP I to VLE RNA, through direct RNA–protein interactions. Recruitment of Vg1RBP/vera is an early step as well, but association with VLE RNA is indirect, mediated by protein–protein interactions. Initial recruitment of Vg1RBP/vera does not rely on PTB/hnRNP I, as mutations (ΔVM1) that prevent both binding of PTB/hnRNP I to VLE RNA and its association with the Vg1 RNP, block direct binding of Vg1RBP/vera to VLE RNA, but allow recruitment of Vg1RBP/vera to the Vg1 RNP (Figure A.5A,B). This early step in the localization pathway is likely to occur in the nucleus, as evidenced by comparison of the timing of direct Vg1RBP/vera–VLE RNA interaction with the time course of VLE localization *in vivo*. Vg1RBP/vera is not bound to VLE RNA at 1 hour post-injection (Figures A.1D, A.2B), at which point VLE RNA is still in the nucleus (Figure A.1A). At this same time point, PTB/hnRNP I is bound directly to VLE RNA (Figure A.2B), and both Vg1RBP/vera and PTB/hnRNP I are associated

with the Vg1 RNP (Figure A.2C). We propose (Figure A.6) that PTB/hnRNP I facilitates remodeling of the Vg1 RNP such that Vg1RBP/vera can contact VLE RNA directly. Support for this proposal comes from our results (Figures A.4, A.5) showing that mutant VLE RNAs (ΔVM1) unable to bind PTB/hnRNP I can still recruit Vg1RBP/vera, but that remodeling of the Vg1RBP/vera interaction to allow direct VLE RNA binding is blocked. We suggest that this remodeling event is a necessary step in the localization pathway, as the ΔVM1 VLE RNAs, which fail to remodel the Vg1RBP/vera–VLE RNA interaction, also fail to localize *in vivo* (Figures A.3, A.4, A.6).

One question raised by these results is how PTB/hnRNP I might act to facilitate remodeling of the Vg1 RNP. It has been shown previously that the interaction between Vg1RBP/vera and PTB/hnRNP I is remodeled upon export from the nucleus to the cytoplasm, with the nuclear interaction being potentially direct, mediated by protein–protein contacts (Kress et al., 2004). Theses results could point towards a role for PTB/hnRNP I in blocking direct Vg1RBP/vera–RNA interactions in the nucleus during the early steps in the localization pathway. However, PTB/hnRNP I cannot act by simply blocking access of Vg1RBP/vera to VLE RNA early in localization, as VLE RNAs (ΔVM1) lacking PTB/hnRNP I fail to bind Vg1RBP/vera directly (Figures A.4, A.5). Instead, our results indicate that binding of PTB/hnRNP I to VM1 motifs within VLE RNA is required for Vg1RBP/vera to access its RNA binding sites (E2 motifs). Consistent with this idea, reduction of PTB/hnRNP I binding activity also reduces binding of

Vg1RBP/vera to VLE RNA *in vitro*. However, binding of PTB/hnRNP I to VLE RNA is not sufficient to permit Vg1RBP/vera–VLE RNA interaction, as evidenced by our analysis of the Vg1 RNP early in the localization pathway (Figures A.1, A.2). At early time points, PTB/hnRNP I is bound to VLE RNA, but Vg1RBP/vera is not directly bound to VLE RNA. It is only later, either during or likely after export of the Vg1 RNP from the nucleus to the cytoplasm, that direct interaction between Vg1RBP/vera and VLE RNA can be detected (Figures A.1, A.2). It is notable that export of PTB/hnRNP I from the nucleus to the cytoplasm is accompanied by its phosphorylation (Xie et al., 2003). Thus it is possible that phosphorylation of PTB/hnRNP I may play a role in remodeling the Vg1 RNP by modulating protein–protein interactions within the Vg1 RNP.

A role for PTB/hnRNP I in RNP remodeling does not exclude functions for other nuclear (Czaplinski et al., 2005) and cytoplasmic (Kress et al., 2004; Yoon and Mowry, 2004; Zhou and King, 1996b) components of the Vg1 RNP. For example, Vg1RBP/vera must be recruited to the Vg1 RNP in the nucleus, but PTB/hnRNP I cannot play this role, as recruitment can occur in the absence of PTB/hnRNP I binding (Figures A.4, A.5, A.6). It is possible that access of Vg1RBP/vera to VLE RNA is blocked in the nucleus by interactions with other nuclear components of the Vg1 RNP and that PTB/hnRNP I may be required to promote RNP remodeling by displacing this factor after export of the Vg1 RNP to the cytoplasm. PTB/hnRNP I could also promote RNP remodeling by recruiting components of the Vg1 RNP during later steps in the localization pathway.

Precedent for such a role can be found for PTB/hnRNP I homologs in other systems. For example, in neurons a PTB/hnRNP I isoform, nPTB, has been shown to act in recruitment of other factors to an RNP complex (Markovtsov et al., 2000). In the *Xenopus* oocyte cytoplasm, additional factors are recruited to the Vg1 RNP (Kress et al., 2004) and could play roles in Vg1 RNP remodeling. Potential functions for other components of the Vg1 RNP in regulating transitions between steps in the RNA localization pathway remain to be explored.

Our results have revealed a function for PTB/hnRNP I in remodeling of the Vg1 RNP during cytoplasmic RNA transport. PTB/hnRNP I is assembled into the Vg1 RNP early in the RNA localization pathway, along with Vg1RBP/vera. At a later step in the localization pathway, the interaction between Vg1RBP/vera and Vg1 RNA is remodeled, resulting in a direct RNA–protein interaction. PTB/hnRNP I is necessary for this remodeling event, and mutations that block direct Vg1 RBP/vera–VLE RNA interaction also disrupt vegetal localization *in vivo*. The identification of PTB/hnRNP I as a factor that promotes a necessary remodeling step in the Vg1 RNA localization pathway provides insight into the molecular pathway of vegetal RNA localization. We suggest that RNP remodeling events, similar to those observed here, may serve to regulate transitions between critical steps in other RNA localization pathways.

Materials and Methods

Mutagenesis and cloning

To introduce point mutations into E2 and VM1 motifs within the minimal VLE, primers containing mutations in either VM1 (Lewis et al., 2004) or E2 (Deshler et al., 1998) sites (VM1: UUUCU→AUACA, E2: UUCAC→ UUUGC) were used to amplify fragments from pSP73-2x135 (Gautreau et al., 1997) by PCR. The resulting fragments were cloned into pSP73 (Promega) and the mutations were verified by DNA sequencing.

Synthesis of RNA transcripts

To prepare fluorescent transcripts for microinjection, VLE RNA was transcribed from linearized pSP73-2x135 or the various VM1 and E2 site mutants in reactions containing transcription buffer [40 mM Tris-HCl (pH 7.5), 6 mM $MgCl_2$, 2 mM spermidine, 10 mM DTT, 40 units RNasin RNase inhibitor (Promega)], 0.5 mM each of CTP and ATP, 0.45 mM UTP, 1 mM diguanosine triphosphate, 0.1 mM GTP, 1 µCi of□[□-^{32}P]UTP (800 Ci/mmole; DuPont/NEN), and 50 µM Alexa Fluor 546-14-UTP (Molecular Probes). The RNAs were purified and resuspended to a concentration of 50 nM. For RNA–binding assays, RNAs were transcribed in reactions containing 1× transcription buffer (Promega), 0.5 mM each of CTP and ATP, 50 µM GTP, 0.5 mM diguanosine triphosphate, and 50 µCi of□[-^{32}P]UTP (800 Ci/mmole; DuPont/NEN). RNA transcripts were resuspended at 1 ng/□l for *in vitro* UV crosslinking and 250 nM for microinjection. FLAG-tagged versions of Vg1RBP/vera, PTB/hnRNP I (Kress et al., 2004) and

XStau (Yoon and Mowry, 2004) were transcribed using the mMessage mMachine kit (Ambion) according to the manufacturer's instructions. Prior to microinjection, Vg1RBP/vera-FLAG RNA was resuspended to 750 nM, PTB/hnRNP I-FLAG RNA was resuspended to 250 nM, and XStau-FLAG RNA was resuspended to 500 nM. Sequence-specific competitor RNAs were synthesized from linearized pSP73-2x135 (12), wild-type and mutant 3×VM1 (5) using the MEGAscript kit (Ambion) according to the manufacturer's protocol. *E. coli* rRNA used as nonspecific competitor was a generous gift from A. Dahlberg.

Oocyte culture

Oocytes were obtained surgically from *Xenopus laevis* females (Nasco) and defoliculated by incubation in 2 mg/ml collagenase (Sigma-Aldrich). The oocytes were washed with MBSH buffer [88 mM NaCl, 1 mM KCl, 2.4 mM $NaHCO_3$. 0.82 mM $MgSO_4 \cdot 7H_2O$, 0.33 mM $Ca(NO_3)_2 \cdot 4H_2O$, 0.41 mM $CaCl_2 \cdot 6H_2O$, 10 mM Hepes (pH 7.6)], and stage III oocytes (Dumont, 1972) were manually sorted. After microinjection, oocytes were cultured in oocyte culture medium [50% L15 medium, 15 mM Hepes (pH 7.6), 1 mM glutamine, 1 mg/ml insulin, 100 mg/ml gentamicin, 50 U/ml nystatin, 50 U/ml penicillin, 50 mg/ml streptomycin and 5-10% frog serum containing vitellogenin], as described in (Wallace and Misulovin, 1978).

In vivo RNA localization assay

Albino stage III oocytes were microinjected with ~3 nl of fluorescently labeled RNA and cultured for up to four days (Wallace and Misulovin, 1978), followed by fixation in MEMFA (Harland, 1991) and storage in 100% methanol at -20°C. For microscopy, oocytes were cleared in 2:1 benzyl benzoate:benzyl alcohol. Oocytes were scored for localization on a Leica MZFL II fluorescence dissecting microscope. Confocal images were obtained using a Leica TCS SP2 AOBS spectral confocal microscope.

In vivo RNA binding assays

Stage III oocytes were microinjected with ~3 nl of RNA transcripts encoding FLAG-tagged proteins (Vg1RBP/vera-FLAG, PTB/hnRNP I-FLAG or XStau-FLAG). Following a 16 hr. incubation in OCM, the oocytes were subsequently injected with ~3 nl of radiolabeled probe RNA and either processed immediately (1 hr.) or cultured overnight (16 hrs.) in OCM. The oocytes were homogenized in YSS buffer [50 mM Tris (pH 8.0), 75 mM NaCl, 1 mM $MgCl_2$, 0.05% Igepal (Sigma), 1 U/ml RNasin (Promega), 0.1 µg/ml leupeptin, 0.1 µg/ml antipain, 0.1 µg/ml trypsin inhibitor, 0.4 mM Pefabloc SC (Sigma), 1.0 mM DTT, and 100 mM sucrose] at a concentration of 0.5 oocyte per µl. Following centrifugation at 10,000× *g* for 10 minutes, the lysate supernatant was crosslinked by a 15 min. incubation in 0.1% formaldehyde, followed by quenching with 0.25 M glycine for 5 minutes. For crosslink-IP analysis to assess direct RNA–protein interactions, the lysate was crosslinked by UV irradiation for 10 minutes in a Stratalinker (Stratagene). Immunoprecipitations were performed by rocking the 25-40 oocyte

equivalents of lysate with 10 µl anti-FLAG beads (Sigma) in a total volume of 500 □l of YSS for 2 hours at room temperature. After treatment with RNase A (1 mg/ml, Sigma) for 15 minutes at 37°C, the crosslinked proteins were separated by SDS-PAGE and visualized by autoradiography. For RNA-IP analysis, anti-FLAG IP was performed as above, except that 10 oocyte equivalents of lysate were used and samples were not subjected to UV irradiation. RNA was isolated from the immunoprecipitates by addition of 200 µl RNA elution buffer [10 mM Tris (pH 7.5), 0.8 M ammonium acetate, 10 mM EDTA, 0.1% SDS, 50 µg/ml yeast tRNA] and incubation at 70°C for 15 minutes. After phenol:chloroform extraction and ethanol precipitation, the isolated RNA was separated on a denaturing polyacrylamide gel and visualized by autoradiography.

In vitro RNA binding assays

Preparation of oocyte S10 and S100 extracts was performed as described in (Kress et al., 2004; Mowry, 1996) and fractionation of oocyte lysate by heparin agarose chromatography was performed as in (Cote et al., 1999). *In vitro* binding was performed as in Lewis *et al.* (Lewis et al., 2004), in 10 µl reactions containing ~5 µg of oocyte lysate, or ~4 ng partially purified Vg1RBP/vera or PTB/hnRNP I, 600 ng of unlabeled competitor RNA and 1 ng ^{32}P-labeled VLE RNA. After incubation for 10 min., followed by UV crosslinking for 10 minutes using a Stratalinker (Stratagene), and treatment with RNase A (1 mg/ml, Sigma) for 15 minutes at 37°C, crosslinked proteins were separated by SDS-PAGE and

visualized by autoradiography or phorophorimage analysis. Quantitation was carried out using a Typhoon 9410 variable mode imager.

Acknowledgments

This work was supported by Public Health Service grant GM071049 from the National Institute of General Medicine to K.L.M. R.A.L. was a pre-doctoral trainee, supported in part by grant T32-GM07601 from the National Institute of General Medicine. We thank Jeffrey Laney, Michael McKeown, Timothy Messitt, Catherine Pratt, Adrian Reich and Tricia Serio for critical reading of the manuscript and for helpful advice and discussions.

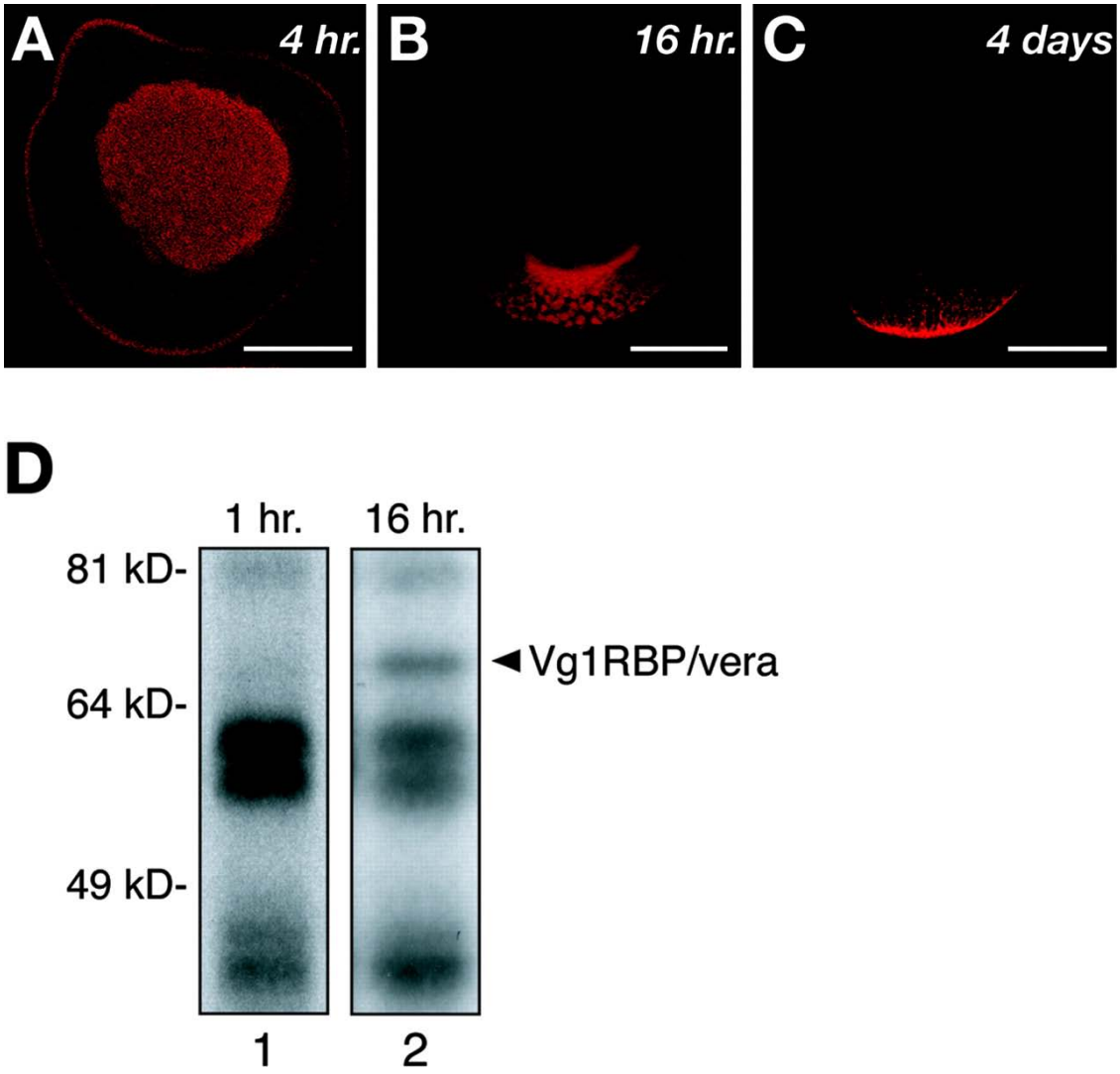

Figure A.1. Time course of RNA–protein interactions during vegetal RNA localization in *Xenopus* oocytes. **A-C)** Alexa Fluor-546-labeled VLE RNA transcripts were injected into the nuclei of stage III *Xenopus* oocytes. Oocytes were fixed at the indicated time points post-injection: 4 hours (A), 16 hours (B), 4 days (C), and viewed by confocal microscopy. The injected RNA (red) is evident in the nucleus in panel A, is asymmetrically distributed within the vegetal hemisphere cytoplasm in panel B, and is restricted to the vegetal cortex in panel C. The vegetal hemisphere is oriented towards the bottom (A-C), and the scale

bars are 100 μm. **D)** Radiolabeled VLE RNA transcripts were injected into the nuclei of stage III *Xenopus* oocytes. Oocyte lysates were prepared at either 1 hour (lane 1) or 16 hours (lane 2) post-injection and crosslinked by UV irradiation. After RNase treatment, labeled proteins were resolved by SDS-PAGE and visualized by autoradiography. The position of Vg1RBP/vera is indicated at the right and molecular weight standards are on the left.

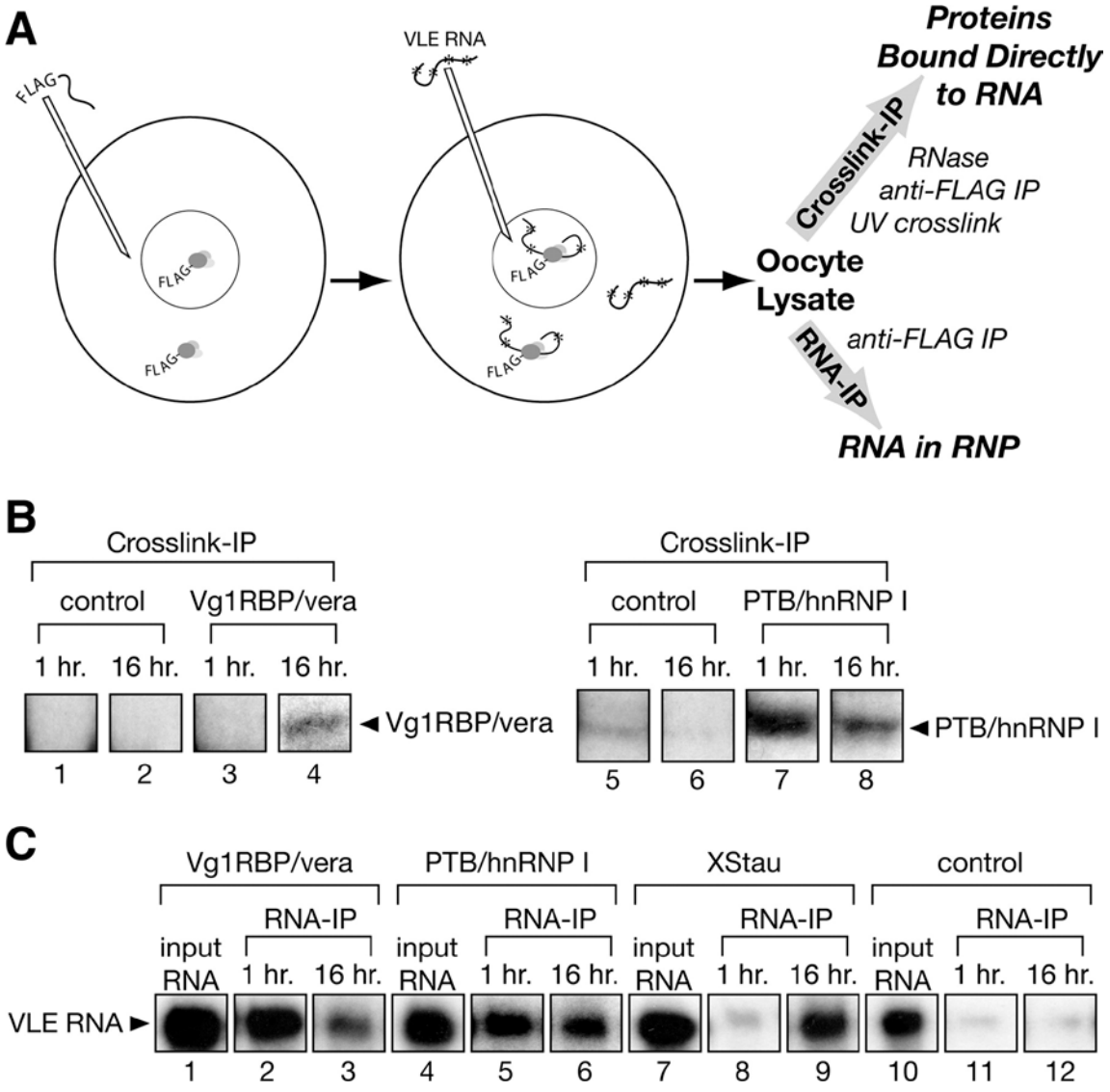

Figure A.2. Interaction between Vg1RBP/vera and VLE RNA is remodeled during localization. **A)** The experimental strategy for identifying proteins directly bound to RNA vs. RNAs contained in RNP complexes is diagrammed. Stage III *Xenopus* oocytes are microinjected with RNA transcripts encoding FLAG-tagged proteins. After overnight culture to allow protein expression, ^{32}P-labeled VLE RNA transcripts are injected into the oocyte nuclei. Oocyte lysates are prepared and split into two aliquots. One aliquot is analyzed by "crosslink-IP" in which

crosslinking by UV irradiation is followed by anti-FLAG IP and RNAse treatment. The RNA-bound proteins, labeled by covalent attachment of RNA oligonucleotides, are resolved by SDS-PAGE and visualized by autoradiography. The other aliquot is analyzed by "RNA-IP", in which anti-FLAG immunoprecipitation is carried out directly, and RNAs associated with the FLAG-tagged proteins are detected by autoradiography following polyacrylamide (PA) gel electrophoresis. **B)** Crosslink-IP analysis. ^{32}P-labeled VLE RNA was injected into nuclei of oocytes expressing Vg1RBP/vera-FLAG (lanes 3, 4), PTB/hnRNP I-FLAG (lanes 7, 8), or control oocytes without expression of FLAG-tagged proteins (lanes 1, 2, 5, 6). Oocyte lysates were prepared either 1 hour (lanes 1, 3, 5, 7) or 16 hours (lanes 2, 4, 6, 8) post-injection and subjected to "crosslink-IP' as detailed in A (above). Autoradiograms of crosslinked proteins resolved by SDS-PAGE are shown, and the positions of Vg1RBP/vera-FLAG (lanes 1-4) and PTB/hnRNP I-FLAG (lanes 4-8) are indicated to the right. **C)** RNA-IP analysis. ^{32}P-labeled VLE RNA was injected into nuclei of oocytes expressing Vg1RBP/vera-FLAG (lanes 1-3), PTB/hnRNP I-FLAG (lanes 4-6), XStau-FLAG (lanes 7-9), or control oocytes without expression of FLAG-tagged proteins (lanes 10-12). Oocyte lysates were prepared either 1 hour (lanes 2, 5, 8, 11) or 16 hours (lanes 2, 6, 9, 12) post-injection and subjected to "RNA-IP" as detailed in A (above). Autoradiograms of isolated VLE RNA resolved by PA gel electrophoresis are shown and the position of VLE RNA is indicated at the left. For each panel, samples were run on the same gel, except lanes 7-9 (XStau) in

panel C, which were run together on a separate gel. Lane order was changed for clarity of presentation.

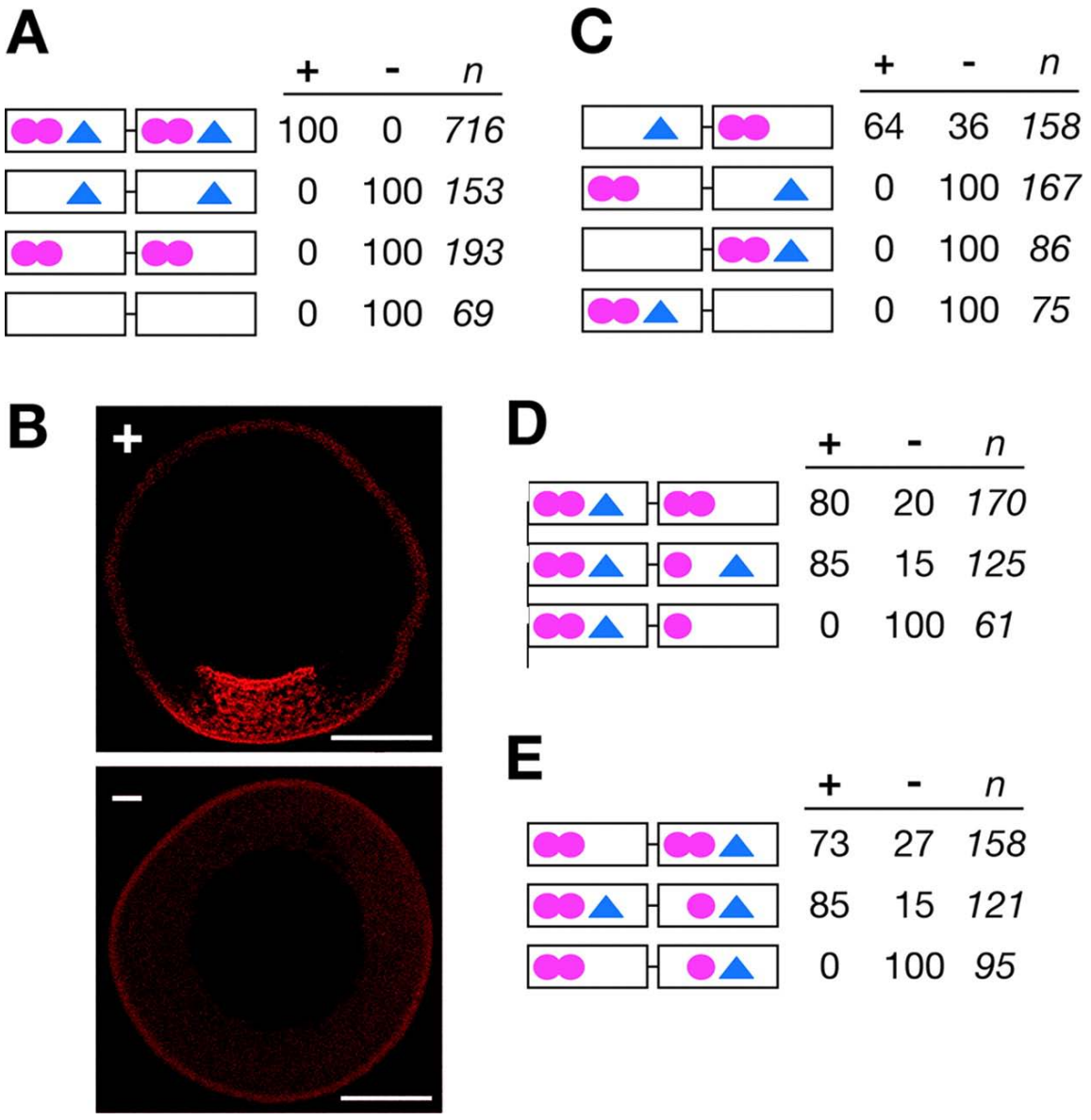

Figure A.3. E2 and VM1 motifs exhibit spacing and synergistic effects within the VLE. **A)** Schematics of wild-type VLE and mutant RNAs, with VM1 motifs (YYUCU, where Y = U or C) shown as circles and E2 motifs (WYCAC, where W = A or C and Y = U or C) represented as triangles. Introduction of mutations into the VM1 sites (YYUCU → AYACA) or E2 sites (WYCAC → UUUGC) is indicated by removal of the site(s) from the diagrams. The results of *in vivo* localization

assays (% localization) are indicated at the right: + represents normal vegetal localization (set to 100% for wild-type) and – indicates no detectable localization. The number of oocytes (*n*) injected for each transcript is indicated at the far right. **B)** *Xenopus* stage III oocytes were injected with Alexa-546 labeled RNA transcripts and scored for localization as indicated above, A. An example of normal vegetal localization (+) is shown on the top and an example with no detectable localization (-) is at the bottom. Localization of the injected RNA (red) is evident by accumulation of the RNA in the vegetal cytoplasm, which is at the bottom of the image. The scale bars represent 100μm. **C-E)** Schematics of VLE RNA transcripts containing mutations in E2 motifs (triangles) or VM1 sites (circles), with localization analyses as detailed in A, above.

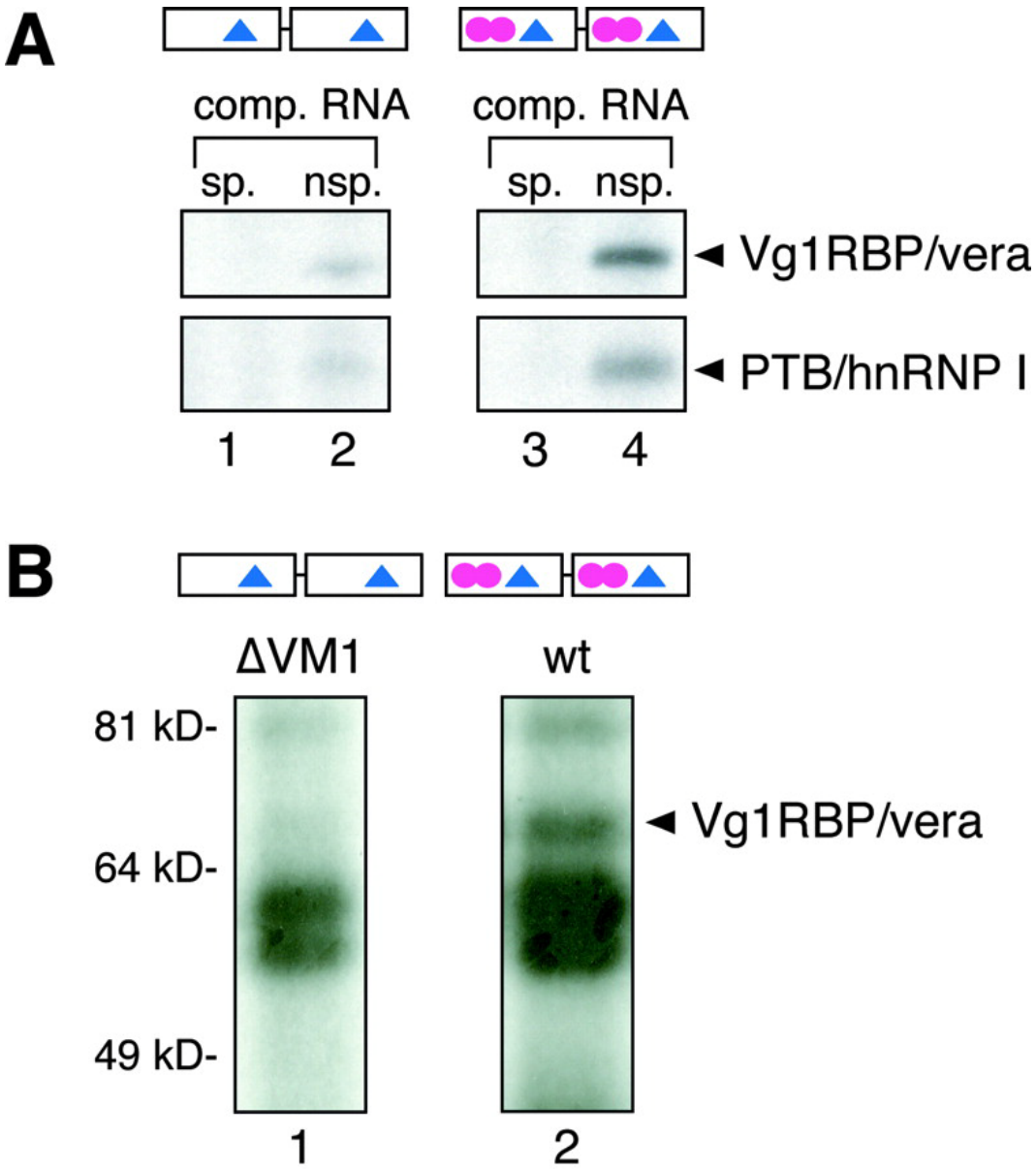
A
comp. RNA
comp. RNA
sp.
nsp.
sp.
nsp.
Vg1RBP/vera
PTB/hnRNP I
1
2
3
4
B
ΔVM1
wt
81 kD-
64 kD-
49 kD-
Vg1RBP/vera
1
2
C
ΔVM1
wt

Figure A.4. VM1 site mutations eliminate direct binding of both PTB/hnRNP I and Vg1RBP/vera to VLE RNA. **A)** UV crosslinking analysis was performed using radiolabeled VM1-mutant (ΔVM1; lanes 1, 2) and wild-type (lanes 3, 4) VLE RNA to test the ability to be directly bound by partially purified preparations of Vg1RBP/vera (top panels) or PTB/hnRNP I (bottom panels). Specificity of *in vitro* binding was assessed by challenging the binding reactions with unlabeled specific (sp.; lanes 1, 3) or nonspecific (nsp.; lanes 2, 4) competitor RNAs. **B)** Radiolabeled VM1-mutant (ΔVM1; lane 1) and wild-type (wt; lane 2) VLE RNA was injected into the nuclei of stage III oocytes. After culturing for 16 hours, oocyte lysates were prepared, crosslinked by UV irradiation, and treated with RNase. Proteins interacting with the injected RNA were resolved by SDS-PAGE and autoradiography. The position of Vg1RBP/vera is indicated at the right, and molecular weight markers are shown on the left. **C)** Stage III oocytes were injected with Alexa-546 labeled VM1-mutant (ΔVM1; left) and wild-type (wt; right) VLE RNA transcripts. VM1-mutant VLE RNA (left) shows no detectable localization after culture, whereas vegetal localization of the injected RNA (red) is evident in oocytes injected with wild-type VLE RNA (right). The oocytes are oriented with the vegetal hemisphere towards the bottom; scale bar = 100μm.

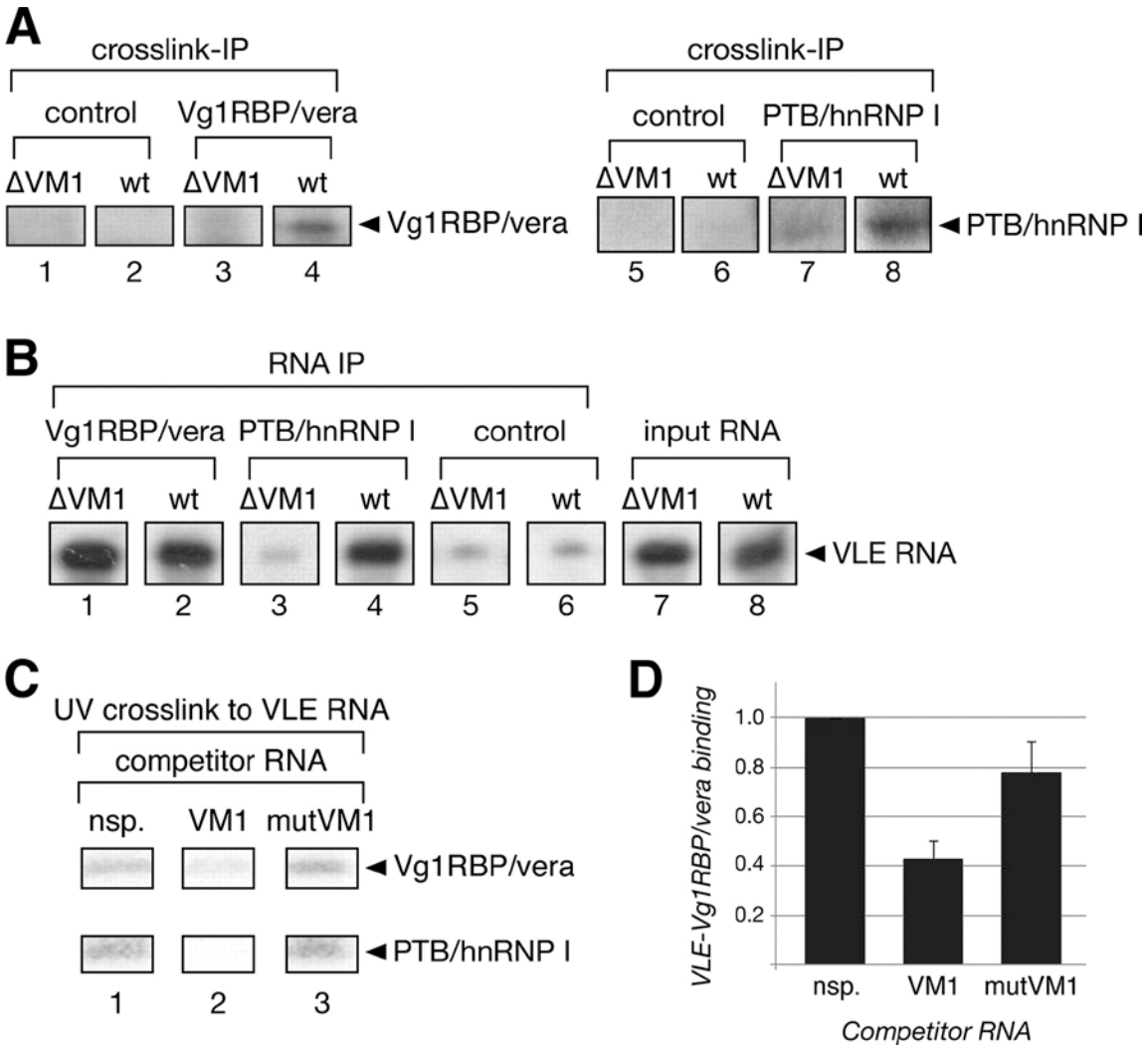

Figure A.5. Binding of PTB/hnRNP I to VLE RNA is required for direct interaction between Vg1RBP/vera and VLE RNA. **A)** Crosslink-IP analysis (as in detailed in Fig. A.2A) was carried out using oocytes expressing Vg1RBP/vera-FLAG (lanes 3, 4), PTB/hnRNP I-FLAG (lanes 7, 8), or control oocytes without expression of FLAG-tagged proteins (lanes 1, 2, 5, 6). ^{32}P-labeled VM1-mutant (ΔVM1; lanes 1, 3, 5, 7) or wild-type (wt; lanes 2, 4, 6, 8) VLE RNA transcripts were injected into the oocyte nuclei, and lysates were prepared after 16 hours culture. After crosslinking by UV irradiation, RNase treatment and anti-FLAG IP, proteins

directly bound to the injected RNA transcripts were resolved by SDS-PAGE, and detected by autoradiography. The positions of Vg1RBP/vera-FLAG (lanes 1-4) and PTB/hnRNP I-FLAG (lanes 4-8) are indicated to the right. **B)** RNA-IP analysis (as diagrammed in Fig. A.2A) was carried out using oocytes expressing Vg1RBP/vera-FLAG (lanes 1, 2), PTB/hnRNP I-FLAG (lanes 3, 4), or control oocytes without expression of FLAG-tagged proteins (lanes 5, 6). ^{32}P-labeled VM1-mutant (∆VM1; lanes 1, 3, 5, 7) or wild-type (wt; lanes 2, 4, 6, 8) VLE RNA transcripts were injected into the oocyte nuclei, and lysates were prepared either immediately (input RNA; lanes 7-8) or after 16 hours culture (lanes 1-6). RNA was isolated after anti-FLAG IP and resolved by polyacrylamide gel electrophoresis; the position of input VLE RNA is indicated at the right. **C)** UV crosslinking analysis was performed using radiolabeled VLE RNA and stage III oocyte lysates. *In vitro* binding reactions included 500–fold molar excess of nonspecific RNA (nsp, lane 1) or 500–fold binding site excess of wild-type VM1 RNA (VM1, lane 2) or RNAs containing mutated VM1 sites (mutVM1, lane 3). VLE–bound Vg1RBP/vera is at the top, and VLE–bound PTB/hnRNP I is at the bottom. **D)** Quantitation of UV crosslinking results (as in panel C). Binding of Vg1RBP/vera to VLE RNA was quantitated by phosphorimage analysis, and the level of VLE–bound Vg1RPB/vera obtained in the presence of 500-1000–fold molar excess of nonspecific RNA (nsp.) was set to 1. The results of three experiments are graphed, and the level of VLE–bound Vg1RBP/vera in the presence of 500-1000–fold binding site excess of unlabeled wild-type VM1 RNA (VM1) averaged 0.44 (st. dev. = 0.07) and averaged 0.78 (st. dev. = 0.12) in the

presence of mutant VM1 RNA (mutVM1). For panels A-C, samples were run on the same gel, but lane order was changed for presentation in the figure.

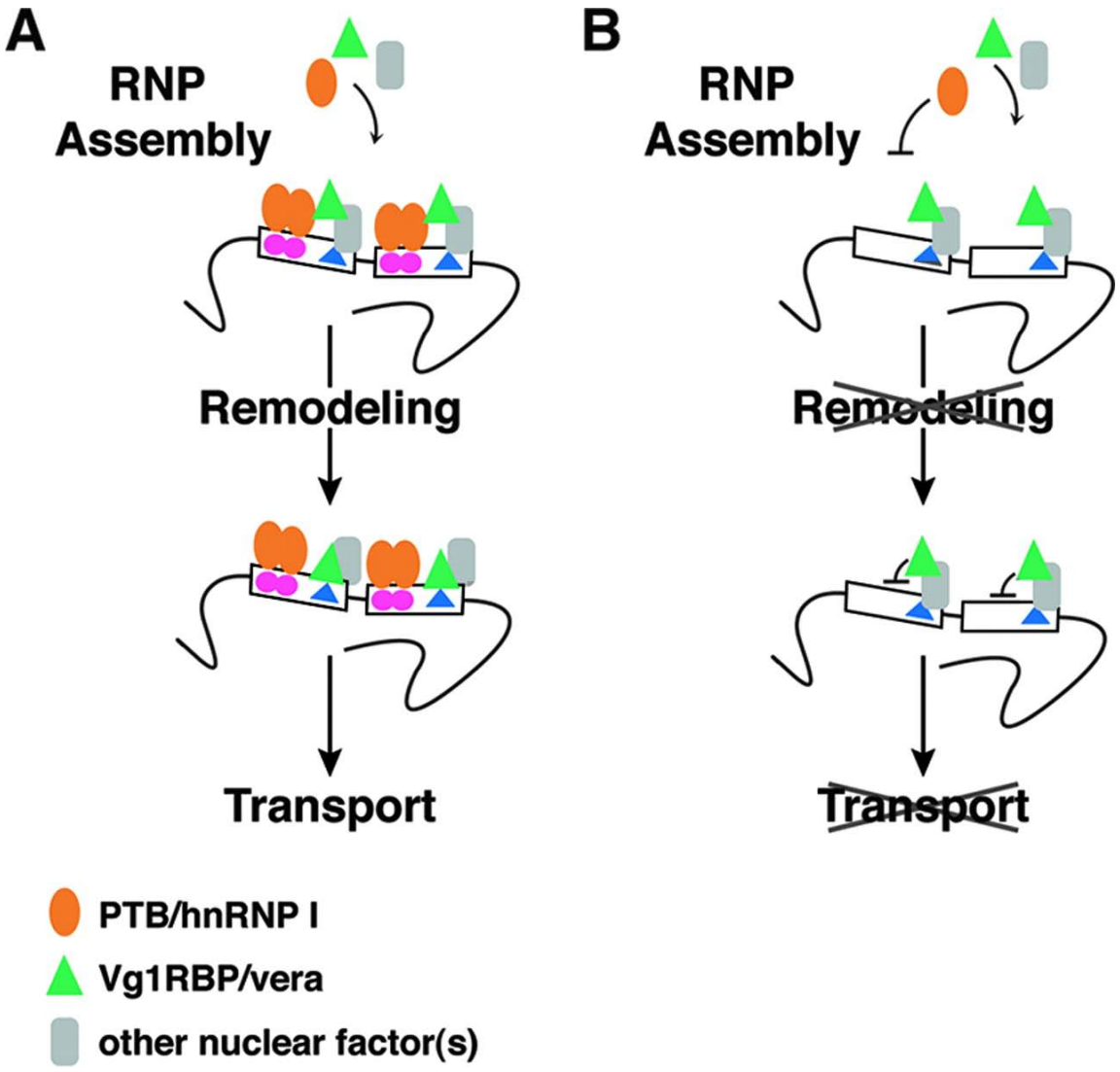

Figure A.6. Model of RNA–protein interactions affecting RNP assembly and remodeling during RNA localization. **A)** RNP assembly initiates in the nucleus, and during the early steps in the vegetal RNA localization pathway, PTB/hnRNP I (orange ovals) and potentially other nuclear factors (gray squares) are bound directly to VLE RNA sequences. Vg1RBP/vera (green triangles) is associated only indirectly with VLE RNA, through protein-protein interactions. The RNP is remodeled at later times during the vegetal RNA localization pathway, such that Vg1RBP/vera binds directly to VLE RNA. **B)** VLE RNA transcripts containing

mutations within VM1 sites cannot bind either directly or indirectly to PTB/hnRNP I. VM1-mutant VLE RNA transcripts bind Vg1RBP/vera (green triangles) indirectly, through protein-protein interactions, but remodeling of the RNP to allow direct interaction between Vg1RBP/vera and VLE RNA is blocked, as is vegetal RNA localization.

Appendix B: Vg1 RNP Granule Formation Is a Rate Limiting Step in RNA Localization that Requires PTB and Vera

James A. Gagnon and Kimberly L. Mowry

Introduction

Many localized RNAs form large particles or granules (hereafter referred to as granules; the terms are used interchangeably) during transport (Ainger et al., 1993; Bratu et al., 2003; Cote et al., 1999; Farina et al., 2003; Kohrmann et al., 1999; MacDougall et al., 2003). These RNP granules are thought to represent large aggregates of RNP complexes. However, the molecular nature of transport granules, how they form, their function, and their relationship with other types of cytoplasmic granules is not yet clear (reviewed in Anderson and Kedersha, 2006; Parker and Sheth, 2007). Evidence that the observed granules represent transport granules first came from visualization of granule movement (Ainger et al., 1993; Bratu et al., 2003; Kohrmann et al., 1999; MacDougall et al., 2003). Second, RNA–binding proteins that function in localization have been observed in such granules. Examples include Staufen, which is found in RNA granules that are transported to dendrites in hippocampal neurons (Kohrmann et al., 1999), ZBP-1 (the chick homolog of Vera), which co-localizes with β-actin mRNA-containing granules in fibroblasts (Farina et al., 2003), and hnRNP I/PTB, which we have shown to be colocalized with Vg1 mRNA in large granules (Cote et al., 1999). It is unknown whether these factors facilitate formation of RNP granules or merely mark them.

Two hypotheses exist for the function of transport granules. One theory is that transport granules represent an efficient method of transporting RNAs. Transport granules appear to package many RNA molecules into a single RNP, which

would represent an obvious energy savings for the cell relative to transporting individual RNAs. Molecular motors traffic many large cargos such as organelles and vesicles, so it is logical that RNAs should be formed into larger cargos. Second, transport granules have been proposed to promote translational repression of cargo RNAs during transport. Translational silencing of *oskar* mRNA in *Drosophila* oocytes was found to be dependent on the formation of large granules which represent oligomerized mRNAs (Chekulaeva et al., 2006). Cis- elements in the 3' UTR of *oskar* mRNA promote oligomerization. These data support a model in which RNA-binding proteins mediate oligomerization as a mechanism of translational repression.

Translational silencing is relieved after RNA localization. It is an intriguing possibility that the silencing particles may be analogous to P bodies, which have been shown to reversibly sequester mRNAs from the translational machinery (Brengues et al., 2005). In mammalian cells, ZBP-1, an RNA-binding protein, promotes transport of β-actin RNA to neuronal protusions (Ross et al., 1997). It also plays a role in translational repression of β-actin RNA. Phosphorylation of ZBP-1 at neuronal protrusions relieves ZBP-1 binding and causes translational derepression of β-actin RNA (Huttelmaier et al., 2005). This provides a crucial mechanistic link between RNA localization and translation- ZBP-1 is loaded to RNA in the nucleus, represses translation during transport, and allows spatial regulation of gene expression (Farina et al., 2003; Huttelmaier et al., 2005). It remains unclear how ZBP-1 may facilitate RNP granule formation.

hnRNP I/PTB and Vg1RBP/Vera (a homolog of ZBP-1) are both RNA-binding proteins that interact with Vg1 RNA in both the nucleus and cytoplasm of *Xenopus* oocytes and are required for Vg1 localization (Cote et al., 1999; Deshler et al., 1997; Kress et al., 2004; Lewis et al., 2008). The crystal structure of the mammalian homologs of each protein and extensive mapping of their binding sites within zipcodes has revealed that they both contain multiple active RNA binding domains capable of binding RNA (Chao et al., 2010; Oberstrass et al., 2005), suggesting that they may each be capable of nucleating RNP granules. Indeed, *oskar* RNA granules appear to be reduced in size and are more numerous in *Drosophila* oocytes lacking PTB (Besse et al., 2009). Strong biochemical evidence that PTB or Vera are required for oligomerization of localized RNAs and an understanding of their mechanism of action is lacking.

We have developed an *in vitro* system for granule assembly to resolve the function of RNA granules in RNA transport. Until now, virtually all analyses of any type of RNP granule have been carried out *in vivo* through co-localization studies (reviewed in Anderson and Kedersha, 2006). We demonstrate, using this novel assay and confocal microscopy, that localized RNAs form granules more efficiently than non-localized RNAs. Granules formed *in vitro* are of similar size to endogenous RNA granules, suggesting that they may be functional. To test this hypothesis, we microinjected *in vitro* formed granules into oocytes and observed an increase in overall rate of localization, suggesting that granule formation is a rate limiting step in RNA localization. Finally, we demonstrate a

role for the RNA binding proteins hnRNP I/PTB and Vg1RNP/Vera in granule formation, and develop a model in which PTB and Vera nucleate oligomerization of Vg1 RNA.

Results

RNA transport has been observed to occur in large granules, and we hypothesize that formation of these so-called transport granules represents a critical step in the RNA localization pathway. However, little is known about the assembly and composition of RNA transport granules in this or any system (Anderson and Kedersha, 2009). Moreover, the function of these RNA granules remains unclear.

We initially noticed that localized RNAs always form granules during the transport process, while non-localized RNAs do not (Figure B.1). We have never observed an RNA that localizes but doesn't form granules, or a non-localized RNA that retains the ability to form particles, suggesting that these two processes are tightly linked. In order to define the structure and function of RNA granules containing localized RNAs, we established an *in vitro* system for granule assembly (Figure B.2). For this we prepared lysates from stage I-III oocytes, incubated with either VLE RNA or non-relevant RNA (control), and captured large complexes by centrifugation. As shown in Figure B.3A, complex formation directed by VLE RNA is ~2-fold greater than that obtained with control RNA, suggesting that factors that specifically bind the VLE RNA mediate its formation into large granules. Analysis of the RNP complexes formed *in vitro* by confocal microscopy (Figure B.3B) reveals large granules that are similar in size (1-2 μm) to those observed during vegetal localization *in vivo* (Figure B.3D,D′). Non-localizing RNAs, which do not form granules *in vivo*, also fail to form granules *in*

vitro (Figure B.3C). These data support the idea that our novel assay can recapitulate *in vivo* granule formation in the test tube.

We hypothesized that formation of RNAs into transport-competent cargos may be a rate-limiting step during RNA localization. We tested *in vivo* function of RNA granules formed *in vitro* by injecting granules prepared with fluorescently-labeled VLE RNA into stage IV oocytes (Figure B.3E). At this stage of oogenesis, localization of injected RNA is markedly slower than at stage III (data not shown), and we hoped to monitor changes in the rate localization more effectively at this later stage. Indeed, VLE RNA in pre-formed granules is localized more rapidly than naked RNA, suggesting that RNA granules formed *in vitro* are functional *in vivo*, and that granule formation is a rate-limiting step in RNA localization.

RNP granule formation may require remodeling of the Vg1 RNP. Because PTB-dependent remodeling of Vera-VLE RNA interactions occurs during localization in the cytoplasm (Lewis et al., 2008), we asked whether PTB and/or Vera might be required for granule formation. Using the granule formation assay, we tested VLE RNAs carrying mutations in either the PTB or Vera binding sites (Figure B.4). Mutation of either PTB or Vera binding sites strongly impairs granule formation, suggesting that PTB and Vera are required for formation of RNA granules in vitro. Further experiments will be necessary to define the mechanism by which PTB and/or Vera oligomerize Vg1 mRNA.

RNA granules have been hypothesized to function in repressing translation (Anderson and Kedersha, 2009). As an initial step towards testing this hypothesis, we tested granule forming ability on a timecourse of oogenesis. We generated lysates from staged oocytes and conducted granule formation assays as before. As shown in Figure B.5, lysates made from stage I-III oocytes demonstrated a stronger ability to form granules than lysates made from stage IV or V oocytes, when localization is slower and translation initiates. This data draws a temporal correlation between granule formation, RNA localization and translational repression.

Methods

Fluorescent RNA generation and microinjection.

RNAs were fluorescently labeled with Alexa-546 and microinjected into staged *Xenopus* oocytes as previously described (Gagnon and Mowry, 2010). VLE, VLE ΔVM1 and VLE ΔE2 have been previously described (Lewis et al., 2008). Unlabeled RNAs were generated from an T7 mMachine kit (Ambion). All imaging was done on a Zeiss LSM510 confocal microscope.

Granule formation assay

Radiolabeled and unlabeled RNA and occasionally fluorescent RNA are incubated with an oocyte lysate (>30 μg/μl) in siliconized glass vials for thirty minutes to allow higher-order complexes to form. Incubations are either imaged by confocal microscopy or spun at 100 Kg for twenty minutes to segregate single RNPs (supernatant) from granules (pellet). Supernatant is removed to a separate vial, and both vials are counted on a scintillation counter to determine segregation of radiolabeled RNA as a measure of granule formation.

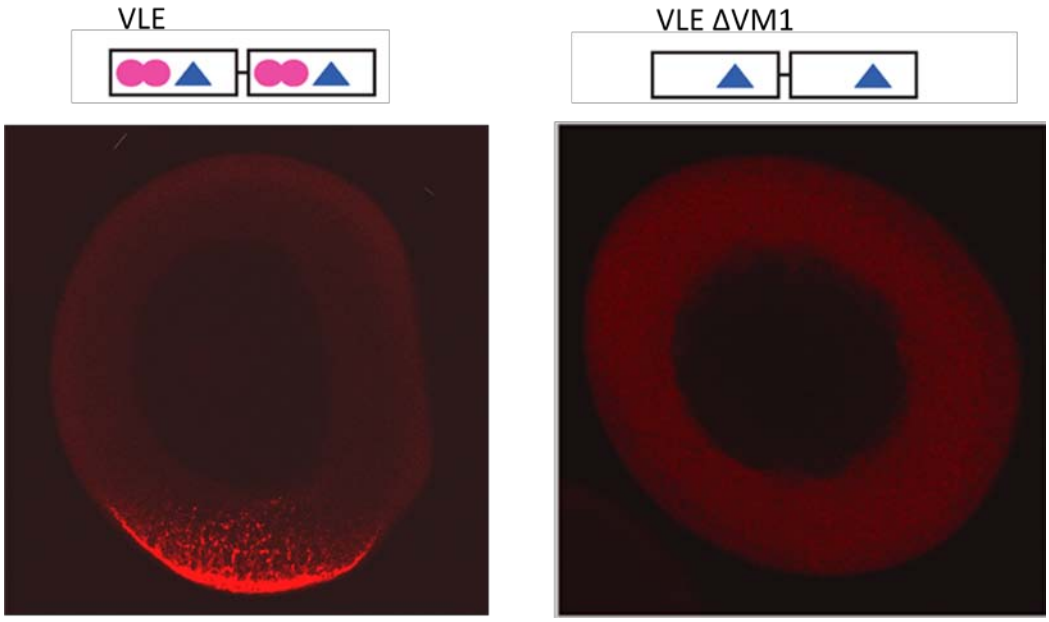

Figure B.1. RNAs capable of localization form particles while non-localizing RNAs do not. (A) VLE RNA or (B) VLE RNA lacking hnRNP I/PTB binding sites (VLE ΔVM1) was microinjected and oocytes cultured for 16 hours before fixation, dehydration and imaging by confocal microscopy. Images courtesy of Ray Lewis.

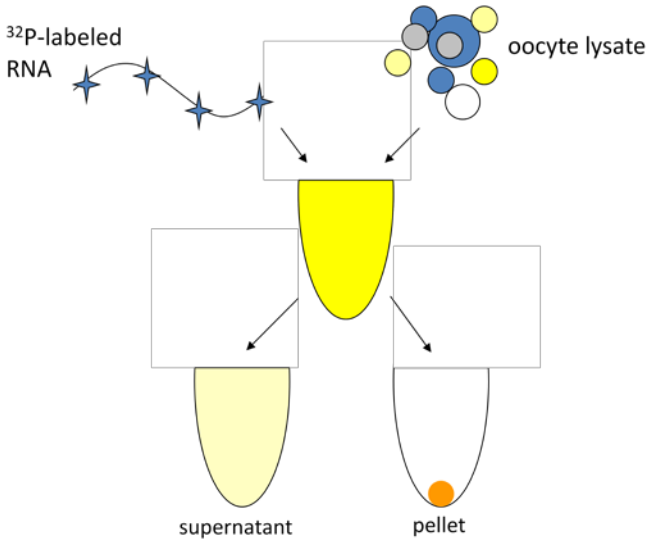

Figure B.2. An *in vitro* assay for granule formation. Radiolabeled and unlabeled RNA are incubated with an oocyte lysate (>30 μg/μl) in siliconized glass vials for thirty minutes to allow higher-order complexes to form. Incubations are spun at 100 Kg for twenty minutes to segregate single RNPs (supernatant) from granules (pellet). Supernatant is removed to a separate vial, and both vials are counted on a scintillation counter to determine segregation of radiolabeled RNA as a measure of granule formation.

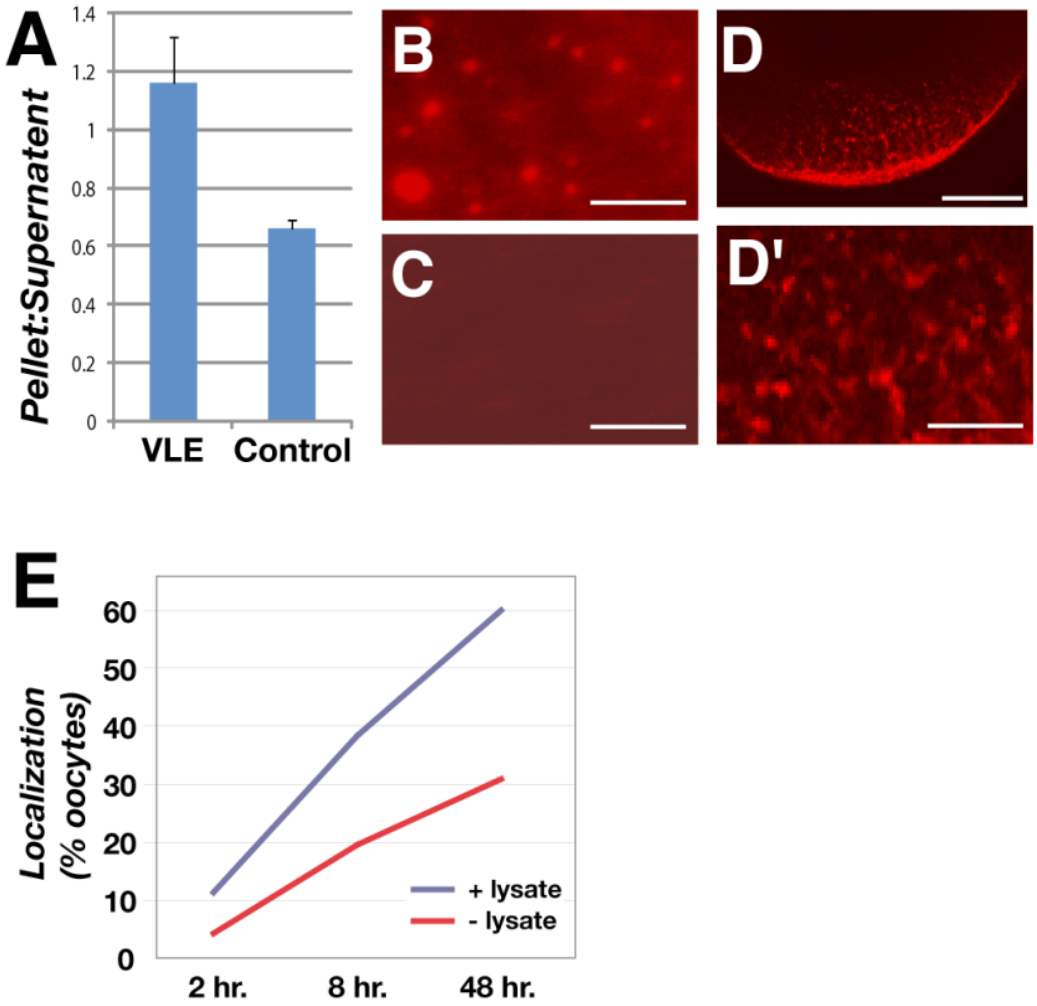

Figure B.3. *In vitro* assembled RNA granules. **(A)** Oocyte lysates were incubated with radiolabeled wt VLE RNA (VLE) or non-localizing (control; pSP73). After centrifugation, the ratio of RNA in the pellet relative to the supernatant was determined. **(B-C)** Oocyte lysates were incubated as in (A), except that RNAs were also labeled with Alexa-546 and imaged by confocal microscopy. **(B)** VLE RNA-containing granules (scale bar=5 μm). **(C)** Non-localizing RNA; granules are not evident (scale bar=5 μm). **(D)** Alexa-546-

labeled VLE RNA during localization in a st. III oocyte (scale bar=50 μm); higher magnification view of granules from the vegetal cytoplasm is shown in **D′** (scale bar=5 μm) **(E)** Alexa-546-labeled VLE RNA was incubated with oocyte lysates, as in (A) to allow granule formation (+ lysate). Control VLE RNA was incubated without lysate (– lysate). RNAs (+ or – lysate) were injected into st. IV oocytes, which were cultured to allow localization *in vivo*. Oocytes were fixed and imaged at 2, 8 and 48 hrs. Oocytes scored as positive for localization exhibited accumulation of the injected RNA in the vegetal cytoplasm. The graph shows the percent of oocytes showing vegetal localization; + lysate is shown in blue and – lysate is red.

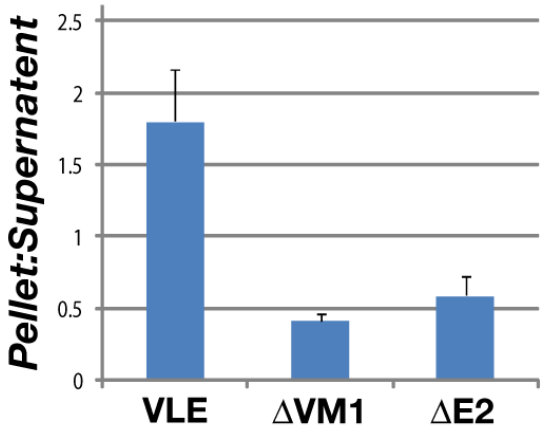

Figure B.4. Roles for PTB and Vera in transport granule assembly. Oocyte lysates were incubated with radio-labeled wt VLE RNA (VLE), or VLE RNAs with mutated PTB (ΔVM1) or Vera (ΔE2) binding sites, and analyzed as before.

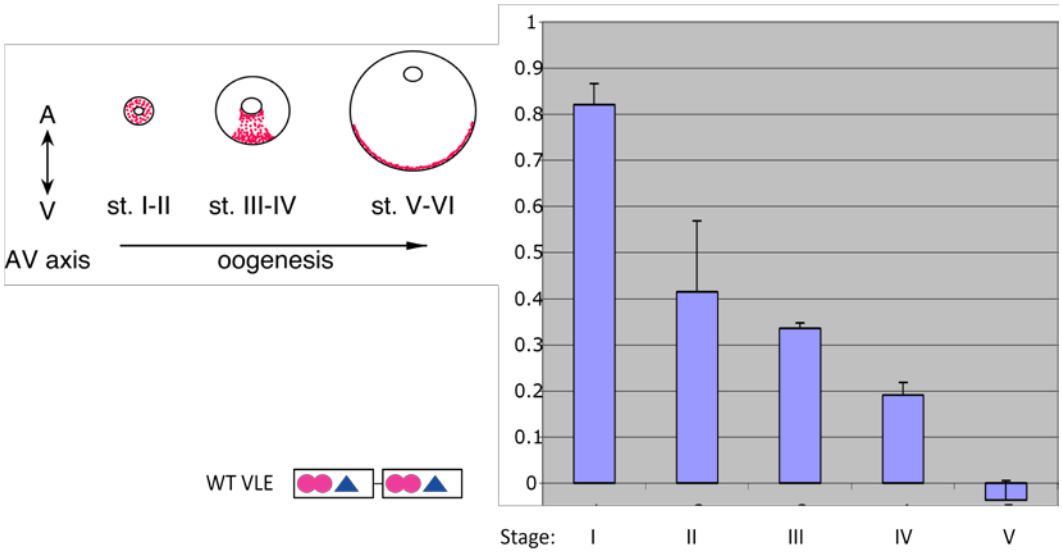

Figure B.5. Correlation between granule forming ability, localization and translational repression during oogenesis. Oocytes from stages I – V were sorted, made into lysates of similar concentrations, and lysates used in a granule formation assay as before. Granule forming ability is highest in stages I-III, when RNA is translationally repressed and actively localized, and lower in later stages, when translation initiates and localization is less efficient.

Appendix C: Visualizing RNA localization in *Xenopus* oocytes

James A. Gagnon and Kimberly L. Mowry

Visualizing RNA localization in *Xenopus* oocytes.
Gagnon JA, Mowry KL.
J Vis Exp. 2010 Jan 14;(35). pii: 1704. doi: 10.3791/1704.

Abstract

RNA localization is a conserved mechanism of establishing cell polarity. Vg1 mRNA localizes to the vegetal pole of *Xenopus laevis* oocytes and acts to spatially restrict gene expression of Vg1 protein. Tight control of Vg1 distribution in this manner is required for proper germ layer specification in the developing embryo. RNA sequence elements in the 3' UTR of the mRNA, the Vg1 localization element (VLE) are required and sufficient to direct transport. To study the recognition and transport of Vg1 mRNA *in vivo*, we have developed an imaging technique that allows extensive analysis of trans-factor directed transport mechanisms via a simple visual readout.

To visualize RNA localization, we synthesize fluorescently labeled VLE RNA and microinject this transcript into individual oocytes. After oocyte culture to allow transport of the injected RNA, oocytes are fixed and dehydrated prior to imaging by confocal microscopy. Visualization of mRNA localization patterns provides a readout for monitoring the complete pathway of RNA transport and for identifying roles in directing RNA transport for cis-acting elements within the transcript and trans-acting factors that bind to the VLE (Lewis et al., 2008; Messitt et al., 2008). We have extended this technique through co-localization with additional RNAs and proteins (Gagnon and Mowry, 2009; Messitt et al., 2008), and in combination with disruption of motor proteins and the cytoskeleton (Messitt et al., 2008) to probe mechanisms underlying mRNA localization.

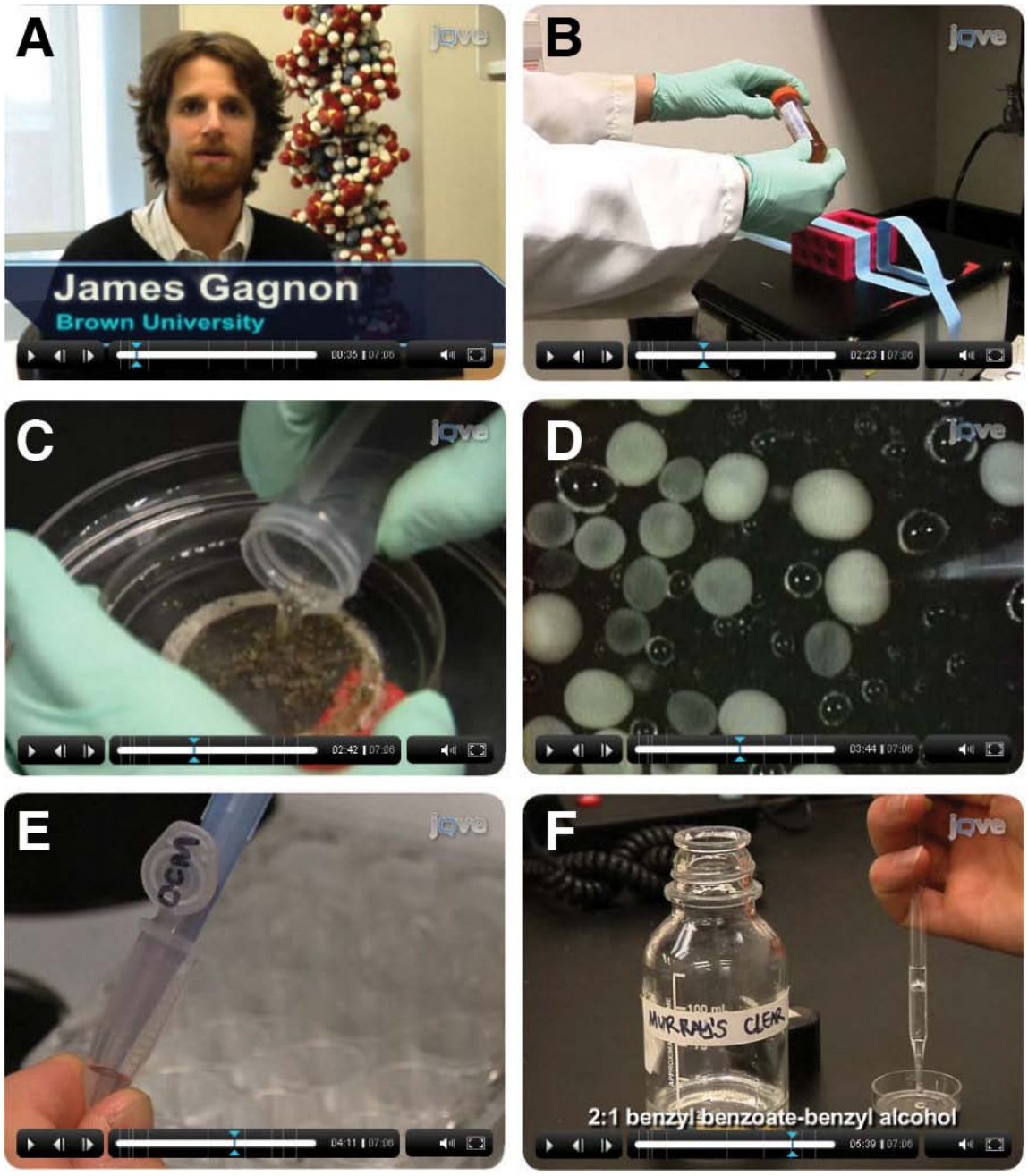

Figure C.1. *Screenshots from JoVE video protocol.* (A) Introduction. (B) Collagenase treatment. (C) Sieving oocytes. (D) Microinjection. (E) Culturing oocytes. (F) Clearing oocytes for microscopy. Video article and protocol can be found here: http://www.jove.com/index/Details.stp?ID=1704

Literature Cited

Adelstein, R.S., and Eisenberg, E. (1980). Regulation and kinetics of the actin-myosin-ATP interaction. Annu Rev Biochem *49*, 921-956.

Ainger, K., Avossa, D., Morgan, F., Hill, S.J., Barry, C., Barbarese, E., and Carson, J.H. (1993). Transport and localization of exogenous myelin basic protein mRNA microinjected into oligodendrocytes. J Cell Biol *123*, 431-441.

Alarcon, V.B., and Elinson, R.P. (2001). RNA anchoring in the vegetal cortex of the Xenopus oocyte. J Cell Sci *114*, 1731-1741.

Ally, S., Larson, A.G., Barlan, K., Rice, S.E., and Gelfand, V.I. (2009). Opposite-polarity motors activate one another to trigger cargo transport in live cells. J Cell Biol *187*, 1071-1082.

Anderson, P., and Kedersha, N. (2006). RNA granules. J Cell Biol *172*, 803-808.

Anderson, P., and Kedersha, N. (2009). RNA granules: post-transcriptional and epigenetic modulators of gene expression. Nat Rev Mol Cell Biol *10*, 430-436.

Andken, B.B., Lim, I., Benson, G., Vincent, J.J., Ferenc, M.T., Heinrich, B., Jarzylo, L.A., Man, H.Y., and Deshler, J.O. (2007). 3'-UTR SIRF: a database for identifying clusters of whort interspersed repeats in 3' untranslated regions. BMC Bioinformatics *8*, 274.

Andresen, M., Schmitz-Salue, R., and Jakobs, S. (2004). Short tetracysteine tags to beta-tubulin demonstrate the significance of small labels for live cell imaging. Mol Biol Cell *15*, 5616-5622.

Aronov, S., Aranda, G., Behar, L., and Ginzburg, I. (2002). Visualization of translated tau protein in the axons of neuronal P19 cells and characterization of tau RNP granules. J Cell Sci *115*, 3817-3827.

Aronov, S., and Gerst, J.E. (2004). Involvement of the late secretory pathway in actin regulation and mRNA transport in yeast. J Biol Chem *279*, 36962-36971.

Bashirullah, A., Cooperstock, R.L., and Lipshitz, H.D. (1998). RNA localization in development. Annu Rev Biochem *67*, 335-394.

Bashirullah, A., Halsell, S.R., Cooperstock, R.L., Kloc, M., Karaiskakis, A., Fisher, W.W., Fu, W., Hamilton, J.K., Etkin, L.D., and Lipshitz, H.D. (1999). Joint action of two RNA degradation pathways controls the timing of maternal transcript elimination at the midblastula transition in Drosophila melanogaster. EMBO J *18*, 2610-2620.

Beach, D.L., Salmon, E.D., and Bloom, K. (1999). Localization and anchoring of mRNA in budding yeast. Curr Biol *9*, 569-578.

Berezuk, M.A., and Schroer, T.A. (2007). Dynactin enhances the processivity of kinesin-2. Traffic *8*, 124-129.

Bergsten, S.E., and Gavis, E.R. (1999). Role for mRNA localization in translational activation but not spatial restriction of nanos RNA. Development *126*, 659-669.

Berleth, T., Burri, M., Thoma, G., Bopp, D., Richstein, S., Frigerio, G., Noll, M., and Nusslein-Volhard, C. (1988). The role of localization of bicoid RNA in organizing the anterior pattern of the Drosophila embryo. EMBO J *7*, 1749-1756.

Berliner, E., Young, E.C., Anderson, K., Mahtani, H.K., and Gelles, J. (1995). Failure of single-headed kinesin to track parallel to microtubule protofilaments. Nature *373*, 718-721.

Bertrand, E., Chartrand, P., Schaefer, M., Shenoy, S.M., Singer, R.H., and Long, R.M. (1998). Localization of ASH1 mRNA particles in living yeast. Mol Cell *2*, 437-445.

Besse, F., Lopez de Quinto, S., Marchand, V., Trucco, A., and Ephrussi, A. (2009). Drosophila PTB promotes formation of high-order RNP particles and represses oskar translation. Genes Dev *23*, 195-207.

Betley, J.N., Frith, M.C., Graber, J.H., Choo, S., and Deshler, J.O. (2002). A ubiquitous and conserved signal for RNA localization in chordates. Curr Biol *12*, 1756-1761.

Betley, J.N., Heinrich, B., Vernos, I., Sardet, C., Prodon, F., and Deshler, J.O. (2004). Kinesin II mediates Vg1 mRNA transport in Xenopus oocytes. Curr Biol *14*, 219-224.

Birsoy, B., Kofron, M., Schaible, K., Wylie, C., and Heasman, J. (2006). Vg 1 is an essential signaling molecule in Xenopus development. Development *133*, 15-20.

Blangy, A., Arnaud, L., and Nigg, E.A. (1997). Phosphorylation by p34cdc2 protein kinase regulates binding of the kinesin-related motor HsEg5 to the dynactin subunit p150. J Biol Chem *272*, 19418-19424.

Blangy, A., Chaussepied, P., and Nigg, E.A. (1998). Rigor-type mutation in the kinesin-related protein HsEg5 changes its subcellular localization and induces microtubule bundling. Cell Motil Cytoskeleton *40*, 174-182.

Blower, M.D., Feric, E., Weis, K., and Heald, R. (2007). Genome-wide analysis demonstrates conserved localization of messenger RNAs to mitotic microtubules. J Cell Biol *179*, 1365-1373.

Bohl, F., Kruse, C., Frank, A., Ferring, D., and Jansen, R.P. (2000). She2p, a novel RNA-binding protein tethers ASH1 mRNA to the Myo4p myosin motor via She3p. EMBO J *19*, 5514-5524.

Bratu, D.P., Cha, B.J., Mhlanga, M.M., Kramer, F.R., and Tyagi, S. (2003). Visualizing the distribution and transport of mRNAs in living cells. Proc Natl Acad Sci U S A *100*, 13308-13313.

Brendza, R.P., Serbus, L.R., Duffy, J.B., and Saxton, W.M. (2000). A function for kinesin I in the posterior transport of oskar mRNA and Staufen protein. Science *289*, 2120-2122.

Brengues, M., Teixeira, D., and Parker, R. (2005). Movement of eukaryotic mRNAs between polysomes and cytoplasmic processing bodies. Science *310*, 486-489.

Bridgman, P.C. (2009). Myosin motor proteins in the cell biology of axons and other neuronal compartments. Results Probl Cell Differ *48*, 91-105.

Bubunenko, M., Kress, T.L., Vempati, U.D., Mowry, K.L., and King, M.L. (2002). A consensus RNA signal that directs germ layer determinants to the vegetal cortex of *Xenopus* oocytes. Dev Biol *248*, 82-92.

Bullock, S.L. (2007). Translocation of mRNAs by molecular motors: Think complex? Sem Cell Dev Biol *18*, 194-201.

Bullock, S.L., and Ish-Horowicz, D. (2001). Conserved signals and machinery for RNA transport in Drosophila oogenesis and embryogenesis. Nature *414*, 611-616.

Bullock, S.L., Nicol, A., Gross, S.P., and Zicha, D. (2006). Guidance of bidirectional motor complexes by mRNA cargoes through control of dynein number and activity. Curr Biol *16*, 1447-1452.

Bullock, S.L., Stauber, M., Prell, A., Hughes, J.R., Ish-Horowicz, D., and Schmidt-Ott, U. (2004). Differential cytoplasmic mRNA localisation adjusts pair-rule transcription factor activity to cytoarchitecture in dipteran evolution. Development *131*, 4251-4261.

Burkhardt, J.K., Echeverri, C.J., Nilsson, T., and Vallee, R.B. (1997). Overexpression of the dynamitin (p50) subunit of the dynactin complex disrupts

dynein-dependent maintenance of membrane organelle distribution. J Cell Biol *139*, 469-484.

Carson, J.H., Worboys, K., Ainger, K., and Barbarese, E. (1997). Translocation of myelin basic protein mRNA in oligodendrocytes requires microtubules and kinesin. Cell Motil Cytoskeleton *38*, 318-328.

Cha, B.J., Serbus, L.R., Koppetsch, B.S., and Theurkauf, W.E. (2002). Kinesin I-dependent cortical exclusion restricts pole plasm to the oocyte posterior. Nat Cell Biol *4*, 592-598.

Chang, P., Torres, J., Lewis, R.A., Mowry, K.L., Houliston, E., and King, M.L. (2004). Localization of RNAs to the mitochondrial cloud in Xenopus oocytes through entrapment and association with endoplasmic reticulum. Mol Biol Cell *15*, 4669-4681.

Chao, J.A., Patskovsky, Y., Patel, V., Levy, M., Almo, S.C., and Singer, R.H. (2010). ZBP1 recognition of beta-actin zipcode induces RNA looping. Genes Dev *24*, 148-158.

Chekulaeva, M., Hentze, M.W., and Ephrussi, A. (2006). Bruno acts as a dual repressor of oskar translation, promoting mRNA oligomerization and formation of silencing particles. Cell *124*, 521-533.

Choo, S., Heinrich, B., Betley, J.N., Chen, Z., and Deshler, J.O. (2005). Evidence for common machinery utilized by the early and late RNA localization pathways in Xenopus oocytes. Dev Biol *278*, 103-117.

Clark, I., Giniger, E., Ruohola-Baker, H., Jan, L.Y., and Jan, Y.N. (1994). Transient posterior localization of a kinesin fusion protein reflects anteroposterior polarity of the Drosophila oocyte. Curr Biol *4*, 289-300.

Cole, D.G., Chin, S.W., Wedaman, K.L., Hall, K., Vuong, T., and Scholey, J.M. (1993). Novel heterotrimeric kinesin-related proteins purified from sea urchin eggs. Nature *366*.

Colegrove-Otero, L.J., Devaux, A., and Standart, N. (2005). The Xenopus ELAV protein ElrB represses Vg1 mRNA translation during oogenesis. Mol Cell Biol *25*, 9028-9039.

Coller, J., and Wickens, M. (2007). Tethered function assays: an adaptable approach to study RNA regulatory proteins. Methods Enzymol *429*, 299-321.

Compton, D.A. (1998). Focusing on spindle poles. J Cell Sci *111 (Pt 11)*, 1477-1481.

Condeelis, J., and Singer, R.H. (2005). How and why does beta-actin mRNA target? Biol Cell *97*, 97-110.

Cote, C.A., Gautreau, D., Denegre, J.M., Kress, T.L., Terry, N.A., and Mowry, K.L. (1999). A Xenopus protein related to hnRNP I has a role in cytoplasmic RNA localization. Mol Cell *4*, 431-437.

Crick, F. (1970). Central dogma of molecular biology. Nature *227*, 561-563.

Czaplinski, K., Kocher, T., Schelder, M., Segref, A., Wilm, M., and Mattaj, I.W. (2005). Identification of 40LoVe, a Xenopus hnRNP D family protein involved in localizing a TGF-beta-related mRNA during oogenesis. Dev Cell *8*, 505-515.

Czaplinski, K., and Mattaj, I.W. (2006). 40LoVe interacts with Vg1RBP/Vera and hnRNP I in binding the Vg1-localization element. RNA *12*, 213-222.

Czaplinski, K., and Singer, R.H. (2006). Pathways for mRNA localization in the cytoplasm. Trends Bioch Sci *31*, 687-693.

Dale, L., Matthews, G., and Colman, A. (1993). Secretion and mesoderm-inducing activity of the TGF-beta-related domain of Xenopus Vg1. EMBO J *12*, 4471-4480.

De Marco, V., Burkhard, P., Le Bot, N., Vernos, I., and Hoenger, A. (2001). Analysis of heterodimer formation by Xklp3A/B, a newly cloned kinesin-II from Xenopus laevis. EMBO J *20*, 3370-3379.

Deacon, S.W., Serpinskaya, A.S., Vaughan, P.S., Lopez Fanarraga, M., Vernos, I., Vaughan, K.T., and Gelfand, V.I. (2003). Dynactin is required for bidirectional organelle transport. J Cell Biol *160*, 297-301.

Delanoue, R., and Davis, I. (2005). Dynein anchors its mRNA cargo after apical transport in the Drosophila blastoderm embryo. Cell *122*, 97-106.

Delanoue, R., Herpers, B., Soetaert, J., Davis, I., and Rabouille, C. (2007). Drosophila Squid/hnRNP helps Dynein switch from a gurken mRNA transport motor to an ultrastructural static anchor in sponge bodies. Dev Cell *13*, 523-538.

Deshler, J.O., Highett, M.I., Abramson, T., and Schnapp, B.J. (1998). A highly conserved RNA-binding protein for cytoplasmic mRNA localization in vertebrates. Curr Biol *8*, 489-496.

Deshler, J.O., Highett, M.I., and Schnapp, B.J. (1997). Localization of Xenopus Vg1 mRNA by Vera protein and the endoplasmic reticulum. Science *276*, 1128-1131.

Diefenbach, R.J., Mackay, J.P., Armati, P.J., and Cunningham, A.L. (1998). The C-terminal region of the stalk domain of ubiquitous human kinesin heavy chain contains the binding site for kinesin light chain. Biochemistry *37*, 16663-16670.

Dienstbier, M., Boehl, F., Li, X., and Bullock, S.L. (2009). Egalitarian is a selective RNA-binding protein linking mRNA localization signals to the dynein motor. Genes Dev *23*, 1546-1558.

Ding, Y., Chan, C.Y., and Lawrence, C.E. (2006). Clustering of RNA secondary structures with application to messenger RNAs. J Mol Biol *359*, 554-571.

Dreyfuss, G., Kim, V.N., and Kataoka, N. (2002). Messenger-RNA-binding proteins and the messages they carry. Nat Rev Mol Cell Biol *3*, 195-205.

Driever, W., and Nusslein-Volhard, C. (1988). The bicoid protein determines position in the Drosophila embryo in a concentration-dependent manner. Cell *54*, 95-104.

Du, T.G., Schmid, M., and Jansen, R.P. (2007). Why cells move messages: The biological functions of mRNA localization. Sem Cell Dev Biol *18*, 171-177.

Dumont, J.N. (1972). Oogenesis in Xenopus laevis (Daudin). I. Stages of oocyte development in laboratory maintained animals. J Morphol *136*, 153-179.

Duncan, J.E., and Warrior, R. (2002). The cytoplasmic dynein and kinesin motors have interdependent roles in patterning the Drosophila oocyte. Curr Biol *12*, 1982-1991.

Eberwine, J., Belt, B., Kacharmina, J.E., and Miyashiro, K. (2002). Analysis of subcellularly localized mRNAs using in situ hybridization, mRNA amplification, and expression profiling. Neurochem Res *27*, 1065-1077.

Falley, K., Schutt, J., Iglauer, P., Menke, K., Maas, C., Kneussel, M., Kindler, S., Wouters, F.S., Richter, D., and Kreienkamp, H.J. (2009). Shank1 mRNA: dendritic transport by kinesin and translational control by the 5'untranslated region. Traffic *10*, 844-857.

Farina, K.L., Huttelmaier, S., Musunuru, K., Darnell, R., and Singer, R.H. (2003). Two ZBP1 KH domains facilitate beta-actin mRNA localization, granule formation, and cytoskeletal attachment. J Cell Biol *160*, 77-87.

Forrest, K.M., and Gavis, E.R. (2003). Live imaging of endogenous RNA reveals a diffusion and entrapment mechanism for nanos mRNA localization in Drosophila. Curr Biol *13*, 1159-1168.

Forristall, C., Pondel, M., Chen, L., and King, M.L. (1995). Patterns of localization and cytoskeletal association of two vegetally localized RNAs, Vg1 and Xcat-2. Development *121*, 201-208.

Frey, S., Pool, M., and Seedorf, M. (2001). Scp160p, an RNA-binding, polysome-associated protein, localizes to the endoplasmic reticulum of Saccharomyces cerevisiae in a microtubule-dependent manner. J Biol Chem *276*, 15905-15912.

Fusco, D., Accornero, N., Lavoie, B., Shenoy, S.M., Blanchard, J.M., Singer, R.H., and Bertrand, E. (2003). Single mRNA molecules demonstrate probabilistic movement in living mammalian cells. Curr Biol *13*, 161-167.

Gagnon, J.A., and Mowry, K.L. (2009). VISIONS: the art of science. Mol Reprod Dev *76*, 1115.

Gagnon, J.A., and Mowry, K.L. (2010). Visualizing RNA localization in Xenopus oocytes. J Vis Exp.

Gard, D.L. (1994). Gamma-tubulin is asymmetrically distributed in the cortex of Xenopus oocytes. Dev Biol *161*, 131-140.

Gautreau, D., Cote, C.A., and Mowry, K.L. (1997). Two copies of a subelement from the Vg1 RNA localization sequence are sufficient to direct vegetal localization in Xenopus oocytes. Development *124*, 5013-5020.

Gavis, E.R., and Lehmann, R. (1994). Translational regulation of nanos by RNA localization. Nature *369*, 315-318.

Gelfand, V., Le Bot, N., Tuma, M., and Vernos, I. (2001). A dominant negative approach for functional studies of the kinesin II complex. In Methods in Molecular Biology: Kinesin Protocols, I. Vernos, ed. (Totowa, NJ, Humana Press, Inc.), pp. 191-204.

Gill, S.R., Schroer, T.A., Szilak, I., Steuer, E.R., Sheetz, M.P., and Cleveland, D.W. (1991). Dynactin, a conserved, ubiquitously expressed component of an activator of vesicle motility mediated by cytoplasmic dynein. J Cell Biol *115*, 1639-1650.

Giorgi, C., and Moore, M.J. (2007). The nuclear nurture and cytoplasmic nature of localized RNPs. Sem Cell Dev Biol, in press.

Glotzer, J.B., Saffrich, R., Glotzer, M., and Ephrussi, A. (1997). Cytoplasmic flows localize injected *oskar* RNA in *Drosophila* oocytes. Curr Biol *7*, 326-337.

Gonsalvez, G.B., Little, J.L., and Long, R.M. (2004). ASH1 mRNA anchoring requires reorganization of the Myo4p-She3p-She2p transport complex. J Biol Chem *279*, 46286-46294.

Gonsalvez, G.B., Urbinati, C.R., and Long, R.M. (2005). RNA localization in yeast: moving towards a mechanism. Biol Cell *97*, 75-86.

Gonzalez, I., Buonomo, S.B., Nasmyth, K., and von Ahsen, U. (1999). ASH1 mRNA localization in yeast involves multiple secondary structural elements and Ash1 protein translation. Curr Biol *9*, 337-340.

Gross, S.P., Vershinin, M., and Shubeita, G.T. (2007). Cargo transport: two motors are sometimes better than one. Curr Biol *17*, R478-486.

Hamada, M., Kiryu, H., Sato, K., Mituyama, T., and Asai, K. (2009). Prediction of RNA secondary structure using generalized centroid estimators. Bioinformatics *25*, 465-473.

Harland, R.M. (1991). In situ hybridization: An improved whole-mount method for *Xenopus* embryos. In *Xenopus laevis*: Practical Uses in Cell and Molecular Biology, B.K. Kay, and H.B. Peng, eds. (San Diego, Academic Press), pp. 685-695.

Havin, L., Git, A., Elisha, Z., Oberman, F., Yaniv, K., Schwartz, S.P., Standart, N., and Yisraeli, J.K. (1998). RNA-binding protein conserved in both microtubule- and microfilament-based RNA localization. Genes Dev *12*, 1593-1598.

Hendricks, A.G., Perlson, E., Ross, J.L., Schroeder, H.W., 3rd, Tokito, M., and Holzbaur, E.L. (2010). Motor Coordination via a Tug-of-War Mechanism Drives Bidirectional Vesicle Transport. Curr Biol.

Hirokawa, N. (1994). Microtubule organization and dynamics dependent on microtubule-associated proteins. Curr Opin Cell Biol *6*, 74-81.

Hirokawa, N. (2006). mRNA transport in dendrites: RNA granules, motors, and tracks. J Neurosci *26*, 7139-7142.

Hirokawa, N., Noda, Y., Tanaka, Y., and Niwa, S. (2009). Kinesin superfamily motor proteins and intracellular transport. Nat Rev Mol Cell Biol *10*, 682-696.

Hirokawa, N., Pfister, K.K., Yorifuji, H., Wagner, M.C., Brady, S.T., and Bloom, G.S. (1989). Submolecular domains of bovine brain kinesin identified by electron microscopy and monoclonal antibody decoration. Cell *56*, 867-878.

Holt, C.E., and Bullock, S.L. (2009). Subcellular mRNA localization in animal cells and why it matters. Science *326*, 1212-1216.

Holzbaur, E.L., and Goldman, Y.E. (2010). Coordination of molecular motors: from in vitro assays to intracellular dynamics. Curr Opin Cell Biol *22*, 4-13.

Hook, P., and Vallee, R.B. (2006). The dynein family at a glance. J Cell Sci *119*, 4369-4371.

Houliston, E., LeGuellec, R., Kress, M., Philippe, M., and Le Guellec, K. (1994). The kinesin-related protein Eg5 associates with both interphase and spindle microtubules during *Xenopus* early development. Dev Biol *164*, 147-159.

Houston, D.W., and King, M.L. (2000). A critical role for Xdazl, a germ plasm-localized RNA, in the differentiation of primordial germ cells in Xenopus. Development *127*, 447-456.

Huttelmaier, S., Zenklusen, D., Lederer, M., Dictenberg, J., Lorenz, M., Meng, X., Bassell, G.J., Condeelis, J., and Singer, R.H. (2005). Spatial regulation of beta-actin translation by Src-dependent phosphorylation of ZBP1. Nature *438*, 512-515.

Ingold, A.L., Cohn, S.A., and Scholey, J.M. (1988). Inhibition of kinesin-driven microtubule motility by monoclonal antibodies to kinesin heavy chains. J Cell Biol *107*, 2657-2667.

Irie, K., Tadauchi, T., Takizawa, P.A., Vale, R.D., Matsumoto, K., and Herskowitz, I. (2002). The Khd1 protein, which has three KH RNA-binding motifs, is required for proper localization of ASH1 mRNA in yeast. EMBO J *21*, 1158-1167.

Janke, C., and Kneussel, M. (2010). Tubulin post-translational modifications: encoding functions on the neuronal microtubule cytoskeleton. Trends Neurosci *33*, 362-372.

Jansen, R.P., Dowzer, C., Michaelis, C., Galova, M., and Nasmyth, K. (1996). Mother cell-specific HO expression in budding yeast depends on the unconventional myosin myo4p and other cytoplasmic proteins. Cell *84*, 687-697.

Januschke, J., Gervais, L., Dass, S., Kaltschmidt, J.A., Lopez-Schier, H., St Johnston, D., Brand, A.H., Roth, S., and Guichet, A. (2002). Polar transport in the Drosophila oocyte requires Dynein and Kinesin I cooperation. Curr Biol *12*, 1971-1981.

Kanai, Y., Dohmae, N., and Hirokawa, N. (2004). Kinesin transports RNA: isolation and characterization of an RNA-transporting granule. Neuron *43*, 513-525.

Kardon, J.R., and Vale, R.D. (2009). Regulators of the cytoplasmic dynein motor. Nat Rev Mol Cell Biol *10*, 854-865.

Karki, S., and Holzbaur, E.L. (1999). Cytoplasmic dynein and dynactin in cell division and intracellular transport. Curr Opin Cell Biol *11*, 45-53.

Keppler, A., Pick, H., Arrivoli, C., Vogel, H., and Johnsson, K. (2004). Labeling of fusion proteins with synthetic fluorophores in live cells. Proc Natl Acad Sci U S A *101*, 9955-9959.

Kertesz, M., Wan, Y., Mazor, E., Rinn, J.L., Nutter, R.C., Chang, H.Y., and Segal, E. (2010). Genome-wide measurement of RNA secondary structure in yeast. Nature *467*, 103-107.

Kiebler, M.A., and Bassell, G.J. (2006). Neuronal RNA granules: movers and makers. Neuron *51*, 685-690.

Kim, S., and Coulombe, P.A. (2010). Emerging role for the cytoskeleton as an organizer and regulator of translation. Nat Rev Mol Cell Biol *11*, 75-81.

King, M.L., Messitt, T.J., and Mowry, K.L. (2005). Putting RNAs in the right place at the right time: RNA localization in the frog oocyte. Biol Cell *97*, 19-33.

Kirchner, J., Woehlke, G., and Schliwa, M. (1999). Universal and unique features of kinesin motors: insights from a comparison of fungal and animal conventional kinesins. Biol Chem *380*, 915-921.

Kislauskis, E.H., Zhu, X., and Singer, R.H. (1997). beta-Actin messenger RNA localization and protein synthesis augment cell motility. J Cell Biol *136*, 1263-1270.

Kloc, M., and Etkin, L.D. (1994). Delocalization of Vg1 mRNA from the vegetal cortex in Xenopus oocytes after destruction of Xlsirt RNA. Science *265*, 1101-1103.

Kloc, M., and Etkin, L.D. (1995). Two distinct pathways for the localization of RNAs at the vegetal cortex in Xenopus oocytes. Development *121*, 287-297.

Kloc, M., and Etkin, L.D. (1998). Apparent continuity between the messenger transport organizer and late RNA localization pathways during oogenesis in Xenopus. Mech Dev *73*, 95-106.

Kloc, M., and Etkin, L.D. (2005). RNA localization mechanisms in oocytes. J Cell Sci *118*, 269-282.

Kloc, M., Wilk, K., Vargas, D., Shirato, Y., Bilinski, S., and Etkin, L.D. (2005). Potential structural role of non-coding and coding RNAs in the organization of the cytoskeleton at the vegetal cortex of Xenopus oocytes. Development *132*, 3445-3457.

Kohrmann, M., Luo, M., Kaether, C., DesGroseillers, L., Dotti, C.G., and Kiebler, M.A. (1999). Microtubule-dependent recruitment of Staufen-green fluorescent protein into large RNA-containing granules and subsequent dendritic transport in living hippocampal neurons. Mol Biol Cell *10*, 2945-2953.

Krauss, J., Lopez de Quinto, S., Nusslein-Volhard, C., and Ephrussi, A. (2009). Myosin-V regulates oskar mRNA localization in the Drosophila oocyte. Curr Biol *19*, 1058-1063.

Krendel, M., and Mooseker, M.S. (2005). Myosins: tails (and heads) of functional diversity. Physiology (Bethesda) *20*, 239-251.

Kress, T.L., Yoon, Y.J., and Mowry, K.L. (2004). Nuclear RNP complex assembly initiates cytoplasmic RNA localization. J Cell Biol *165*, 203-211.

Krieg, P.A., and Melton, D.A. (1984). Functional messenger RNAs are produced by SP6 in vitro transcription of cloned cDNAs. Nucleic Acids Res *12*, 7057-7070.

Kroll, T.T., Zhao, W.M., Jiang, C., and Huber, P.W. (2002). A homolog of FBP2/KSRP binds to localized mRNAs in *Xenopus* oocytes. Development *129*, 5609-5619.

Kural, C., Kim, H., Syed, S., Goshima, G., Gelfand, V.I., and Selvin, P.R. (2005). Kinesin and dynein move a peroxisome in vivo: a tug-of-war or coordinated movement? Science *308*, 1469-1472.

Kwon, S., Abramson, T., Munro, T.P., John, C.M., Köhrmann, M., and Schnapp, B.J. (2002). UUCAC- and vera-dependent localization of VegT RNA in *Xenopus* oocytes. Curr Biol *12*, 558-564.

Lane, J.D., and Allan, V.J. (1999). Microtubule-based endoplasmic reticulum motility in *Xenopus laevis*: Activation of membrane-associated kinesin during development. Mol Biol Cell *10*, 1909-1922.

Latham, V.M., Yu, E.H., Tullio, A.N., Adelstein, R.S., and Singer, R.H. (2001). A Rho-dependent signaling pathway operating through myosin localizes beta-actin mRNA in fibroblasts. Curr Biol *11*, 1010-1016.

Lawrence, C.J., Dawe, R.K., Christie, K.R., Cleveland, D.W., Dawson, S.C., Endow, S.A., Goldstein, L.S., Goodson, H.V., Hirokawa, N., Howard, J.*, et al.* (2004). A standardized kinesin nomenclature. J Cell Biol *167*, 19-22.

Lawrence, J.B., and Singer, R.H. (1986). Intracellular localization of messenger RNAs for cytoskeletal proteins. Cell *45*, 407-415.

Le Bot, N., Antony, C., White, J., Karsenti, E., and Vernos, I. (1998). Role of Xklp3, a subunit of the *Xenopus* kinesin II heterotrimeric complex, in membrane transport between the endoplasmic reticulum and the Golgi apparatus. J Cell Biol *143*, 1559-1573.

Lecuyer, E., Yoshida, H., Parthasarathy, N., Alm, C., Babak, T., Cerovina, T., Hughes, T.R., Tomancak, P., and Krause, H.M. (2007). Global analysis of mRNA localization reveals a prominent role in organizing cellular architecture and function. Cell *131*, 174-187.

Lehmann, R., and Nusslein-Volhard, C. (1991). The maternal gene nanos has a central role in posterior pattern formation of the Drosophila embryo. Development *112*, 679-691.

Levi, V., Serpinskaya, A.S., Gratton, E., and Gelfand, V. (2006). Organelle transport along microtubules in *Xenopus* melanophores: evidence for cooperation between multiple motors. Biophys J *90*.

Lewis, R.A., Gagnon, J.A., and Mowry, K.L. (2008). PTB/hnRNP I is required for RNP remodeling during RNA localization in Xenopus oocytes. Mol Cell Biol *28*, 678-686.

Lewis, R.A., Kress, T.L., Cote, C.A., Gautreau, D., Rokop, M.E., and Mowry, K.L. (2004). Conserved and clustered RNA recognition sequences are a critical feature of signals directing RNA localization in Xenopus oocytes. Mech Dev *121*, 101-109.

Lewis, R.A., and Mowry, K.L. (2007). Ribonucleoprotein remodeling during RNA localization. Differentiation *75*, 507-518.

Ling, S.C., Fahrner, P.S., Greenough, W.T., and Gelfand, V.I. (2004). Transport of Drosophila fragile X mental retardation protein-containing ribonucleoprotein granules by kinesin-1 and cytoplasmic dynein. Proc Natl Acad Sci U S A *101*, 17428-17433.

Lipshitz, H.D., and Smibert, C.A. (2000). Mechanisms of RNA localization and translational regulation. Curr Opin Genet Dev *10*, 476-488.

Long, R.M., Gu, W., Lorimer, E., Singer, R.H., and Chartrand, P. (2000). She2p is a novel RNA-binding protein that recruits the Myo4p-She3p complex to ASH1 mRNA. EMBO J *19*, 6592-6601.

Long, R.M., Singer, R.H., Meng, X., Gonzalez, I., Nasmyth, K., and Jansen, R.P. (1997). Mating type switching in yeast controlled by asymmetric localization of ASH1 mRNA. Science *277*, 383-387.

Luders, J., and Stearns, T. (2007). Microtubule-organizing centres: a re-evaluation. Nat Rev Mol Cell Biol *8*, 161-167.

MacArthur, H., Bubunenko, M., Houston, D.W., and King, M.L. (1999). Xcat2 RNA is a translationally sequestered germ plasm component in Xenopus. Mech Dev *84*, 75-88.

MacDougall, N., Clark, A., MacDougall, E., and Davis, I. (2003). Drosophila gurken (TGFalpha) mRNA localizes as particles that move within the oocyte in two dynein-dependent steps. Dev Cell *4*, 307-319.

Marello, K., La Rovere, J., and Sommerville, J. (1991). Binding of *Xenopus* oocyte masking proteins to mRNA sequences. Nucl Acids Res *20*, 5593-5600.

Markovtsov, V., Nikolic, J.M., Goldman, J.A., Turck, C.W., Chou, M.Y., and Black, D.L. (2000). Cooperative assembly of an hnRNP complex induced by a tissue-specific homolog of polypyrimidine tract binding protein. Mol Cell Biol *20*, 7463-7479.

Martin, K.C., and Ephrussi, A. (2009). mRNA localization: gene expression in the spatial dimension. Cell *136*, 719-730.

Martin, K.C., and Zukin, R.S. (2006). RNA trafficking and local protein synthesis in dendrites: an overview. J Neurosci *26*, 7131-7134.

Martin, M., Iyadurai, S.J., Gassman, A., Gindhart, J.G., Jr., Hays, T.S., and Saxton, W.M. (1999). Cytoplasmic dynein, the dynactin complex, and kinesin are interdependent and essential for fast axonal transport. Mol Biol Cell *10*, 3717-3728.

Melton, D.A. (1987). Translocation of a localized maternal mRNA to the vegetal pole of *Xenopus* oocytes. Nature *328*, 80-82.

Messitt, T.J., Gagnon, J.A., Kreiling, J.A., Pratt, C.A., Yoon, Y.J., and Mowry, K.L. (2008). Multiple kinesin motors coordinate cytoplasmic RNA transport on a subpopulation of microtubules in Xenopus oocytes. Dev Cell *15*, 426-436.

Miki, H., Okada, Y., and Hirokawa, N. (2005). Analysis of the kinesin superfamily: Insights into structure and function. Trends Cell Biol *15*, 467-476.

Mimori-Kiyosue, Y., Shiina, N., and Tsukita, S. (2000). The dynamic behavior of the APC-binding protein EB1 on the distal ends of microtubules. Curr Biol *10*, 865-868.

Minakhina, S., and Steward, R. (2005). Axes formation and RNA localization. Curr Opin Genet Dev *15*, 416-421.

Mingle, L.A., Okuhama, N.N., Shi, J., Singer, R.H., Condeelis, J., and Liu, G. (2005). Localization of all seven messenger RNAs for the actin-polymerization nucleator Arp2/3 complex in the protrusions of fibroblasts. J Cell Sci *118*, 2425-2433.

Mische, S., Li, M., Serr, M., and Hays, T.S. (2007). Direct observation of regulated ribonucleoprotein transport across the nurse cell/oocyte boundary. Mol Biol Cell *18*, 2254-2263.

Moore, M.J. (2005). From birth to death: the complex lives of eukaryotic mRNAs. Science *309*, 1514-1518.

Mowry, K.L. (1996). Complex formation between stage-specific oocyte factors and a Xenopus mRNA localization element. Proc Natl Acad Sci U S A *93*, 14608-14613.

Mowry, K.L., and Melton, D.A. (1992). Vegetal messenger RNA localization directed by a 340-nt RNA sequence element in Xenopus oocytes. Science *255*, 991-994.

Nakamura, A., Amikura, R., Hanyu, K., and Kobayashi, S. (2001). Me31B silences translation of oocyte-localizing RNAs through the formation of cytoplasmic RNP complex during *Drosophila* oogenesis. Development *128*, 3233-3242.

Nakata, T., and Hirokawa, N. (1995). Point mutation of adenosine triphosphate-binding motif generated rigor kinesin that selectively blocks anterograde lysosome membrane transport. J Cell Biol *131*, 1039-1053.

Niethammer, P., Kronja, I., Kandels-Lewis, S., Rybina, S., Bastiaens, P., and Karsenti, E. (2007). Discrete states of a protein interaction network govern interphase and mitotic microtubule dynamics. PLOS Biol *5*, e29.

Oberstrass, F.C., Auweter, S.D., Erat, M., Hargous, Y., Henning, A., Wenter, P., Reymond, L., Amir-Ahmady, B., Pitsch, S., Black, D.L.*, et al.* (2005). Structure of PTB bound to RNA: specific binding and implications for splicing regulation. Science *309*, 2054-2057.

Ohashi, S., Koike, K., Omori, A., Ichinose, S., Ohara, S., Kobayashi, S., and Anzai, K. (2002). Identification of mRNA/protein (mRNP) complexes containing pur-alpha, mStaufen, fragile X protein, and myosin Va and their association with rough endoplasmic reticulum equipped with a kinesin motor. J Cell Biol *277*, 37804-37810.

Otero, L.J., Devaux, A., and Standart, N. (2001). A 250-nucleotide UA-rich element in the 3' untranslated region of Xenopus laevis Vg1 mRNA represses translation both in vivo and in vitro. RNA *7*, 1753-1767.

Palacios, I.M. (2007). How does an RNA find its way? Intracellular localisation of transcripts. Sem Cell Dev Biol *18*, 163-170.

Palacios, I.M., Gatfield, D., St Johnston, D., and Izaurralde, E. (2004). An eIF4AIII-containing complex required for mRNA localization and nonsense-mediated mRNA decay. Nature *427*, 753-757.

Palacios, I.M., and St Johnston, D. (2002). Kinesin light chain-independent function of the Kinesin heavy chain in cytoplasmic streaming and posterior localisation in the Drosophila oocyte. Development *129*, 5473-5485.

Parker, R., and Sheth, U. (2007). P bodies and the control of mRNA translation and degradation. Mol Cell *25*, 635-646.

Pfeiffer, D.C., and Gard, D.L. (1999). Microtubules in Xenopus oocytes are oriented with their minus-ends towards the cortex. Cell Motil Cytoskeleton *44*, 34-43.

Poon, M.M., Choi, S.H., Jamieson, C.A., Geschwind, D.H., and Martin, K.C. (2006). Identification of process-localized mRNAs from cultured rodent hippocampal neurons. J Neurosci *26*, 13390-13399.

Quintyne, N.J., Gill, S.R., Eckley, D.M., Crego, C.L., Compton, D.A., and Schroer, T.A. (1999). Dynactin is required for microtubule anchoring at centrosomes. J Cell Biol *147*, 321-334.

Rayment, I., and Holden, H.M. (1994). The three-dimensional structure of a molecular motor. Trends Biochem Sci *19*, 129-134.

Redeker, V. (2010). Mass spectrometry analysis of C-terminal posttranslational modifications of tubulins. Methods Cell Biol *95*, 77-103.

Richards, T.A., and Cavalier-Smith, T. (2005). Myosin domain evolution and the primary divergence of eukaryotes. Nature *436*, 1113-1118.

Riedl, J., Crevenna, A.H., Kessenbrock, K., Yu, J.H., Neukirchen, D., Bista, M., Bradke, F., Jenne, D., Holak, T.A., Werb, Z.*, et al.* (2008). Lifeact: a versatile marker to visualize F-actin. Nat Methods *5*, 605-607.

Ross, A.F., Oleynikov, Y., Kislauskis, E.H., Taneja, K.L., and Singer, R.H. (1997). Characterization of a beta-actin mRNA zipcode-binding protein. Mol Cell Biol *17*, 2158-2165.

Schroer, T.A. (2004). Dynactin. Annu Rev Cell Dev Biol *20*, 759-779.

Shaner, N.C., Campbell, R.E., Steinbach, P.A., Giepmans, B.N., Palmer, A.E., and Tsien, R.Y. (2004). Improved monomeric red, orange and yellow fluorescent proteins derived from Discosoma sp. red fluorescent protein. Nat Biotechnol *22*, 1567-1572.

Sharp, P.A. (2009). The centrality of RNA. Cell *136*, 577-580.

Shav-Tal, Y., and Singer, R.H. (2005). RNA localization. J Cell Sci *118*, 4077-4081.

Singer, R.H. (2008). Highways for mRNA transport. Cell *134*, 722-723.

Sossin, W.S., and DesGroseillers, L. (2006). Intracellular trafficking of RNA in neurons. Traffic *7*, 1581-1589.

Sprague, B.L., and McNally, J.G. (2005). FRAP analysis of binding: proper and fitting. Trends Cell Biol *15*, 84-91.

St Johnston, D. (2005). Moving messages: the intracellular localization of mRNAs. Nat Rev Mol Cell Biol *6*, 363-375.

St Johnston, D., and Ahringer, J. (2010). Cell polarity in eggs and epithelia: parallels and diversity. Cell *141*, 757-774.

Stearns, T. (1995). Green fluorescent protein. The green revolution. Curr Biol *5*, 262-264.

Stearns, T., Evans, L., and Kirschner, M. (1991). Gamma-tubulin is a highly conserved component of the centrosome. Cell *65*, 825-836.

Stearns, T., and Kirschner, M. (1994). In vitro reconstitution of centrosome assembly and function: the central role of gamma-tubulin. Cell *76*, 623-637.

Subach, F.V., Patterson, G.H., Manley, S., Gillette, J.M., Lippincott-Schwartz, J., and Verkhusha, V.V. (2009). Photoactivatable mCherry for high-resolution two-color fluorescence microscopy. Nat Methods *6*, 153-159.

Sundell, C.L., and Singer, R.H. (1991). Requirement of microfilaments in sorting of actin messenger RNA. Science *253*, 1275-1277.

Suzuki, T., Tian, Q.B., Kuromitsu, J., Kawai, T., and Endo, S. (2007). Characterization of mRNA species that are associated with postsynaptic density fraction by gene chip microarray analysis. Neurosci Res *57*, 61-85.

Tadauchi, T., Matsumoto, K., Herskowitz, I., and Irie, K. (2001). Post-transcriptional regulation through the HO 3'-UTR by Mpt5, a yeast homolog of Pumilio and FBF. EMBO J *20*, 552-561.

Takizawa, P.A., Sil, A., Swedlow, J.R., Herskowitz, I., and Vale, R.D. (1997). Actin-dependent localization of an RNA encoding a cell-fate determinant in yeast. Nature *389*, 90-93.

Tekotte, H., and Davis, I. (2002). Intracellular mRNA localization: motors move messages. Trends Genet *18*, 636-642.

Thomsen, G.H., and Melton, D.A. (1993). Processed Vg1 protein is an axial mesoderm inducer in Xenopus. Cell *74*, 433-441.

Tuma, M.C., Zill, A., Le Bot, N., Vernos, I., and Gelfand, V. (1998). Heterotrimeric kinesin II is the microtubule motor protein responsible for pigment dispersion in *Xenopus* melanophores. J Cell Biol *143*, 1547-1558.

Uchida, A., Alami, N.H., and Brown, A. (2009). Tight functional coupling of kinesin-1A and dynein motors in the bidirectional transport of neurofilaments. Mol Biol Cell *20*, 4997-5006.

Uteng, M., Hentrich, C., Miura, K., Bieling, P., and Surrey, T. (2008). Poleward transport of Eg5 by dynein-dynactin in Xenopus laevis egg extract spindles. J Cell Biol *182*, 715-726.

Vale, R.D. (2003). The molecular motor toolbox for intracellular transport. Cell *112*, 467-480.

Vale, R.D., and Milligan, R.A. (2000). The way things move: looking under the hood of molecular motor proteins. Science *288*, 88-95.

Vale, R.D., Reese, T.S., and Sheetz, M.P. (1985). Identification of a novel force-generating protein, kinesin, involved in microtubule-based motility. Cell *42*, 39-50.

Vershinin, M., Carter, B.C., Razafsky, D.S., King, S.J., and Gross, S.P. (2007). Multiple-motor based transport and its regulation by Tau. Proc Nat Acad Sci USA *104*, 87-92.

Vicente-Manzanares, M., Ma, X., Adelstein, R.S., and Horwitz, A.R. (2009). Non-muscle myosin II takes centre stage in cell adhesion and migration. Nat Rev Mol Cell Biol *10*, 778-790.

Wallace, R.A., and Misulovin, Z. (1978). Long-term growth and differentiation of *Xenopus* oocytes in a defined medium. Proc Natl Acad Sci USA *75*, 5534-5538.

Wallace, R.A., Misulovin, Z., and Wiley, H.S. (1980). Growth of anuran oocytes in serum-supplemented medium. Reprod Nutr Dev *20*, 699-708.

Wang, D.O., Kim, S.M., Zhao, Y., Hwang, H., Miura, S.K., Sossin, W.S., and Martin, K.C. (2009). Synapse- and stimulus-specific local translation during long-term neuronal
plasticity. Science *324*, 1536-1540.

Wang, D.O., Martin, K.C., and Zukin, R.S. (2010). Spatially restricting gene expression by local translation at synapses. Trends Neurosci *33*, 173-182.

Waterman-Storer, C.M., Karki, S.B., Kuznetsov, S.A., Tabb, J.S., Weiss, D.G., Langford, G.M., and Holzbaur, E.L. (1997). The interaction between cytoplasmic dynein and dynactin is required for fast axonal transport. Proc Natl Acad Sci U S A *94*, 12180-12185.

Wedaman, K.L., Meyer, D.W., Rashid, D.J., Cole, D.G., and Scholey, J.M. (1996). Sequence and submolecular localization of the 115-kD accessory subunit of the heterotrimeric kinesin-II (KRP85/95) complex. J Cell Biol *132*, 371-380.

Weeks, D.L., and Melton, D.A. (1987). A maternal mRNA localized to the vegetal hemisphere in Xenopus eggs codes for a growth factor related to TGF-beta. Cell *51*, 861-867.

Weil, T.T., Forrest, K.M., and Gavis, E.R. (2006). Localization of bicoid mRNA in late oocytes is maintained by continual active transport. Dev Cell *11*, 251-262.

Weil, T.T., Xanthakis, D., Parton, R., Dobbie, I., Rabouille, C., Gavis, E.R., and Davis, I. (2010). Distinguishing direct from indirect roles for bicoid mRNA localization factors. Development *137*, 169-176.

Welte, M.A. (2004). Bidirectional transport along microtubules. Curr Biol *14*, R525-537.

Westermann, S., and Weber, K. (2003). Post-translational modifications regulate microtubule function. Nat Rev Mol Cell Biol *4*, 938-947.

Wilkie, G.S., and Davis, I. (2001). Drosophila wingless and pair-rule transcripts localize apically by dynein-mediated transport of RNA particles. Cell *105*, 209-219.

Wright, B.D., Henson, J.H., Wedaman, K.P., Willy, P.J., Morand, J.N., and Scholey, J.M. (1991). Subcellular localization and sequence of sea urchin kinesin heavy chain: Evidence for its association with membranes in the mitotic apparatus and interphase cytoplasm. J Cell Biol *113*, 817-833.

Wright, B.D., Terasaki, M., and Scholey, J.M. (1993). Roles of kinesin and kinesin-like proteins in sea urchin embryonic cell division: Evaluation using antibody microinjection. J Cell Biol *123*, 681-689.

Xie, J., Lee, J.-A., Kress, T.L., Mowry, K.L., and Black, D.L. (2003). Protein kinase A phosphorylation modulates transport of polypyrimidine tract-binding protein. Proc Natl Acad Sci USA *100*, 8776-8781.

Yang, J.T., Laymon, R.A., and Goldstein, L.S. (1989). A three-domain structure of kinesin heavy chain revealed by DNA sequence and microtubule binding analyses. Cell *56*, 289-298.

Yisraeli, J.K. (2005). VICKZ proteins: a multi-talented family of regulatory RNA-binding proteins. Biol Cell *97*, 87-96.

Yisraeli, J.K., and Melton, D.A. (1988). The material mRNA Vg1 is correctly localized following injection into Xenopus oocytes. Nature *336*, 592-595.

Yisraeli, J.K., Sokol, S., and Melton, D.A. (1990). A two-step model for the localization of maternal mRNA in Xenopus oocytes: involvement of microtubules and microfilaments in the translocation and anchoring of Vg1 mRNA. Development *108*, 289-298.

Yoon, Y.J., and Mowry, K.L. (2004). Xenopus Staufen is a component of a ribonucleoprotein complex containing Vg1 RNA and kinesin. Development *131*, 3035-3045.

Zaessinger, S., Busseau, I., and Simonelig, M. (2006). Oskar allows nanos mRNA translation in Drosophila embryos by preventing its deadenylation by Smaug/CCR4. Development *133*, 4573-4583.

Zearfoss, N.R., Chan, A.P., Kloc, M., Allen, L.H., and Etkin, L.D. (2003). Identification of new Xlsirt family members in the Xenopus laevis oocyte. Mech Dev *120*, 503-509.

Zhang, J., Houston, D.W., King, M.L., Payne, C., Wylie, C., and Heasman, J. (1998). The role of maternal VegT in establishing the primary germ layers in Xenopus embryos. Cell *94*, 515-524.

Zhang, Q., Yaniv, K., Oberman, F., Wolke, U., Git, A., Fromer, M., Taylor, W.L., Meyer, D., Standart, N., Raz, E.*, et al.* (1999). Vg1 RBP intracellular distribution and evolutionarily conserved expression at multiple stages during development. Mech Dev *88*, 101-106.

Zhao, W.M., Jiang, C., Kroll, T.T., and Huber, P.W. (2001). A proline-rich protein binds to the localization element of Xenopus Vg1 mRNA and to ligands involved in actin polymerization. EMBO J *20*, 2315-2325.

Zhou, Y., and King, M.L. (1996a). Localization of Xcat-2 RNA, a putative germ plasm component, to the mitochondrial cloud in Xenopus stage I oocytes. Development *122*, 2947-2953.

Zhou, Y., and King, M.L. (1996b). RNA transport to the vegetal cortex of *Xenopus* oocytes. Dev Biol *179*, 173-183.

Zimyanin, V.L., Belaya, K., Pecreaux, J., Gilchrist, M.J., Clark, A., Davis, I., and St Johnston, D. (2008). In vivo imaging of oskar mRNA transport reveals the mechanism of posterior localization. Cell *134*, 843-853.